

UNIVERSIDAD SAN FRANCISCO DE QUITO USFQ

Colegio de Posgrados

**Design and Analysis of Metamaterial Absorbers for Radiated Emission
Reduction**

**Tesis en torno a una hipótesis o problema de investigación y su
contrastación**

Daniel Ignacio Collahuazo Soria

**Francesca Venneri Doctor of Philosophy
Director de Trabajo de Titulación**

Trabajo de titulación de posgrado presentado como requisito
para la obtención del título de Máster en Nanoelectrónica

Quito, 5 de Enero de 2023

UNIVERSIDAD SAN FRANCISCO DE QUITO USFQ
COLEGIO DE POSGRADOS

HOJA DE APROBACIÓN DE TRABAJO DE TITULACIÓN

**Design and Analysis of Metamaterial Absorbers for Radiated Emission
Reduction**

Daniel Ignacio Collahuazo Soria

Nombre del Director del Programa:	Luis Miguel Prócel
Título académico:	Doctor of Philosophy
Director del programa de:	Maestría en Nanoelectrónica

Nombre del Decano del colegio Académico:	Eduardo Alba
Título académico:	Doctor of Philosophy
Decano del Colegio:	Colegio de Ciencias e Ingenierías

Nombre del Decano del Colegio de Posgrados:	Hugo Burgos
Título académico:	Doctor of Philosophy

Quito, Enero de 2023

© DERECHOS DE AUTOR

Por medio del presente documento certifico que he leído todas las Políticas y Manuales de la Universidad San Francisco de Quito USFQ, incluyendo la Política de Propiedad Intelectual USFQ, y estoy de acuerdo con su contenido, por lo que los derechos de propiedad intelectual del presente trabajo quedan sujetos a lo dispuesto en esas Políticas.

Asimismo, autorizo a la USFQ para que realice la digitalización y publicación de este trabajo en el repositorio virtual, de conformidad a lo dispuesto en la Ley Orgánica de Educación Superior del Ecuador.

Nombre del estudiante: Daniel Ignacio Collahuazo Soria

Código de estudiante: 00215162

C.I.: 1720276714

Lugar y fecha: Quito, 5 de Enero de 2023.

ACLARACIÓN PARA PUBLICACIÓN

Nota: El presente trabajo, en su totalidad o cualquiera de sus partes, no debe ser considerado como una publicación, incluso a pesar de estar disponible sin restricciones a través de un repositorio institucional. Esta declaración se alinea con las prácticas y recomendaciones presentadas por el Committee on Publication Ethics COPE descritas por Barbour et al. (2017) Discussion document on best practice for issues around theses publishing, disponible en <http://bit.ly/COPETheses>.

UNPUBLISHED DOCUMENT

Note: The following graduation project is available through Universidad San Francisco de Quito USFQ institutional repository. Nonetheless, this project – in whole or in part – should not be considered a publication. This statement follows the recommendations presented by the Committee on Publication Ethics COPE described by Barbour et al. (2017) Discussion document on best practice for issues around theses publishing available on <http://bit.ly/COPETheses>.

DEDICATORIA

To my Princesa de la noche heredera de Caín.

AGRADECIMIENTOS

Me gustaría expresar mi más sincero agradecimiento a mi asesora Prof. Francesca Venneri por el apoyo continuo de mi investigación de maestría y por las clases que tomé con ella en el campo de la compatibilidad electromagnética, por su tiempo, orientación, paciencia, motivación e inmenso conocimiento.

Agradezco a la Universidad San Francisco de Quito (USFQ) y a la Universidad della Calabria (UNICAL) por los conocimientos impartidos y ayuda prestada durante el transcurso de mis estudios.

Quiero agradecer a mi familia: mis padres Luis Ignacio y Cecilia y mis hermanas Nora y Cristina, por su apoyo en momentos difíciles a lo largo de mi vida, especialmente en estos años de estudios.

Y por último, un gran agradecimiento a mis amigos y gente que conocí en esta parte de mi vida, con los que compartí días de estrés, nervios, viajes y deportes y noches de trabajo y diversión.

Daniel C.

RESUMEN

En esta tesis, un absorbedor basado en el concepto de superficie selectiva de frecuencia (FSS) es adoptado para bloquear la onda de frecuencia indeseada.

El material que será usado para realizar el blindaje es llamado metamaterial; los metamateriales son estructuras compuestas que consisten en inclusiones incrustadas periódicamente en una matriz. Cuando el tamaño de las inclusiones y los períodos espaciales son pequeños en comparación con la longitud de onda del campo Electromagnético (EM) generado por una fuente, estos materiales artificiales pueden ser homogeneizados. Estos materiales artificiales son caracterizados por parámetros constitutivos efectivos que dependen de las propiedades geométricas y físicas de las inclusiones y del medio. Los metamateriales exhiben propiedades EM que los materiales convencionales no poseen, como la capacidad de comportarse como un absorbedor selectivo de frecuencia.

Este trabajo de tesis ilustra las principales características y los criterios de diseño de metamateriales absorbedores para emisión de radiofrecuencia (RF).

En el Capítulo 1, una introducción sobre los metamateriales y su estructura es ilustrada.

El Capítulo 2 proporciona una breve descripción general de las emisiones radiadas no intencionales; en particular, discutirá los estándares de EMC para emisión radiada, mediciones y pruebas de emisión radiada, algunas soluciones como blindaje y absorbentes.

El Capítulo 3 ilustra el análisis y la simulación de una celda unitaria de metamaterial de una sola capa para la reducción de las emisiones radiadas a 8 GHz.

En el Capítulo 4, se presenta el análisis de celdas absorbentes miniaturizadas para la reducción de emisiones radiadas. Finalmente se diseña una estructura metamaterial miniaturizada (53% de reducción de tamaño respecto a las soluciones existentes) consiguiendo valores de absorción muy elevados cercanos al 100%.

El Capítulo 5 muestra el análisis de estabilidad angular del metamaterial absorbedor fractal diseñado. En conclusión, la estructura absorbente diseñada es estable con respecto al ángulo de incidencia, lo que permite reducir las emisiones radiadas no deseadas de direcciones aleatorias y desconocidas.

Palabras clave: superficie selectiva de frecuencia (FSS), metamaterial, absorbedores, emisiones radiadas no intencionales, celda unitaria, estabilidad angular.

ABSTRACT

In this thesis, an absorber based on the concept of frequency selective surface (FSS) is adopted to block the undesired wave frequency.

The material that will be used to develop the shield is called metamaterial; metamaterials are composite structures consisting of inclusions periodically embedded in a host matrix. When the size of the inclusions and the spatial periods are small compared with the wavelength of the EM field generated by a source, such artificial materials can be homogenized. These artificial materials are characterized by effective constitutive parameters that depend on the geometrical and physical properties of the inclusions and of the host medium. Metamaterials exhibit EM properties that conventional materials do not possess, such as the ability to behave as a frequency selective absorber.

This thesis work illustrates the main characteristics and the design criteria of metamaterial absorbers for radio frequency (RF) emission.

In Chapter 1, an introduction on metamaterials and their structure is illustrated.

Chapter 2 provides a brief overview of unintentional radiated emissions; in particular, it will discuss EMC standards for radiated emission, measurements and test of radiated emission, some solutions such as shielding and absorbers.

Chapter 3 illustrates the analysis and simulation of a single layer metamaterial unit cell for the reduction of radiated emissions at 8 GHz.

In Chapter 4, the analysis of miniaturized absorber cells for radiated emission reduction is presented. A miniaturized metamaterial structure is finally designed (53% size reduction with respect to existing solutions) achieving very high absorption values close to 100%.

Chapter 5 shows the angular stability analysis of the designed fractal metamaterial absorber. In conclusion, the designed absorbing structure is stable with respect to the angle of incidence, allowing the reduction of unwanted radiated emissions from random and unknown directions.

Key words: frequency selective surface (FSS), metamaterial, absorbers, unintentional radiated emissions, unit cell, angular stability.

TABLE OF CONTENTS

ABSTRACT	9
TABLE OF CONTENTS.....	11
INTRODUCTION.....	21
CHAPTER I.....	24
METAMATERIALS	24
1.1 Introduction.....	24
1.2 History of metamaterials.....	25
1.3 Electromagnetic properties	27
<i>1.3.1 Plane wave propagation into metamaterial.....</i>	<i>28</i>
<i>1.3.2 Classification of metamaterials</i>	<i>30</i>
1.4 Metamaterial’s properties	32
1.5 Applications of metamaterials	33
<i>1.5.1 Medical sector.....</i>	<i>33</i>
<i>1.5.2 Automotive sector.....</i>	<i>34</i>
<i>1.5.3 Aerospace sector</i>	<i>34</i>
<i>1.5.4 Biosensors application</i>	<i>34</i>
1.6 Metamaterial absorber	35
<i>1.6.1 Impedance Matching.....</i>	<i>37</i>
<i>1.6.2 Interference theory.....</i>	<i>39</i>
1.7 Classification Electromagnetic-Wave Absorbers	41
<i>1.7.1 Broadband Perfect Absorbers.....</i>	<i>41</i>
<i>1.7.2 Resonant Absorbers.....</i>	<i>44</i>
1.8 Differences and Advantages of metamaterial-Based Perfect Absorbers	47
CHAPTER II	49
UNINTENTIONAL RADIATED EMISSION.....	49
2.1 Definition	49
2.2 Radiated and Conducted Emissions.....	50

2.3 EMC Standards for Radiated Emission	53
2.3.1 US Standards.....	53
2.3.2 EU Standards	55
2.4 Measurements and test of Radiated Emission	58
2.5 Solutions: Shielding and Absorbers.....	62
2.5.1 Shielding.....	62
2.5.2 EM Absorbers.....	67
2.6 Metamaterial-based solution discussed in the paper “Design and Evaluation of Radiated Emission Metamaterial Absorbers”	70
2.6.1 Source of Radiation.....	70
2.6.2 Solution: Impedance Matching Metamaterial Absorber.....	71
CHAPTER III.....	76
ANALYSIS AND SIMULATION OF A SINGLE LAYER METAMATERIAL UNIT CELL FOR THE REDUCTION OF RADIATED EMISSIONS	76
3.1 Introduction.....	76
3.2 Unit cell geometry.....	77
3.3 Design of resonant metamaterial unit cell	79
3.4 Unit cell behavior vs dielectric loss tangent	86
3.5 Unit cell behavior vs thickness of the metal layer	90
3.6 Metamaterial absorber	95
3.6.1 $D=4.7mm$ and $L=3.49mm$	95
3.6.2 $D=4.2mm$ and $L=3.23mm$	102
3.7 Final considerations	103
3.8 Design of a single layer metamaterial unit cell for the reduction of radiated emissions.....	106
CHAPTER IV	110
ANALYSIS AND DESIGN OF MINIATURIZED ABSORBER CELLS FOR RADIATED EMISSION REDUCTION	110
4.1 Introduction.....	110
4.2 Fractal Structure.....	111
4.3 Analysis versus the scaling factor S.....	113
4.3.1 Unit Cell $D \times D = 4.7 mm \times 4.7 mm$	113

4.3.2 Unit Cell $D \times D = 4.2 \text{ mm} \times 4.2 \text{ mm}$	121
4.3.3 Unit Cell $D \times D = 3.8 \text{ mm} \times 3.8 \text{ mm}$	122
4.3.4 Unit Cell $D \times D = 3.2 \text{ mm} \times 3.2 \text{ mm}$	125
4.3.5 Unit Cell $D \times D = 2.5 \text{ mm} \times 2.5 \text{ mm}$	131
4.4 Final considerations	139
CHAPTER V.....	140
ANGULAR STABILITY OF THE DESIGNED FRACTAL METAMATERIAL ABSORBERS	140
5.1 Introduction.....	140
5.2 Analysis for the horizontally polarized E-field (TE mode) and vertically polarized E-field (TM mode).....	141
5.3 Final comments	152
CONCLUSIONS.....	154
REFERENCES	156

LIST OF TABLES

Table 2.1 FCC Emission limits for Class A digital devices (10 meters)	54
Table 2.2 FCC Emission limits for Class B digital devices (3 meters)	55
Table 2.3 CISPR 32 Emission limits for Class A digital devices (30 meters).....	56
Table 2.4 FCC Emission limits for Class B digital devices (10 meters).....	56
Table 4.1 Unit cells behaviors versus the ratio A_p/A_c	124
Table 4.2 Unit cells behaviors versus the ratio A_p/A_c	138
Table 5.1 Summary of the absorption coefficient for different incident angles (TE and TM modes) from all unit cells	153

LIST OF FIGURES

Fig. 1.1 Historical development of metamaterials	26
Fig. 1.2 Forward and backward waves: (a) Plane wave in a usual isotropic medium; (b) Plane wave in a Veselago medium	30
Fig. 1.3 Classification of materials.....	30
Fig. 1.4 Comparison of Snell’s law in different medium.....	32
Fig. 1.5 First experimental demonstration of a metamaterial perfect absorber.....	36
Fig. 1.6 Applications of metamaterial absorbers with respect to different frequencies.....	37
Fig. 1.7 Multiple reflections and interference model of metamaterial absorber.	40
Fig. 1.8 Commercial EM-wave absorber material	42
Fig. 1.9 Types of porous absorbing materials	44
Fig. 1.10 Common designs for resonant absorbers	46
Fig. 2.1 Generation of unwanted electromagnetic energy	51
Fig. 2.2 Principal methods to reduce EMI	52
Fig. 2.3 Radiated Emissions Limits for Class A digital devices	57
Fig. 2.4 Radiated Emissions Limits for Class B digital devices	58
Fig. 2.5 OATS in Queretaro, Mexico	59
Fig. 2.6 Broadband antennas for EMC measurements	60
Fig. 2.7 Semi anechoic Chamber	61
Fig. 2.8 Illustration of the setup for measurement of radiated emissions	61
Fig. 2.9 Measurement equipment for radiated emissions	62
Fig. 2.10 Illustration of the use of a shielded enclosure	63
Fig. 2.11 Illustration of the incident wave through the shield	65
Fig. 2.12 Illustration of EM radiation and absorption in the current scenario	69
Fig. 2.13 PCIe switch	70
Fig. 2.14 Side and top views of the two- layer metamaterial absorber	72
Fig. 2.15 Effect of the dielectric substrate thickness on the reflection coefficient	73
Fig. 2.16 Effect of the metallic patch thickness on the reflection coefficient	74
Fig. 2.17 Effect of the square metallic patch width on the reflection coefficient	74
Fig. 2.18 Effect of the gap (for a fixed patch width) on the reflection coefficient	75

Fig. 3.1 Illustration 3D view of the unit cell	78
Fig. 3.2 Layers of the unit cell	78
Fig. 3.3 Plot of the real part of the cell impedance for different values of L (D=4.7mm)	79
Fig. 3.4 Plot of the imaginary part of the cell impedance for different values of L (D=4.7mm)	80
Fig. 3.5 Behavior of the impedance for different values of L (D=4.7mm): (a) Real part; (b) Imaginary part.....	80
Fig. 3.6 Reflection coefficient for different values of L (D=4.7mm)	81
Fig. 3.7 Reflection coefficient for different values of L (D=4.7mm) (processing in Matlab)	82
Fig. 3.8 Absorption of the unit cell for different values of L (D=4.7mm)	83
Fig. 3.9 Absorption of the unit cell for different values of L (D=4.7mm) (processing in Matlab)	83
Fig. 3.10 Behavior of the impedance for different values of L (D=4.2mm)	84
Fig. 3.11 Behavior of the impedance for different values of L (D=7.5mm)	85
Fig. 3.12 Behavior of the impedance for different values of L (D=9.4mm)	85
Fig. 3.13 Behavior of the impedance for different values of loss tangent (D=4.7mm L=3.49mm)	87
Fig. 3.14 (a) Reflection coefficient for different values of loss tangent; (b) Absorption for different values of loss tangent. (D=4.7mm L=3.49mm)	87
Fig. 3.15 (a) Behavior of the impedance for different values of loss tan at the resonance frequency; (b) Absorption for different values of loss tangent at the resonance frequency. (D=4.7mm L=3.49mm)	88
Fig. 3.16 Impedance for different values of loss tangent (D=4.2mm L=3.23mm)	89
Fig. 3.17 (a) Behavior of the reflection coefficient for different values of loss tangent; (b) Behavior of the absorption for different values of loss tangent. (D=4.2mm L=3.23mm)	89
Fig. 3.18 (a) Behavior of the impedance for different values of loss tan at the resonance frequency; (b) Absorption for different values of loss tangent at the resonance frequency. (D=4.2mm L=3.23mm)	90
Fig. 3.19 Impedance for different values of metal thickness (D=4.7mm L=3.49mm)	91
Fig. 3.20 (a) Reflection coefficient for different values of metal thickness; (b) Absorption for different for different values of metal thickness. (D=4.7mm L=3.49mm)	92
Fig. 3.21 (a) Behavior of the impedance for different values of metal thickness at the resonance frequency; (b) Absorption for different values of metal thickness at the resonance frequency. (D=4.7mm L=3.49mm)	92

Fig. 3.22 Behavior of the impedance for different values of metal thickness (D=4.2mm L=3.23mm)	93
Fig. 3.23 (a) Behavior of the reflection coefficient for different values of loss tangent; (b) Absorption for different values of loss tangent. (D=4.2mm L=3.23mm)	94
Fig. 3.24 (a) Behavior of the impedance for different values of metal thickness at the resonance frequency; (b) Absorption for different values of metal thickness at the resonance frequency. (D=4.2mm L=3.23mm)	95
Fig. 3.25 (a) Behavior of the real part of the impedance for different values of metal conductivity; (b) Behavior of the absorption for different values of metal conductivity. (MT=0.01mm)	96
Fig. 3.26 (a) Behavior of the real part of the impedance due conductivity of the metal layer. (b) Behavior of the absorption due conductivity of the metal layer. (MT= 0.001mm)	97
Fig. 3.27 (a) Behavior of the real part of the impedance due conductivity of the metal layer; (b) Behavior of the absorption due conductivity of the metal layer. (MT = 0.0001mm)	98
Fig. 3.28 (a) Behavior of the real part of the impedance due conductivity of the metal layer. (b) Behavior of the absorption due conductivity of the metal layer. (MT = 1 x 10 ⁻⁵ mm)	99
Fig. 3.29 (a) Behavior of the real part of the impedance due conductivity of the metal layer. (b) Behavior of the absorption due conductivity of the metal layer. (MT = 1 x 10 ⁻⁶ mm) .	100
Fig. 3.30 (a) Behavior of the real part of the impedance due conductivity of the metal layer. (b) Behavior of the absorption due conductivity of the metal layer. (MT = 2 x 10 ⁻⁷ mm) .	101
Fig. 3.31 (a) Behavior of the impedance for different values of conductivity for each metal thickness at the resonance frequency; (b) Absorption for different values of conductivity for each metal thickness at the resonance frequency. (D=4.7 mm, L=3.49 mm)	102
Fig. 3.32 (a) Behavior of the impedance for different values of conductivity for each metal thickness at the resonance frequency; (b) Absorption for different values of conductivity for each metal thickness at the resonance frequency. (D=4.2 mm, L=3.23 mm)	103
Fig. 3.33 (a) Behavior of the impedance for different values of conductivity for each metal thickness at the resonance frequency; (b) Behavior of the absorption for different values of conductivity for each metal thickness at the resonance frequency. (D=4.7 mm, L=3.49 mm)	104
Fig. 3.34 (a) Behavior of the impedance for different values of conductivity for each metal thickness at the resonance frequency; (b) Behavior of the absorption for different values of conductivity for each metal thickness at the resonance frequency. (D=4.2 mm, L=3.23 mm)	105
Fig. 3.35 Illustration 3D of the unit cell	106

Fig. 3.36 Edit layers of the unit cell	106
Fig. 3.37 Behavior of the impedance for different values of L (D=4.7 mm, MT=0.0001 mm)	107
Fig. 3.38 (a) Reflection coefficient; (b) Absorption coefficient. (D=4.7 mm, MT=0.0001 mm)	108
Fig. 3.39 Behavior of the impedance for different values of L (D=4.2 mm, MT=0.0001 mm)	109
Fig. 3.40 (a) Reflection coefficient; (b) Absorption coefficient. (D=4.2 mm, MT=0.0001 mm)	109
Fig. 4.1 Structure of the fractal metamaterial absorber	112
Fig. 4.2 Geometry of the unit cell: (a) View 2D; (b)View 3D	112
Fig. 4.3 Layers of Fractal structure in Ansoft Designer V3	113
Fig. 4.4 Real part of the unit cell impedance for different values of S (D=4.7 mm, L=3.9 mm)	114
Fig. 4.5 Absorption of the unit cell for different values of S (D=4.7 mm, L=3.9 mm)	115
Fig. 4.6 Real part of the unit cell impedance for different values of S (D=4.7 mm, L=4 mm)	116
Fig. 4.7 Absorption of the unit cell for different values of S (D=4.7 mm, L=4 mm)	116
Fig. 4.8 Real part of the unit cell impedance for different values of S (D=4.7 mm, L=4.1 mm)	117
Fig. 4.9 Absorption of the unit cell for different values of S (D=4.7 mm, L=4.1 mm)	117
Fig. 4.10 Real part of the unit cell impedance for different values of S (D=4.7 mm, L=4.2mm)	118
Fig. 4.11 Absorption of the unit cell for different values of S (D=4.7 mm, L=4.2 mm)	119
Fig. 4.12 Unit cell impedance for different values of L and S=0.15 (D=4.7 mm)	120
Fig. 4.13 Absorption of the unit cell for different values of L and S=0.15 (D=4.7 mm)	120
Fig. 4.14 Unit cell impedance for different values of L and S=0.15 (D=4.2 mm)	121
Fig. 4.15 Absorption of the unit cell for different values of L and S=0.15 (D=4.2 mm)	122
Fig. 4.16 Unit cell impedance for different values of L and S=0.15 (D=3.8 mm)	123
Fig. 4.17 Absorption of the unit cell for different values of L and S=0.15 (D=3.8 mm)	123
Fig. 4.18 Unit cell impedance versus the ratio A_p/A_c for different values of D	125
Fig. 4.19 Real part of the unit cell impedance for different values of S (D=3.2 mm L=2.75mm)	126

Fig. 4.20 Absorption of the unit cell for different values of S (D=3.2 mm L=2.75 mm)	126
Fig. 4.21 Real part of the unit cell impedance for different values of S (D=3.2 mm L=2.8mm)	127
.....	
Fig. 4.22 Absorption of the unit cell for different values of S (D=3.2 mm L=2.8 mm)	127
Fig. 4.23 Real part of the unit cell impedance for different values of S (D=3.2 mm L=2.9mm)	128
.....	
Fig. 4.24 Absorption of the unit cell for different values of S (D=3.2 mm L=2.9 mm)	128
Fig. 4.25 Real part of the unit cell impedance for different values of S (D=3.2 mm L=3 mm)	129
.....	
Fig. 4.26 Absorption of the unit for different values of S (D=3.2 mm L=3 mm)	130
Fig. 4.27 Unit cell impedance for different values of L and S=0.15 (D=3.2 mm)	130
Fig. 4.28 Absorption of the unit cell for different values of L and S=0.15 (D=3.2 mm)	131
Fig. 4.29 Real part of the unit cell impedance for different values of S (D=2.5 mm L=2.2mm)	132
.....	
Fig. 4.30 Absorption of the unit cell for different values of S (D=2.5 mm L=2.2 mm)	132
Fig. 4.31 Real part of the unit cell impedance for different values of S (D=2.5 mm L=2.3mm)	133
.....	
Fig. 4.32 Absorption of the unit cell for different values of S (D=2.5 mm L=2.3 mm)	133
Fig. 4.33 Real part of the unit cell impedance for different values of S (D=2.5 mm L=2.4mm)	134
.....	
Fig. 4.34 Absorption of the unit cell for different values of S (D=2.5 mm L=2.4 mm)	135
Fig. 4.35 Real part of the unit cell impedance for different values of S (D=2.5 mm L=2.45mm)	136
.....	
Fig. 4.36 Absorption of the unit cell for different values of S (D=2.5 mm L=2.45 mm)	136
Fig. 4.37 Unit cell impedance for different values of L and S=0.15 (D=2.5 mm)	137
Fig. 4.38 Absorption of the unit cell for different values of L and S=0.15 (D=2.5 mm)	137
Fig. 4.39 Unit cell impedance Vs Relationship Metallic Patch Area/Unit Cell Area	138
Fig. 5.1 Polarization of the incident E-field: (a) Horizontal polarization (TE-mode);	
(b) Vertical polarization (TM-mode)	140
Fig. 5.2 Reflection coefficient for different values of incident angle (TE mode) (D=4.7 mm	
L=4.2 mm S=0.15)	142
Fig. 5.3 Absorption for different values of incident angle (TE-mode) (D=4.7 mm L=4.2 mm	
S=0.15)	142

Fig. 5.4 Reflection coefficient to TM mode for different values of incident angle (D=4.7 mm L=4.2 mm S=0.15)	143
Fig. 5.5 Absorption to TM mode for different values of incident angle (D=4.7 mm L=4.2 mm S=0.15)	144
Fig. 5.6 Comparison of reflection coefficient for TE mode and TM mode (D=4.7 mm L=4.2mm S=0.15)	145
Fig. 5.7 Comparison of absorption for TE mode and TM mode (D=4.7 mm L=4.2 mm S=0.15)	145
Fig. 5.8 Comparison of reflection coefficient for TE mode and TM mode (D=4.2 mm L=3.8mm S=0.15)	146
Fig. 5.9 Comparison of absorption for TE mode and TM mode (D=4.2 mm L=3.8 mm S=0.15)	147
Fig. 5.10 Comparison of reflection coefficient for TE mode and TM mode (D=3.8 mm L=3.5mm S=0.15)	148
Fig. 5.11 Comparison of absorption for TE mode and TM mode (D=3.8 mm L=3.5 mm S=0.15)	148
Fig. 5.12 Comparison of reflection coefficient for TE mode and TM mode (D=3.2 mm L=3mm S=0.15)	149
Fig. 5.13 Comparison of absorption for TE mode and TM mode (D=3.2 mm L=3 mm S=0.15)	150
Fig. 5.14 Comparison of reflection coefficient for TE mode and TM mode (D=2.5 mm L=2.45mm S=0.15)	151
Fig. 5.15 Comparison of absorption for TE mode and TM mode (D=2.5 mm L=2.45 mm S=0.15)	151

INTRODUCTION

The high development of technology in the last years has created in man a dependence to a lot kind of electric and electronic devices, and these devices are generators of electromagnetic emissions (radiated electromagnetic pollution). This kind of emissions give rise to artificial electromagnetic environments, which are defined as the totality of electromagnetic phenomena existing in a specific place.

An electromagnetic device is considered compatible with its environment when its emissions do not interfere with other devices, and is not affected by external emissions. In recent decades, many protection schemes have been developed with the aim of reducing the effect of radiated electromagnetic pollution on equipment and electronic devices sensitive to electromagnetic interference.

EM shielding may be pursued by any of the following main strategies, or by a combination of them:

- Interposition of a “barrier” between the source and the area (volume) where the EM field has to be reduced.
- Introduction of a mean capable of diverging the EM field from the area of interest.
- Introduction of an additional source whose effect is the reduction of the EM field levels in the prescribed area with respect to a situation involving the original source or source system. [1]

This project is focus on the first strategy, the interposition of a barrier is particularly effective in reducing the EM field levels when the shield material is highly conducting or when it is characterized by constitutive parameters such that the level of attenuation of the field propagating through the shield is high.

Here will be used an electromagnetic absorber in the shield, the application of the absorber is to resonances damping. It is usefulness in the improvement of the enclosure's performance. The high conductivity of shield walls works to trap the EM energy penetrated through the shield discontinuities (which may be viewed as traveling back and forth within the shielded volume). Materials capable of effectively dissipating such energy in the shielded region can considerably help in the improvement of shielding performance. [1] The shape and material of EM absorbers vary according to EM constraints, environmental peculiarities, and manufacturer design. Generally, they are used to cover a metallic surface in such a way that:

1. the reflected field is as low as possible;
2. the reflected field phase is opposite, as much as possible, to that of the incident field;
3. the transmitted field is attenuated as much as possible while traveling through the absorber material and before being reflected by the conductive surface over which the EM absorber has been installed.

In this thesis, an absorber based on the concept of frequency selective surface (FSS) is adopted to block the undesired wave frequency.

The material that will be used to develop the shield is called metamaterial; metamaterials are composite structures consisting of inclusions periodically embedded in a host matrix. When the size of the inclusions and the spatial periods are small compared with the wavelength of the EM field generated by a source, such artificial materials can be homogenized. These artificial materials are characterized by effective constitutive parameters that depend on the geometrical and physical properties of the inclusions and of the host medium. Metamaterials

exhibit EM properties that conventional materials do not possess, such as the ability to behave as a frequency selective absorber.

This thesis work illustrates the main characteristics and the design criteria of metamaterial absorbers for radio frequency (RF) emission.

CHAPTER I

METAMATERIALS

1.1 Introduction

One of the remarkable aspects of the human civilizational development is the intention to create or construct something that is not available in natural surroundings. The aim of obtaining materials with specified properties has always been one of the tasks of scientific research. New materials have been synthesized thanks to the development of more and more innovative manipulation methods at the molecular and/or atomic level. Furthermore, spectacular properties of materials can be also obtained by manipulation of certain structures, various composites being thus created.

Electromagnetic properties of all materials existing in nature can be determined by two parameters, the magnetic permeability and the electrical permittivity, which allow us to characterize the response of any material when this interacts with an electromagnetic wave. These properties are mainly determined by the chemical composition of material, that is, by the properties of the assembled atoms and molecules. It is only a small step to replace the atoms of the original concept with structures on a larger scale, called Meta-atoms (composed by usual materials such as metals, dielectrics, etc.) and to pass from materials to metamaterials. [1][2]

As long as the meta-atom sizes and distances between them remain sufficiently small on the wavelength scale of interest, the composites formed by meta-atoms can be considered as

“materials,” which can be described in terms of characteristic parameters (such as permittivity or permeability). Therefore, the same approaches adopted to describe electromagnetic properties of matter in terms of material relations can be applied to metamaterials made of meta-atoms.

Metamaterial can be defined as artificial and effectively homogeneous material formed by “an arrangement of artificial structural elements, designed to achieve advantageous and unusual electromagnetic properties” (this definition is adopted by the Virtual Institute for Artificial Electromagnetic Materials and Metamaterials; see www.metamorphose-vi.org). [3]

In most cases, metamaterials consists of a periodical lattice of identical elements (or sets of elements), being analogy to crystals. We shall consider periodic structures defined by a unit cell of characteristic dimensions “a”, defined by $a \ll \lambda$, where λ is the wavelength of incident electromagnetic waves. In this case, effective permittivity and permeability are a valid concept. [1]

Metamaterials have various applications, starting from perfect lenses and invisible cloaks to antennas and different types of sensors. [1]

1.2 History of metamaterials

The metamaterial concept was introduced by Russian theorist Veselago in 1968, who demonstrated that materials with negative and positive permeability are theoretically possible. In 1999, John B. Pendry described a practical technique to make materials, which are not based on the right hand rule of traditional type. Metamaterials are also known as left handed materials (LHM). The LHM materials have an atypical relationship between the wave propagation vector and the pointing vector, which represents the wave propagation energy

flow. In these metamaterials, in fact, the wave vector and energy density flow are in the opposite direction. However, the new enhancement in metamaterials was initiated by Lucent Technology, in 2002 for resonant antenna production.

The historical development of metamaterial is illustrated in Fig. 1.1. [4]

However, with the continuous development of technologies and nanofabrication, metamaterial structures are becoming an increasingly important topic in scientific research. Furthermore, the number of research papers published in the field of metamaterials is increasing very rapidly.

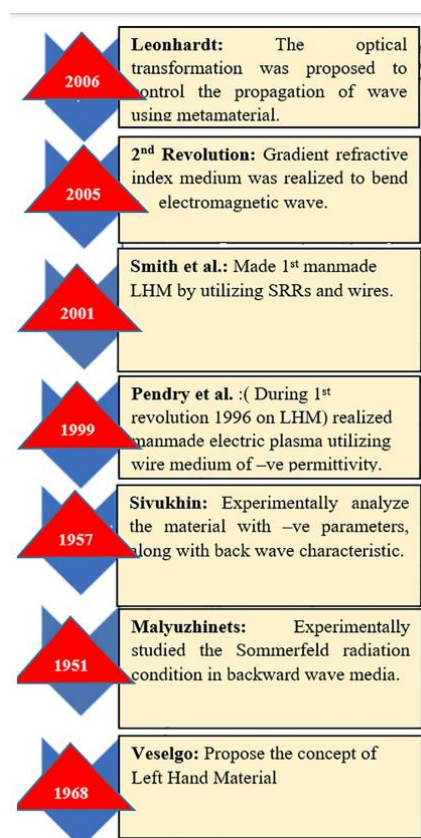


Fig. 1.1 Historical development of metamaterials.

1.3 Electromagnetic properties of metamaterials

Maxwell's equations describe the relation between the physical fields, derived fields and applied charged particles ρ_{ext} and applied stationary current \mathbf{J}_{ext} . We define the fields as the electric field \mathbf{E} , the electric flux density \mathbf{D} , the magnetic-flux density \mathbf{B} and the magnetic field \mathbf{H} .

The Maxwell's equations are:

$$\nabla \cdot \mathbf{D} = \rho_{\text{ext}} \quad (\text{Gauss' Law})$$

$$\nabla \cdot \mathbf{B} = 0 \quad (\text{Gauss' Law for magnetism})$$

$$\nabla \times \mathbf{E} = -\partial\mathbf{B}/\partial t \quad (\text{Faraday's Law})$$

$$\nabla \times \mathbf{H} = \mathbf{J}_{\text{ext}} + \partial\mathbf{D}/\partial t \quad (\text{Ampere-Maxwell Law})$$

Here ρ_{ext} and \mathbf{J}_{ext} are associated with the external charge and the current density. Furthermore, vectors \mathbf{D} , \mathbf{E} , \mathbf{B} and \mathbf{H} are related to each other through the following constitutive equations:

$$\mathbf{D} = \epsilon_0\mathbf{E} + \mathbf{P}$$

$$\mathbf{B} = \mu_0(\mathbf{H} + \mathbf{M})$$

\mathbf{P} and \mathbf{M} are the polarisation and magnetisation of a medium, which are the consequence of each individual electric or magnetic dipole in the material, respectively. [5]

The polarization \mathbf{P} is an averaged quantity, which is the sum of all the microscopic dipoles per unit volume inside a material. And for a linear isotropic media the induced polarization \mathbf{P} is parallel to the electric field \mathbf{E} such that:

$$\mathbf{P} = \epsilon_0\chi_e\mathbf{E}, \quad \chi_e = \text{electric susceptibility of the medium.}$$

If we would insert the previous relation of \mathbf{P} in the constitutive equation of \mathbf{D} we'll yield

$$\mathbf{D} = \varepsilon_0 \mathbf{E} + \varepsilon_0 \chi_e \mathbf{E}$$

$$\mathbf{D} = \varepsilon_0 (1 + \chi_e) \mathbf{E}$$

$$\mathbf{D} = \varepsilon_0 \varepsilon_r \mathbf{E} = \varepsilon \mathbf{E}$$

To define \mathbf{B} , we can do a similar analysis and we will find,

$$\mathbf{B} = \mu_0 (1 + \chi_m) \mathbf{H}, \quad \chi_m = \text{magnetic susceptibility of the medium.}$$

$$\mathbf{B} = \mu_0 \mu_r \mathbf{H} = \mu \mathbf{H}$$

ε and μ are the electric permittivity and the magnetic permeability of the medium, these physical quantities describe the interactions between the fields and the materials.

ε_0 and ε_r are the electric permittivity of free space and material relative permittivity, respectively.

μ_0 and μ_r are the magnetic permeability of free space and material relative permeability, respectively.

1.3.1 Plane wave propagation into metamaterials.

Double-negative materials are, by definition, isotropic materials obeying the constitutive relations

$$\mathbf{D} = \varepsilon \mathbf{E}$$

$$\mathbf{B} = \mu\mathbf{H}$$

where the material parameters ε and μ are real and negative. Since all materials are lossy, it is more accurate to say that both $\text{Re}\{\varepsilon\} < 0$ and $\text{Re}\{\mu\} < 0$. These materials have many alternative names in addition to double-negative (DNG) media: materials with negative parameters, backward-wave media, materials with negative refraction index (NRI), left-handed materials, and Veselago media. [3]

The first experimental realization of double-negative materials (at microwaves, for a single polarization and in-plane propagation directions) was built using split rings and metal wires. [6]

As it can be seen from Maxwell's equations for plane waves in the form $e^{-j\mathbf{k}\cdot\mathbf{r}}$

$$\mathbf{k} \times \mathbf{E} = \omega\mu\mathbf{H}$$

$$\mathbf{k} \times \mathbf{H} = -\omega\varepsilon\mathbf{E}$$

plane waves in double-negative materials are backward waves; that is, the direction of the Poynting vector \mathbf{S} is opposite to the wave vector \mathbf{k} :

$$\mathbf{S} = (1/2) \text{Re}(\mathbf{E} \times \mathbf{H}^*) = (|\mathbf{E}|^2/2\omega\mu) \mathbf{k} = (|\mathbf{H}|^2/2\omega\varepsilon) \mathbf{k}$$

This concept is illustrated in Fig. 1.2. When μ and ε are positive (usual isotropic medium) the direction of the Poynting vector is equal to \mathbf{k} direction (Fig. 1.2 (a)), whilst in the case of Veselago medium (μ and ε negative) the direction of the Poynting vector is opposite to \mathbf{k} direction (Fig. 1.2 (b)).

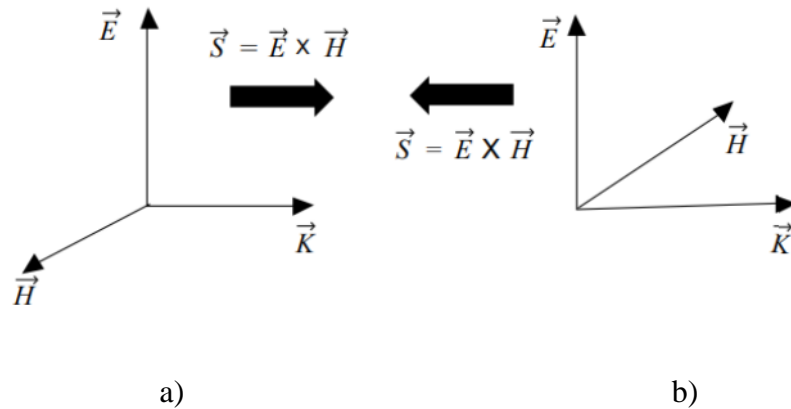


Fig. 1.2 Forward and backward waves: (a) Plane wave in a usual isotropic medium; (b) Plane wave in a Veselago medium.

1.3.2 Classification of metamaterials.

The parameters ϵ and μ describe the propagation of the electromagnetic wave in a medium. The aforementioned constitutive parameters are in principle complex, and their signs are based on the signs of their real parts, while their imaginary parts indicate the presence of electric or magnetic losses, respectively. It is appropriate to consider the classification of materials represented on Fig. 1.3. Materials are divided into four categories based on their permittivity and permeability characteristics.

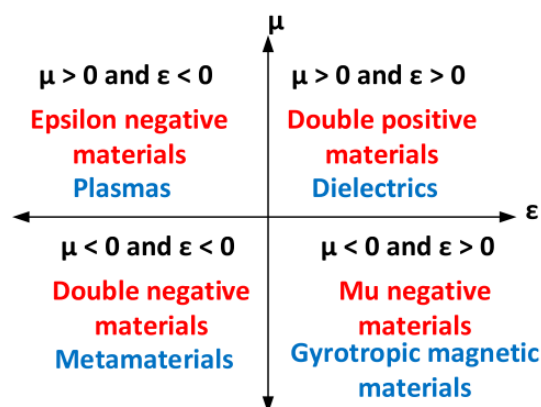


Fig. 1.3 Classification of materials. [7]

Almost all isotropic materials existing in nature have positive values of permittivity and permeability greater than unity. They are therefore determined as DPS (double positive) materials. This category mainly contains dielectrics.

Materials with only ϵ or μ negative are defined as SNG (single negative) materials and are divided into two classes according to the actual negative parameter: ENG (epsilon-negative) and MNG (mu-negative). It should be noted that if one of the two characteristic constants takes on a negative value, the refractive index of the incident beam becomes imaginary and only damped (evanescent) electromagnetic waves can propagate in such material.

The most known natural ENG-material is the plasma, whose dielectric constant is negative in a certain frequency range. Typical ϵ -negative materials are metals since their dielectric constant is described as a function of frequency in the Drude model and below the plasma frequency the metal permittivity is negative. For instance, the noble metals behave like ϵ -negative materials in infrared and optical frequency ranges therefore the propagation of light is impossible in such media.

In MNG-materials, accordingly, permittivity is greater than zero and permeability is less. Some gyro-tropic materials exhibit such characteristic in certain frequency range.

Materials with simultaneously negative values of ϵ and μ do not exist in nature, so they can be artificially produced. Over the last two decades, the research and experiments with these materials and finding ways of application have become a widespread. Such artificial media are named left-handed materials or double negative metamaterials (DNG), or backward wave media. As indicated above, negative material constants lead to negative value of the refractive index of an electromagnetic wave passing through the media. [8]

From the above classification, metamaterials can be defined as a special class of materials that are artificially designed to display negative permittivity and negative permeability. However, with the continuous design and development of more structures with unique properties and applications, a broader definition is used to classify them as metamaterials. [7]

1.4 Properties of metamaterials

In the third quadrant, refractive index in the Snell's law is negative. N. Engheta described that if an incident wave faces negative refraction at the interface, the ray bends in inside direction after refracting in the medium, which is the opposite of what happens in a medium with a positive index (Fig. 1.4) [9]. Therefore, light is refracted in a contrary way as compared to the normal "right handed materials".

In this case $n_1 \sin \theta_1 = n_2 \sin \theta_2$ still describes refraction, where n is the refractive index, but as n_2 is negative, incident and refracted rays are on the same side of the surface normal at an interface of positive and negative index materials (Fig. 1.4(a)).[9]

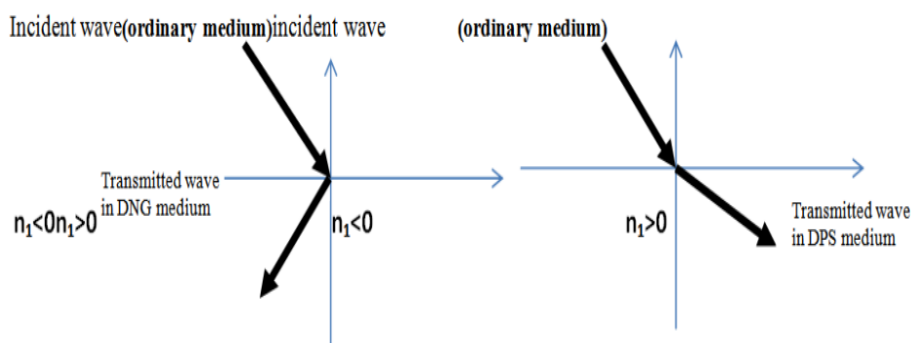


Fig. 1.4 Comparison of Snell's law in different medium.

Other properties of metamaterials due to the negative refractive index are:

- Doppler effect in this material is reversed, if a source moves towards a detector, it is observed that the detected radiation has a lower frequency than that generated when the source is motionless.
- Cherenkov effect, the emission of light due to a charged particle moving in a medium at a speed greater than that which would have light in the medium itself, the light is emitted in a cone pointing backwards in the direction of the motion of the particle.
- The Poynting vector describes the energy flow associated with the propagation of the electromagnetic field, in a medium with negative refraction is opposite to the motion of the wave fronts

1.5 Applications of metamaterials

In 2016, it is estimated that the worldwide metamaterial market size was USD 316 million but in recent days, there is a growing demand for better quality materials with durability properties that are driving the growth of the metamaterials market worldwide. The average size of the metamaterials market, according to the study in the report, is estimated to reach \$ 1.5 billion by 2025. Owing to their superior properties, they are used in distinct sectors (e.g. aerospace, automotive, defence, electronics, public safety, metamaterial antennas, high frequency battlefield communication etc.) [4]

1.5.1 Medical sector (metamaterial as antennas).

This is a category of antennas, which utilize metamaterials to increase the radiated power as well as to improve the efficiency-bandwidth performances of the overall antenna system. In addition, metamaterials can minimize the mutual coupling in array antennas, reducing their dimension. Furthermore, for making high directivity antennas the material of

zero refractive index are used. [10][11]. Nowadays, antenna technology finds greater interest in the healthcare sector, through wireless body area networks, which provide a fundamental contribution in improving the quality of life.

1.5.2 Automotive sector.

Recently, there is an increased demand for new materials in the automotive sector (i.e. high-performance magnetic & absorbing as well as shielding materials) in order to ensure electromagnetic compatibility in motors that use electricity. In addition, many materials (photonic metamaterials) can enhance the capabilities of automotive optical devices. Toyota Central research and development Lab, reported that metamaterials provide highly contribution in the use of automobile such as mobile communication antennas, radar scanning, new magnetic materials for the application of electric motors etc. [12]

1.5.3 Aerospace sector.

The commercial sales of metamaterials-based parts and subsystems for aerospace as well as defence utilizations will reach approximate \$250 million by 2020 & then burgeon \$2.3 billion in 2025. Some applications of metamaterials are invisibility, size reduction of antenna and support structures. Metamaterial-based devices in aerospace sector allow improving the performance of the aircraft. Furthermore, the use of metamaterials have generally the aim to provide highly noise reductions in the internal ducts of the engine itself. [13] [14] [15]

1.5.4 Biosensors application.

Biosensors are currently used for several applications such as environmental monitoring, disease diagnostics as well as the study of biological phenomena. Now a day, bio-sensing methods based on metamaterials are adopted from the microwave up to optical

frequency ranges, owing to their low cost & label-free biomolecule detection. According to the frequency of sensing biomolecules, metamaterial sensors are generally categorized into three groups: plasmonic biosensors, microwave biosensors and terahertz biosensors.

In addition, metamaterials have several other applications (invisible slab, light & sound filtering, spectroscopy, metamaterial absorber, MEMS, remote sensing, revolutionary electronic, WMD detectors, plasmonic devices, NDT test, smart material application, spectroscopy etc. [16][17])

1.6 Metamaterial absorbers

Recently, vigorous researches have been performed in the area of metamaterials (MMs). An outstanding application of metamaterials is MM absorbers (MMA). MMA is a block of material used to absorb some of the energy of an incident plane wave and is usually comprised of three layers. The metallic pattern is the first layer, which is arranged periodically. The second layer consists of a substrate or dielectric layer. Finally, the third layer is a continuous metallic layer. MMAs are also called perfect absorbers with near-unity absorption, showing zero reflection and transmission coefficients for incident plane waves. [18]

The first metamaterial based absorber was introduced by Landy [19], showing a simulated absorptivity of $A \approx 99\%$ at 11.48 GHz (Fig. 1.5 (a)). The MMA had advantage of small size and thin thickness compared with the conventional absorbers. The top layer consists of an electric ring resonator (ERR) which provides, along with the ground plane, the electric response by coupling strongly to incident electric field at a certain resonance frequency. The second metal, spaced apart from the top layer by a dielectric, consists of a cut wire in a parallel plane and contributes to the electric response (see Fig. 1.5 (b)). Magnetic coupling is

achieved via antiparallel currents in the cut wire and the centre wire of the ERR. An incident magnetic field may couple to these antiparallel currents, thus yielding a Lorentz like magnetic response. The combined design allows for individual tuning of the electric and magnetic responses. For example, adjustment of the geometry of the ERR permits tuning the frequency position and strength of a Lorentz resonance, while altering the spacing of the two metallic structures, and their geometry, allows the magnetic response to be modified.

Experimentally, Landy was able to achieve an absorptivity of 88% (Figure 1.5 (c), (d)). The author postulated that discrepancies between simulated and measured results were due to fabrication errors. Although the first experimental work on MMAs was in the microwave frequency range, a work quickly followed in the THz regime. [20]

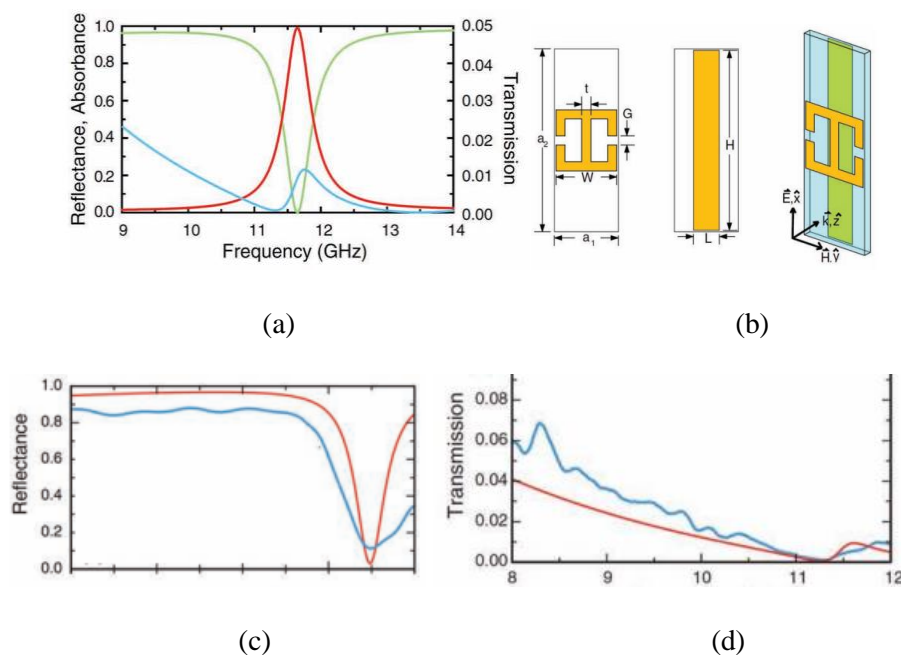


Fig. 1.5 First experimental demonstration of a metamaterial perfect absorber: (a) simulated results displaying transmissivity (blue, right axes), reflectivity (green, left axes), absorptivity (red, left axes); (b) Unit cell: top metamaterial layer (dimensions in mm: $a_1= 4.2\text{mm}$, $a_2= 12\text{mm}$, $W= 4\text{mm}$, $G= 0.6\text{mm}$, $t= 0.6\text{mm}$), cut wire dimensions ($L= 1.7\text{mm}$, $H= 11.8\text{mm}$) and a perspective view; (c) , (d) Experimental (blue) and simulated (red) results for reflectivity and transmissivity.

MMA are usually designed for RF frequency applications, extending from microwaves to optical frequency, for applications such as sensors, photodetectors, solar cells, and emitters.

MMA are classified into three different frequencies and applications (Fig. 1.6). [7]

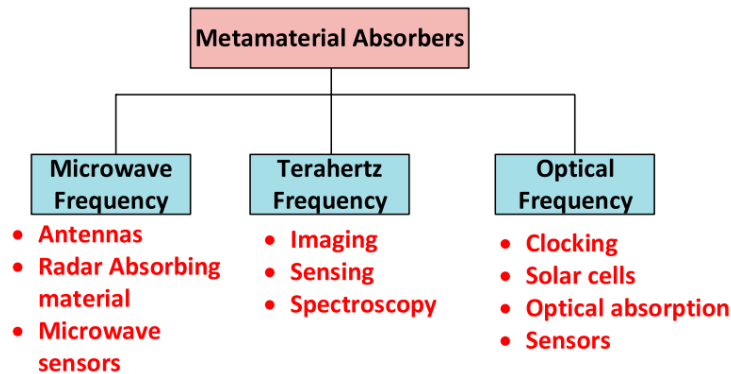


Fig. 1.6 Applications of metamaterial absorbers with respect to different frequencies.

1.6.1 Impedance Matching Concept.

A metamaterial absorber is typically a sandwiched structure, consisting of an array of certain metallic patterns on one side of a substrate and backed with a highly conductive metallic ground plane. Due to the presence of the ground plane, no transmittance could be found on the other side of the metamaterial. This allows us to focus only on the reflection from the metamaterial.

Consider an EM wave impinging normally on a planar boundary of medium, in the most general case, with complex permittivity and permeability. The medium is surrounded by the free space or at least air. The (complex) reflection coefficient is equal to:

$$\mathbf{r} = \frac{Z - Z_0}{Z + Z_0}$$

Where $\mathbf{Z} \equiv \sqrt{\frac{\epsilon}{\mu}}$ is the impedance of the medium and $Z_0 \equiv \sqrt{\frac{\epsilon_0}{\mu_0}} = 377\Omega$ is the impedance of the free space.

For perfect reflection, the absolute magnitude of impedance $|\mathbf{Z}|$ must be either zero or infinity. A metallic plate can easily achieve the impedance with zero magnitude, whilst frequency-selective surface (FSS) can be an example of medium with an impedance of actually infinite amplitude.

To be a perfect MMA the reflection should be zero. If $\mathbf{Z}=Z_0$ then $\mathbf{r}=0$. This condition is called impedance matching, at which the travelling wave cannot ‘see’ the reflecting boundary. To make absorption better than 99 %, $|\mathbf{r}|$ should be less than 0.1. One of the most important factors limiting the small enough reflection on a broad range of frequency is the dispersion of \mathbf{Z} . In general, \mathbf{Z} strongly depends on the frequency of the incident EM wave. If the impedance is very weakly dependent upon the frequency in a wide range of frequencies and is close to that of free space, the reflection is very small in a wide range of frequencies. [17]

According to the Fresnel formula of the reflection coefficient, the reflectivity (R) from the metamaterial is

$$R_{TE} = |r_{TE}|^2 = \left| \frac{\mu_r \cos\theta - \sqrt{n^2 - \sin^2\theta}}{\mu_r \cos\theta + \sqrt{n^2 - \sin^2\theta}} \right|^2$$

$$R_{TM} = |r_{TM}|^2 = \left| \frac{\epsilon_r \cos\theta - \sqrt{n^2 - \sin^2\theta}}{\epsilon_r \cos\theta + \sqrt{n^2 - \sin^2\theta}} \right|^2$$

where the subscripts TE and TM refer to transverse electric (TE) and transverse magnetic (TM) polarized waves, θ is the angle of incidence, and $n=(\epsilon_r \mu_r)^{-1/2}$ is the effective refractive index of the metamaterial.

For the case of normal incident, we have $\theta = 0^\circ$, so that the above equations reduce to:

$$R = \left| \frac{Z - Z_0}{Z + Z_0} \right|^2 = \left| \frac{\sqrt{\mu_r} - \sqrt{\epsilon_r}}{\sqrt{\mu_r} + \sqrt{\epsilon_r}} \right|^2$$

Since the metallic ground leads to zero transmissivity, the absorptivity is equal to:

$$A = 1 - R = 1 - \left| \frac{Z - Z_0}{Z + Z_0} \right|^2 = 1 - \left| \frac{\sqrt{\mu_r} - \sqrt{\epsilon_r}}{\sqrt{\mu_r} + \sqrt{\epsilon_r}} \right|^2$$

To achieve impedance matching in a metamaterial absorber, simultaneous electric and magnetic resonances are required. Even if a perfect impedance matching is achieved, the energy of the transmitted radiation should be dissipated efficiently in the interior of medium. Otherwise, the absorbed energy will be re-emitted in the form of radiation. [20]

1.6.2 Interference theory.

The front layer with certain metallic patterns functions as a partial reflective surface, which can be utilized to modify the complex reflection and transmission coefficients. On the other hand, the highly conductive ground plane works as a perfect reflector, offering a phase delay of 180° to the electromagnetic wave reflecting on it.

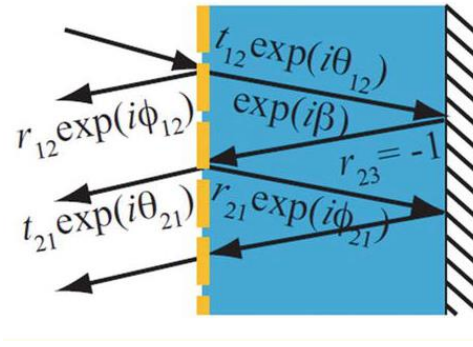


Fig. 1.7 Multiple reflections and interference model of metamaterial absorber. The yellow dashed line refers the resonator array.

As shown in Fig.1.7, the front meta-layer resides at the interface between air and the dielectric substrate. The incident electromagnetic wave is partially reflected back to air with a reflection coefficient $\mathbf{r}_{12}(\omega) = r_{12}(\omega)e^{i\phi_{12}(\omega)}$ and partially transmitted into the substrate with a transmission coefficient $\mathbf{t}_{12}(\omega) = t_{12}(\omega)e^{i\theta_{12}(\omega)}$. The transmitted wave will propagate further until reaching the metallic ground plane. The complex propagation constant inside the dielectric substrate is $\boldsymbol{\beta} = \beta_1 + i\beta_2 = (\epsilon d)^{1/2} k_0 d$, where k_0 is the wavenumber of free space, d is the thickness of the substrate, β_1 represents the propagation phase, and β_2 refers to the absorption in the dielectric substrate. At the ground plane, a total reflection occurs with a reflection coefficient of -1 . [20]

After direct mirror reflection and an additional propagation phase delay $\boldsymbol{\beta}$, partial reflection and transmission occur again at the front interface. The corresponding reflection and transmission coefficients are $\mathbf{r}_{21}(\omega) = r_{21}(\omega)e^{i\phi_{21}(\omega)}$ and $\mathbf{t}_{21}(\omega) = t_{21}(\omega)e^{i\theta_{21}(\omega)}$, respectively. It is worth noting that multiple reflections and transmissions exist inside the dielectric substrate, and the totally output energy at the left side of the metamaterial is the superposition of reflections of all orders:

$$\mathbf{r}(\omega) = \mathbf{r}_{12}(\omega) - \frac{\mathbf{t}_{12}(\omega)\mathbf{t}_{21}(\omega)e^{2i\boldsymbol{\beta}}}{1 + \mathbf{r}_{21}(\omega)e^{2i\boldsymbol{\beta}}}$$

where the first term in the right is the reflection directly from the meta-layer, and the second term is the contribution of the superposition of the multiple higher-order reflections. As long as we know the total reflection \mathbf{r} , the absorption spectrum of the metamaterial absorber could be obtained by

$$A(\omega) = 1 - |\mathbf{r}(\omega)|^2$$

So to maximize the absorption and make it equal to 1, you need to cancel $\mathbf{r}(\omega)$, in correspondence of the desired frequency ω , properly checking the thickness of the substrate and the characteristics of the matrix of the resonant metal elements, or the coefficients $\mathbf{r}_{12}(\omega)$, $\mathbf{t}_{12}(\omega)$, $\mathbf{r}_{21}(\omega)$, $\mathbf{t}_{21}(\omega)$ which depend on the metallic layers.

1.7 Classification of Electromagnetic-Wave Absorbers

Ruck et al. [21] classified perfect EM-wave absorbers into two groups; broadband absorbers and resonant absorbers. So far, the resonant absorbers can have perfect absorption in a narrow bandwidth, while only non-resonant techniques were known to be employed for broadband absorption. It is, of course, possible to make resonant absorbers operating in a broad range of frequencies by stacking several layers; however, these kind of broadband absorbers are very thick and bulky. However, some resonant absorbers can have broadband behaviour without the aforementioned disadvantages. [18]

1.7.1 Broadband Perfect Absorbers.

The broadband absorbers are further divided into two categories; geometric transition absorbers and low-density absorbers.

- **Geometric-Transition Absorbers**

Geometric-transition absorber consists of two-dimensional periodic arrays of lossy-foam pyramids, cones or wedges, and is widely used in anechoic rooms to minimize the reflections from walls. The internal appearance of EM-wave anechoic room is often very similar to that of acoustic anechoic room. Because the basic principle of absorption of acoustic wave is nearly identical to that of EM wave, the similarity of internal appearance is not surprising. The difference is the materials used in anechoic rooms. For acoustic anechoic room acoustic-wave absorbing materials are used, while radiation-absorbing ones are used for EM-wave anechoic room. A commercial absorber is showed in Fig. 1.8.



Fig. 1.8 Commercial EM-wave absorber material.

The basic principle of the operation of geometric-transition absorber is to gradually change the optical property from absorber to free space by introducing a geometrically adjusted absorbing material between them. The term ‘geometric-transition’ is originated from this principle. In order to reduce the transmission of EM wave reflected from the rear metal plate, broadband absorbers should have sufficient attenuation. It implies that the thickness is comparable to the wavelength of incident EM waves.

As aforementioned, the geometrical shape can be pyramids, cones or wedges. Basically, the absorption of EM wave depends on the size of absorbing material, as well as its material

properties. Therefore, geometric-transition absorber is inherently broadband one because of varying characteristic length of geometrically-shaped structures. The gradual change of the optical property suppresses reflection and results in a gradual absorption of EM wave. Furthermore, geometric-transition absorber is operating for arbitrary polarization of incident EM wave and over a wide range of angles of incidence, which is enough for the practical purposes.

- **Low-density absorbers**

Low-density absorbers for acoustic noise reduction utilize very porous or sparse material. On the ceiling of classrooms, business offices, and other rooms requiring noise reduction this type of absorbers is easily found. They are usually made of porous open cell foams, typically open-cell rubber foams or melamine sponges, which are highly effective for absorbing noises from medium- to high-frequency ranges, but not for low-frequency one. The basic principle of low-density acoustic absorber is dissipation of the energy of noise by thermal conduction and viscous friction inside the cell structure. Low-density absorbers of EM waves with porous materials operate in a very similar way of porous acoustic absorber. Once EM wave enter a pore, it hits the surface of absorbing material several times before it eventually leaves the pore. The multiple reflections at the interior surfaces of the pore enhance the absorption because a part of EM wave is absorbed whenever it hit the surface of absorbing material. The multiple reflections also effectively increase the path length, leading to a reduced size of absorbers. In Fig. 1.9 are illustrated the three main types of porous absorbing materials.

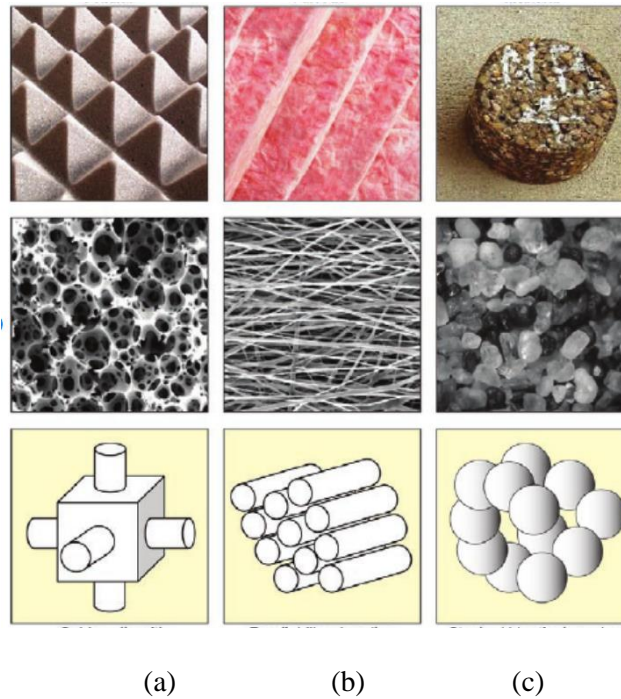


Fig. 1.9 Types of porous absorbing materials: (a) Cellular (Cubic cells with connecting pores);
 (b) Fibrous (Parallel fiber bundles); (c) Granular (Stacked identical spheres)

1.7.2 Resonant Absorbers.

Resonant EM-wave absorbers utilize the quarter-wavelength thickness of the substrate before the grounded metallic plate. The first resonant EM-wave absorber was invented by American engineer Salisbury, and it was called Salisbury screens named after the inventor. The basic principle of the operation of Salisbury screens is exactly the same as that of the AR coatings, each coating layer in the AR stack combines with previous layers to cancel out a broad range of light waves by introducing opposite, or destructive, waves that are out of phase. Thus, reflective properties of that range of light are neutralized. A Salisbury screen consists of three layers; a thin resistive screen, a low-loss dielectric substrate with an exact thickness corresponding to a quarter of the wavelength of incident EM wave, and a continuous metallic surface. If the incident EM wave pass through the first layer, a thin resistive screen, is

reflected by the continuous metallic surface, and eventually reach the resistive screen again, then the distance traveled is exactly a half wavelength, which corresponds to 180° phase change. Therefore, there is an exactly 180° phase difference between the EM wave just incident upon the first layer and the EM waves reflected from the continuous metallic surface, resulting in a destructive interference and, consequently, no reflection.

The Salisbury screen; however, has two major drawbacks; the thickness and the absorption band. To satisfy the complete destructive interference, the dielectric layer has a thickness of quarter wavelength divided by its refractive index. If the wavelength of the incident EM wave is very long then the dielectric layer should be very thick. Because for the Salisbury screen the absorption occurs only at a specific wavelength satisfying the condition for complete destructive interference, the absorption bandwidth is very narrow.

One of the two major drawbacks of Salisbury screen can be relaxed. The narrow bandwidth can be extended by putting one more layers of resistive screen and quarter-wavelength gap in front of Salisbury screen. This modified Salisbury screen is called Jaumann absorber because it was first realized by J. Jaumann during World War II in Germany. Severin was the first one who calculated the reflection spectrum of Jaumann absorber. By putting one more layer of resistive screen and quarter-wavelength gap in front of Salisbury screen with the aid of TLT he was able to calculate the reflection spectrum, which has dual minima with zero reflectivity, of Jaumann absorber.

Another kind of Salisbury screen is Dällenbach-layer absorber (DLA) in which only a homogeneous single layer was placed in front of grounded metallic plane. The thickness, the permittivity and the permeability are adjusted in such a way that the reflection is minimized.

The structure of the basic resonant absorbers is shown in Fig. 1.10.

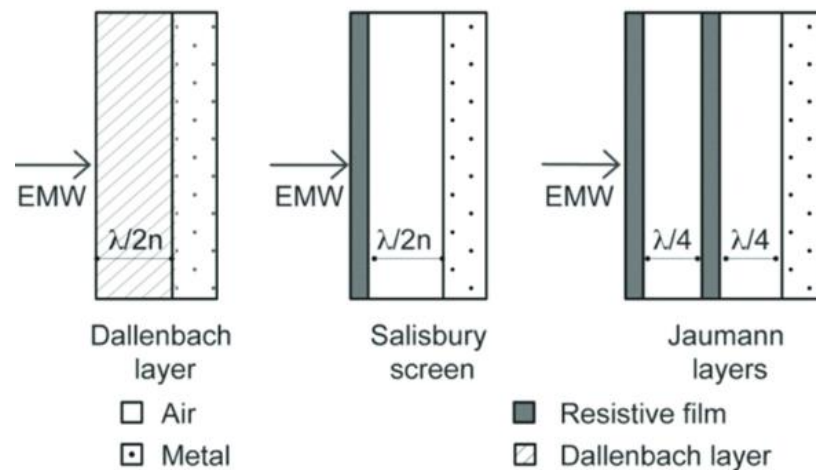


Fig. 1.10 Common designs for resonant absorbers

In a sense, both Salisbury screens and its extension, Jaumann absorbers, are actually a kind of the so-called circuit-analog absorbers (CAs). In Salisbury screens and Jaumann absorbers only one or more resistive sheets are used, and thus their impedances do not contain any imaginary components. The basic structure of CAs is identical to that of Salisbury screens or Jaumann absorbers; tri-layer structure with quarter-wavelength thickness for the middle layer. By putting a layer of periodically-arranged conducting patches instead of continuous resistive sheet the front layer becomes reactive, as well as resistive.

The resistance of patch itself can be modelled as a resistor. The thickness of the patch is important to adjust the resistance. In addition, the linear part of patch plays a role of inductor and the gap between any two adjacent patches plays a role of capacitor. Therefore, the transmission line of CAs can be considered as a one- or two-dimensional infinite array of identical RLC circuits, which are connected in series. The resonance frequency is selected by the resonance of RLC circuits, not by the distance between first and third layers. It is the reason why this type of absorbers is called ‘circuit-analog’ absorbers. Because the resonance

frequency is determined by the frontal surface, we call the frontal surface made of a periodically-patterned metallic patches a ‘frequency-selective’ surface.

In actual applications, absorbers should possess a broadband response and should be independent of the polarization of incident wave and of the angle of incidence. CAs partially solve the problem of narrow bandwidth of Salisbury screen. CAs can also be polarization independent by making pattern of patches in a symmetric shape, such as square, hexagonal, octagonal or circular shapes.

1.8 Differences and Advantages of Metamaterial-Based Perfect Absorbers

MMA is a particular kind of resonant absorbers, more specifically CAs. Most of MMAs consist of three layers; a layer of periodically-arranged metallic patterns, a dielectric layer and a continuous metallic layer. It is nearly the same as the case of CA. MMAs use a layer of periodically-arranged metallic patterns, which is similar to the FSS of CAs; however, the thickness of the dielectric layer could be much smaller than the wavelength, especially, in the GHz regime. To accomplish the total absorption there should be no reflection and no transmission. No transmission can be accomplished by the third layer, a continuous metallic plate, which completely blocks all incident EM waves. [18]

The basic role of dielectric layer is to provide a space to the incident EM wave to stay and be absorbed. It is desirable to use high- ϵ_1 material because it reduces the thickness of dielectric layer with the optical path still maintained. For the incident EM wave, the path should be given by $\mathbf{n} \cdot \mathbf{d}$, where \mathbf{n} is the refractive index and \mathbf{d} is the distance travelled. Although it is generally true, it is not necessary for MMPA to be very thick, satisfying, for instance, the quarter wavelength condition. Unlike MMPAs, the quarter-wavelength condition is crucial for

the operation of AR coating and Salisbury screen. Dielectric materials usually have very small imaginary part of permittivity, and this small imaginary part is sometimes enough to absorb all EM waves incident during travelling inside the dielectric.

The main advantages of such absorbers are compactness and easy manufacturing with polarization independence at the broad frequency band. High absorption coefficient for wide angles of incidence and possibility of dynamical tuning have been obtained. Now, the main aim of studies is to design perfect metamaterial absorbers, which provide absorption coefficient equal unity in a wide range of frequencies. In addition, these devices can absorb electromagnetic energy at certain points and transfer it into heat. Such a property can be applied in high selective thermal emitters. Absorbers with the possibility of tuning the operating frequency can be used as spectrally sensitive detectors or sensors, particularly in micro bolometers and pyroelectric detectors. [8]

CHAPTER II

UNINTENTIONAL RADIATED EMISSION

2.1 Definition

Unintended radiated emissions (UREs) could be defined as electromagnetic radiation that is unintentionally emitted by all electronic devices during their operation. UREs result from a mismatch between ideal and real designs such as the utilization of non-pure sinusoidal signals and non-ideal filters. [21] [22]

URE can cause electromagnetic interference (EMI). Unintentional transmission or reception of electromagnetic energy is not necessarily detrimental, the unintentional transfer of energy causes interference only if the received energy is of sufficient magnitude and/or spectral content at the receptor input to cause the receptor to behave in an undesired way.[21] [23]

Nowadays, commercial or residential facilities contain a large number of electrical devices, which generate URE, for that reason identifying and mitigating EMI is a key element of modern power engineering and associated control systems.

The aim of electromagnetic compatibility (EMC) is to design electronic systems that are electromagnetically compatible with their environment. EMC requirements exist so that electronic systems designers have a set of guidelines that explain the limits of what can be considered electromagnetically compatible. Those EMC guidelines are created by individual product manufacturers, and by the governments. [23]

2.2 Radiated and Conducted Emissions

Electromagnetic compatibility (EMC) is defined as the ability of a device, equipment, or system to work satisfactorily in its electromagnetic environment without producing electromagnetic disturbances to any object in that environment.

An electronic device/system must satisfy three fundamentals criteria:

1. It does not cause interference with other systems.
2. It is not susceptible to emissions from other systems.
3. It does not cause interference with itself. [24]

As mentioned in the previous section, the unwanted electromagnetic radiation that causes potential interference to other items of electronics equipment is called Electromagnetic Interference (EMI).[25]

It is clear that any device, equipment or system that requires electrical energy for its operation is immersed in an environment of radiated or conducted electromagnetic energy, the former has free space as the propagation medium and the latter requires a physical medium such as a conductive material, or a dielectric material. Fig. 2.1 gives a representation of the electromagnetic propagation. [26]

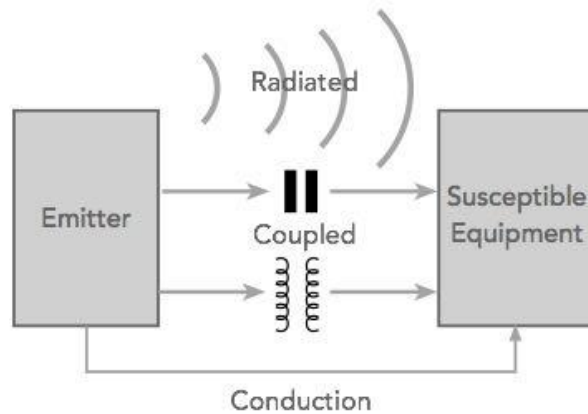


Fig. 2.1 Generation of unwanted electromagnetic energy.

Radiated Emission: This type of EM energy coupling is probably the most obvious. It is the type of EMI coupling that is normally experienced when the source and victim are separated by a large distance - typically more than a wavelength. The source radiates a signal, which may be wanted or unwanted, and the victim receives it in a way that disturbs its performance.

Conducted Emission: Conducted emissions occur when there is a conduction path along which the signals can travel. This may be along power cables or other interconnection cabling.

The conduction may be in one of two modes:

- **Common mode:** This type of EMI coupling occurs when the noise appears in the same phase on the two conductors, e.g. out and return for signals, or $+V_e$ and $-V_e$ for power cables.
- **Differential mode:** This occurs when the noise is out of phase on the two conductors.
- **Capacitive coupling:** This occurs when a changing voltage from the source capacitively transfers a charge to the victim circuitry.

- **Magnetic coupling:** This type of EMI coupling exists when a varying magnetic field exists between the source and victim - typically, two conductors may run close together (less than λ apart). This induces a current in the victim circuitry, thereby transferring the signal from source to victim.

Electromagnetic interferences are present in all areas of electronics. By understanding the source, the coupling methods and the susceptibility of the victim, the level of interference can be reduced to a level where the EMI causes no undue degradation in performance.

The three principal methods to reduce EMI are (Fig. 2.2):

1. Suppress the emission at its source.
2. Make the coupling path as inefficient as possible.
3. Make the receptor less susceptible to the emission.

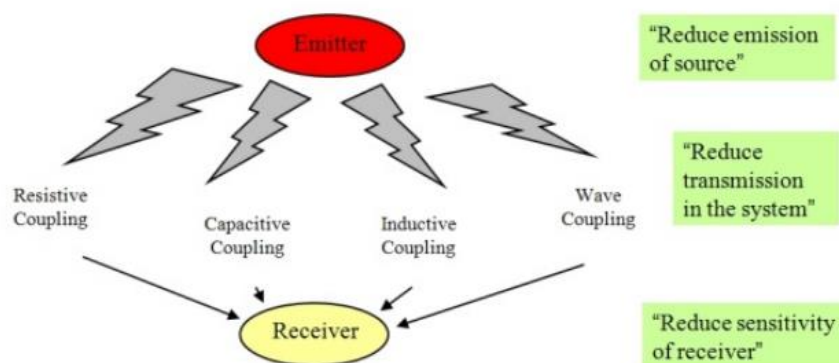


Fig. 2.2 Principal methods to reduce EMI.

2.3 EMC Standards for Radiated Emission

Several international organizations have created standards that are a series of rules and steps that indicate how to perform the tests, the equipment to use, the recommended environment and the EMI limits. These requirements serve to regulate, compare and verify satisfactory compliance with the standards, imposed to minimize the interferences between electronic devices. The standards allow Country to control the amount of “electromagnetic pollution” that the product generates. We will focus in the EMI due to radiated emissions. [27]

2.3.1 US Standards.

The first EMC standards and legislation were introduced in 1979. The Federal Communications Commission, FCC, in the USA imposed legal limits on the electromagnetic emissions from all digital equipments. These limits were imposed as a result of the growing use of digital systems (devices that use a clock of 9 kHz or greater and use “digital techniques”) including small calculators and digital equipments that were interfering with wired and radio communications and broadcast systems.[23] It sets limits on the radiated and conducted emissions of a digital device.

The FCC defines a digital device as any unintentional radiator (device or system) that generates and uses timing pulses at a rate in excess of 9000 pulses (cycles) per second and uses digital techniques.

The FCC further breaks the digital device class of products into Class A and Class B:

- Class A (higher emission limits, industrial): Class A devices are devices that are suitable for use in all areas other than residential. Devices must have emissions, which are below the limits of Class A, but the emissions may exceed the limits of Class B.
- Class B (lower emission limits, residential): Class B devices are devices that are suitable for use in residential areas and. The Class B limits are more stringent than the Class A limits under the reasonable assumption that interference from the device in an industrial environment can be more readily corrected than in a residential environment, where the interference source and the susceptible device are likely to be in closer proximity.[28][29]

The FCC requires measurement of the radiated electric field, and the regulatory limits are given in terms of that field in dBmV/m. The frequency range for radiated emissions begins at 30 MHz and extends to 40 GHz.

The radiated emissions for Class B devices are to be measured at a distance of 3 m from the product, whereas the radiated emissions for Class A products are to be measured at a distance of 10 m. Table 2.1 shows the EMI limits for Class A and Table 2.2 shows the EMI limits for Class B. [30]

Frequency of Emission (MHz)	Field Strength Limit (dB μ V/m)
30 - 88	39
88 - 216	43.5
216 - 960	46.5
above 960	49.5

Table 2.1. FCC Emission limits for Class A digital devices (10 meters)

Frequency of Emission (MHz)	Field Strength Limit (dB μ V/m)
30 - 88	40.0
88 - 216	43.5
216 - 960	46.0
above 960	54.0

Table 2.2. FCC Emission limits for Class B digital devices (3 meters)

2.3.2 EU Standards.

The European Union (EU) EMC Standards are initiated by the International Special Committee on Radio Interference (CISPR, Comité International Spécial des Perturbations Radioélectriques,), which is a committee of the International Electrotechnical Committee (IEC). [27]

One difference between the US regulations and the EU regulations is, that the US regulations (FCC, Title 47, Chapter I) do also specify the limits in the law. Whereas in the EU laws and directives this is not the case, and the testing limits are specified in the EMC Standards, issued by the IEC (International Electrotechnical Commission)/ CISPR organizations.

However, most international countries adopt the CISPR recommendations. The most widely used standard is CISPR 32 that sets limits on the conducted and radiated emissions of signals in the frequency range of 9kHz to 400GHz. CISPR 32 replaced CISPR 13 and the popular CISPR 22 in March 2017. The limits are divided into Class A and Class B equipment, and their meaning is essentially the same as the FCC definitions. [29]

Although there are a large number of EMC standards in the Directive, the primary one we will discuss is the European Norm EN 55032. This is essentially the CISPR 32 standard published by the IEC.

The CISPR 32 (EN 55032) radiated emission limits are tabulated in Table 2.3 for Class A devices and in Table 2.4 for Class B equipment. CISPR 22 regulations require that radiated emissions measurements for Class A devices be measured at a distance of 30 m and Class B devices be measured at a distance of 10 m. Like the FCC radiated emission limits, these are to be measured with a CISPR 32 receiver having a quasi-peak detector (QP). [23][31]

Frequency of Emission (MHz)	Field Strength Limit (dB μ V/m)
30-230	30.0
230-1000	37.0

Table 2.3. CISPR 32 Emission limits for Class A digital devices (30 meters)

Frequency of Emission (MHz)	Field Strength Limit (dB μ V/m)
30-230	30.0
230-1000	37.0

Table 2.4. FCC Emission limits for Class B digital devices (10 meters)

Using the inverse distance method, which assumes that emissions fall off linearly with increasing distance to the measurement antenna, we can scale the measurement limits to a common distance and plot the CISPR 22 and FCC regulations together to compare them. The Fig. 2.3 shows the radiated emissions limits for Class A and The Fig. 2.4 shows the radiated emissions limits for Class B. [32]

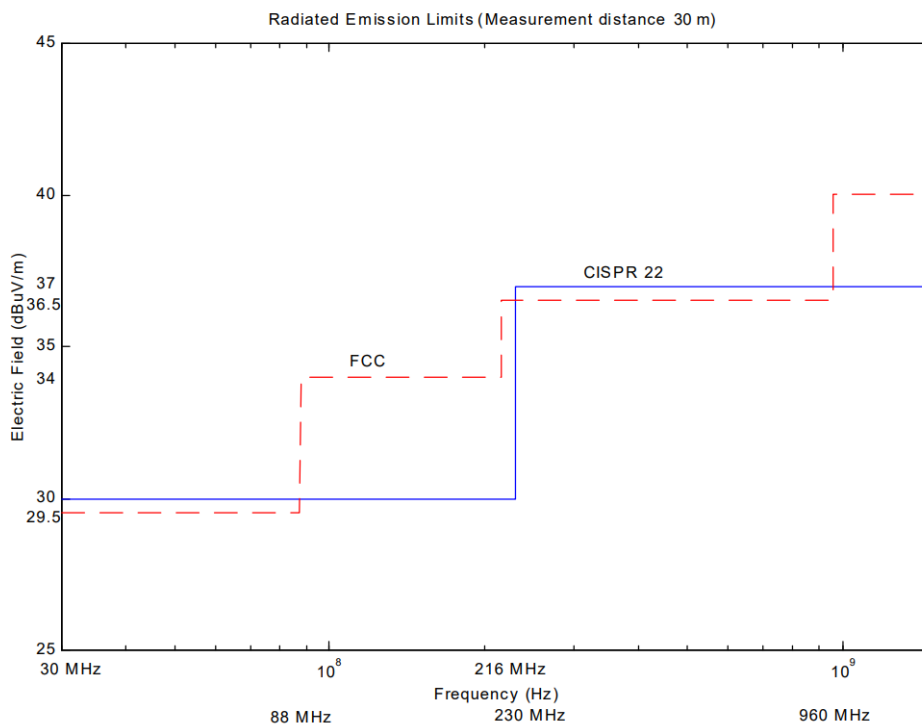


Fig. 2.3 Radiated Emissions Limits for Class A digital devices.

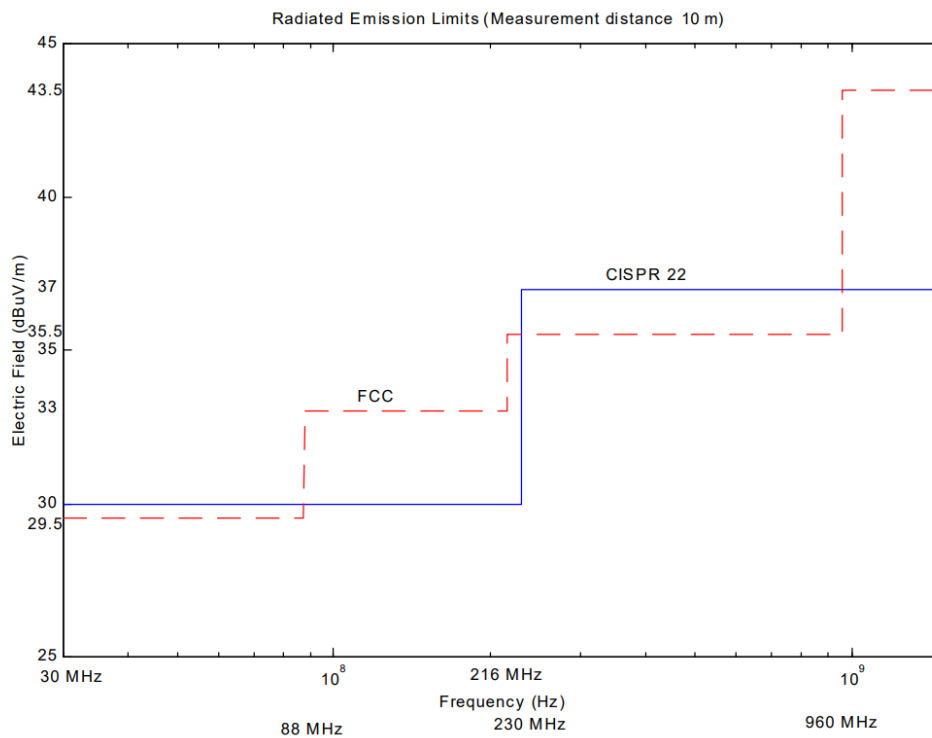


Fig. 2.4 Radiated Emissions Limits for Class B digital devices.

2.4 Measurements and test of Radiated Emission

In order to ensure that the tests for radiated emissions are accurate, the FCC and CISPR have testing standards that explain how compliance tests must be done. This ensures that the testing is accurate and repeatable. The measurement procedure for the FCC measurements is contained in the American National Standards Institute (ANSI) standard ANSI C63.4-2003. The measurement procedures for CISPR 32 (EN 55032) are self-contained in the same standard that defines the limits although CISPR 32 references CISPR 16. [23]

The radiated electric fields for the commercial tests (FCC and CISPR 32) must be measured on an open area test site (OATS). The OATS are spaces located outside the cities, are located in places far away from them due to the possible sources of EMI in the region, emissions at these sites should be minimal. Also OATS should have a conducting ground plane of sufficient size on which both the Device under test (DUT) and receiving antenna are placed. The Fig. 2.5 is a pic of an OATS in Mexico. [27]

For radiated emissions, the FCC specifies that the measurements must be performed on the complete system. All interconnect cables to peripheral equipment must be connected and the system must be in a typical configuration. The cables and the system must also be configured in a representative way such that the emissions are maximized. [32]

The receiving antenna should be a tuned dipole over the frequency range of interest and measurements should be made for vertically polarized radiated fields (dipole is perpendicular to the ground plane) and for horizontally polarized radiated fields (dipole is parallel to the ground plane).[31]



Fig. 2.5 OATS in Queretaro, Mexico.

The preferred measurement antenna for the FCC measurements is a tuned, half-wave dipole. A half-wave dipole is a linear antenna whose length is 0.5λ at the measurement frequency. Thus, for every frequency, the antenna length would have to be adjusted. [23]

The FCC test procedure can be simplified by using a broadband antenna such as a log-periodic or biconical antenna; unlike a tuned dipole, their length does not need to be adjusted with each frequency change. They are commonly used in order to allow the user to automate the radiated emissions test. Fig. 2.6 shows typical broadband antennas. [31]



Fig. 2.6 Broadband antennas for EMC measurements: (a) Biconical antenna b) Log-Periodic antenna.

During the development of products, however, most companies test their products in a semi anechoic chamber, which is a shielded room having radio-frequency absorber material on the sides and at the top of the room to prevent reflections. In order to simulate the OATS, the floor of the semi anechoic chamber should be a conducting ground plane. An example of this room can be seen in the Fig. 2.7, and in the Fig 2.8 is the illustration of the setup. [27][31]

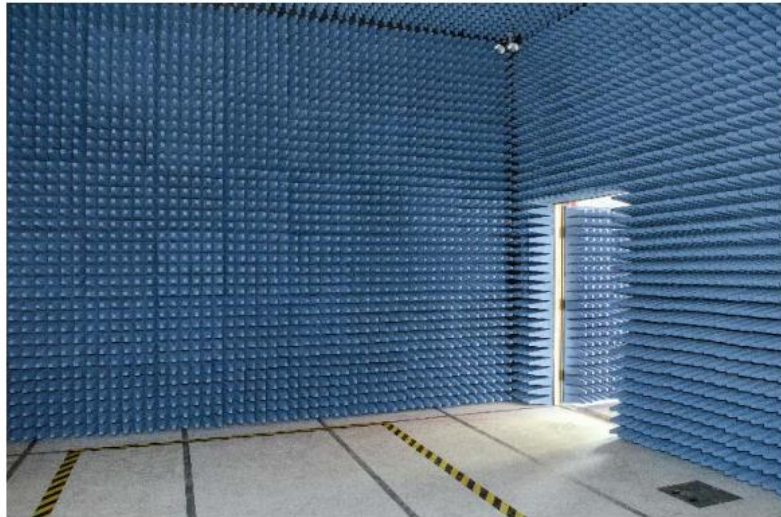


Fig. 2.7 Semi anechoic Chamber

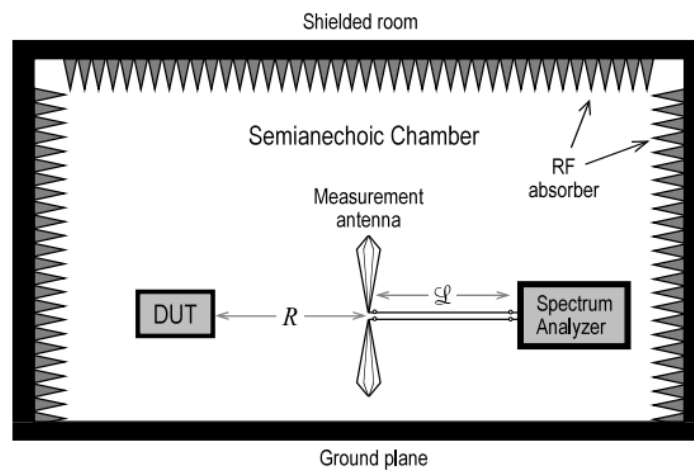


Fig. 2.8 Illustration of the setup for measurement of radiated emissions.

The last test requirement for radiated emissions testing is the bandwidth of the receiver used to measure the signal. The bandwidth must be at least 100 kHz. By having such a large bandwidth, the test will not pick up intended narrowband signals such as clock signals, but it will detect emissions from broadband sources. The FCC and CISPR test procedures require that the receiver use a quasi-peak detector. In the Fig 2.9 there are some receivers. [27][32]



Fig. 2.9 Measurement equipments.

2.5 Solutions: Shielding and Absorbers

2.5.1 Shielding.

Shielding electromagnetic emissions is a complex and formidable task. The effectiveness of any strategy or technique aimed at the reduction of the electromagnetic field levels in a prescribed region depends largely upon the source characteristics, the shield topology, and materials.

An electromagnetic shield can be defined as any means used for the reduction of the electromagnetic field in a prescribed region.

Electromagnetic shielding represents a way toward the improvement of EMC performance of single devices, apparatus, or systems.

EM shielding may be pursued by any of the following main strategies, or by a combination of them:

- Interposition of a “barrier” between the source and the area (volume) where the EM field has to be reduced.
- Introduction of a mean capable of diverging the EM field from the area of interest.
- Introduction of an additional source whose effect is the reduction of the EM field levels in the prescribed area with respect to a situation involving the original source or source system.

[24]

Shielding has two purposes (Fig. 2.10). The first, as shown in Fig. 2.10 (a), is to prevent the emissions of the electronics outside the boundaries of the product. The second purpose of a shield, as shown in Fig. 2.10 (b) is to prevent radiated emissions external to the product from coupling to the product’s electronics, which may cause interference in the product. [23]

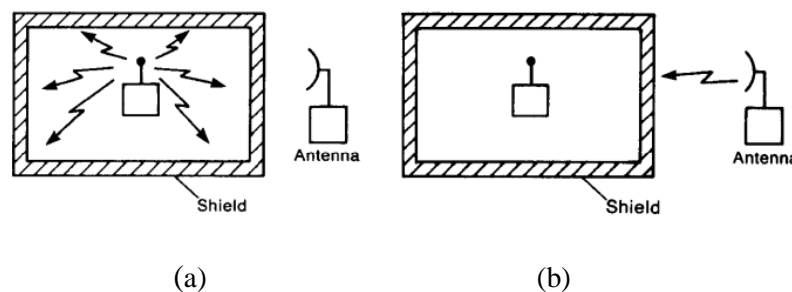


Fig. 2.10 Illustration of the use of a shielded enclosure: (a) to contain radiated emissions; (b) to exclude radiated emissions.

Shielding effectiveness (SE) is a concise parameter generally applied to quantify shielding performance. We may view the effectiveness of a shield as the ratio of the magnitude of the electric (magnetic) field that is incident on the barrier and the magnitude of the electric (magnetic) field that is transmitted through the barrier.

The shielding effectiveness of the barrier is defined for the electric field, in decibels, as

$$SE = 20 \log_{10} \left| \frac{E_i}{E_t} \right|$$

In terms of the magnetic field, the shielding effectiveness could be defined as

$$SE = 20 \log_{10} \left| \frac{H_i}{H_t} \right|$$

If the incident field is a uniform plane wave and the media on each side of the barrier are identical, the above two definitions are identical, since the electric and magnetic fields are related by the intrinsic impedance of the medium for a uniform plane wave.

Several phenomena contribute to the reduction of the incident field (Fig. 2.11). The first effect is the reflection at the left surface of the barrier. The portion of the incident electric field that is reflected is given by the reflection coefficient for that surface. The portion of the wave that crosses this surface proceeds through the shield wall. As it passes through this conductive medium, its amplitude is attenuated according to the factor $e^{-\alpha z}$, where α is the attenuation constant of the material.

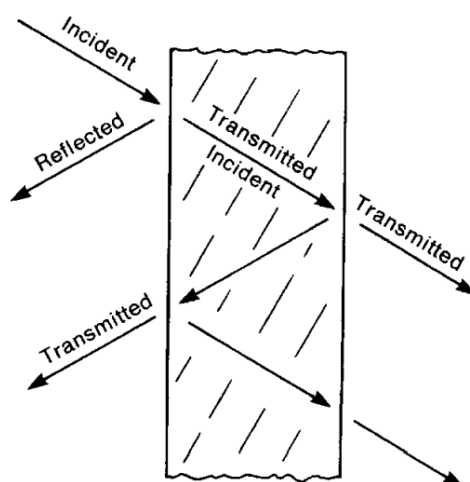


Fig. 2.11 Illustration of the incident wave through the shield.

In the case of good conductors the attenuation constant α is related to the skin depth of the material, δ , as $\alpha=1/\delta$ and $\delta=1/\sqrt{\pi f \mu \sigma}$, where μ is the permeability of the barrier and σ is its conductivity.

If the barrier thickness t is much greater than the skin depth of the barrier material at the frequency of the incident wave, the wave that is transmitted through the first interface is greatly attenuated when it strikes the right interface.

This becomes the incident wave for the right interface. A portion of this incident wave is reflected, and a portion is transmitted across the barrier into the medium on the right of the barrier. The reflected portion of this wave is transmitted back through the barrier and strikes the first interface, being incident from the metal. Once again, a portion of this wave is transmitted through the left interface and adds to the total reflected field in the left medium, and a portion is reflected and proceeds to the right. This portion is again attenuated as it passes through the barrier. Once it has passed through the barrier and strikes the right interface, a portion is reflected and a portion is transmitted through the right interface. The portion transmitted through the right interface adds to the total field that is transmitted through the

shield. The process continues in like fashion, but the additional reflected and transmitted fields are progressively attenuated by their travel through the conductive barrier.

If a shield is designed to have a thickness that is much greater than the skin depth of the material at the frequency of the anticipated incident field, there is little consequence to the continued re-reflection at the interior surfaces of the barrier.[23][34]

The shielding effectiveness can be expressed by the product of three terms each representing one of the phenomena of reflection loss, absorption loss, and multiple reflections. In decibels, these factors add to give:

$$SE_{dB} = R_{dB} + A_{dB} + M_{dB}$$

The first term, R, in equation depends only on the free-space impedance and the impedance of the shield medium, and it accounts for the first field reflection at the two shield interfaces that is due to the mismatch between the two impedances at both the interfaces. R is called the reflection-loss term, and it is always positive or null.

The second term, A, is a function of the shield characteristics only, and it accounts for the attenuation that a plane wave undergoes in traveling through an electrical depth in the shield material. A is called the absorption-loss term, and it is always positive.

The last term, M, is associated with the wave that undergoes multiple reflections and consequent attenuation before passing through the shield. M is called the multiple-reflection-loss term, and it may be positive, null, or negative. M is often negligible with respect to the other two terms, especially in the high-frequency range. [24]

In order to get extremely large values of shielding effectiveness, the shield must completely enclose the electronics and must have no penetrations such as holes, seams, slots or cables.

Any penetrations in a shield unless properly treated, may drastically reduce the effectiveness of the shield [23]

Since emission problems are emerging in higher frequencies, sometimes the commonly practiced solutions using off-the-shelf shielding products are not effective. Depending on shielding effectiveness of the chassis, part of the unintentional radiations from different interfaces inside can leak and emit outside the box and cause an EMC test failure at certain frequencies.

2.5.2 EM Absorbers.

Another solution for radiated emission reduction is the use of absorbers. Metallic shielding described in the previous section is an efficient way to reduce electromagnetic emissions; however, it only prevents EMI in a particular direction by reflecting the radiated emission, but they do not minimize the EM pollution. Whilst the absorbers' based solution minimizes the EMI by absorbing it completely.

Electromagnetic absorbers have a number of applications, such as anechoic chambers used for compliance testing of apparatus and systems instead of open area test sites, reduction of the radar cross sections of objects, improvement of the radiation pattern of antennas, damping of resonances and spurious electromagnetic radiation in metal shielding constructions, etc [33].

For the purpose of EM shielding, the last application is evidently good for an improvement of a shielded room performance. The high conductivity of metal walls works to trap the electromagnetic energy penetrated through the shield discontinuities (which may be viewed as traveling back and forth within the shielded volume). Materials capable of effective

dissipation of such energy in the shielded area can considerably help in the improvement of shielding effectiveness. [24]

The attenuation of the energy of electromagnetic field by radio absorbing materials is provided by their dielectric, conductive and magnetic properties. A common approach is to use a combination of different materials in various forms with a variation of concentration, ratio and dimensions. Many types of designs are applied for the RF absorbers: the layer type, pyramidal, wedge, walkway, convoluted, ferrite tiles, oblique incident and metamaterial absorbers. Pyramidal absorbers are commonly applied for the frequency range above hundreds of megahertz [27].

The EM wave absorber emphasizes low-reflection wave beam amplitude, which means that it has to absorb incident EM waves as much as possible. Modern electronic devices present new demands for low density and thin thickness structures able to offer strong absorption peak in a broadband frequency range. There are two parameters usually adopted to evaluate the absorption ability of EM absorbing materials. One variable is reflection loss (R), determined by amplitudes of reflection wave, transmission wave, and incident wave, and uses decibel (dB) as a unit. R is a negative value determined by a logarithmic function. A good EM absorber R_{dB} should be less than -10 dB through artificial regulation in most cases. [34]

$$R_{dB} = 20 \log_{10} \left| \frac{Z_{in} - Z_0}{Z_{in} + Z_0} \right|$$

Since the metallic ground leads to zero transmissivity, the absorptivity can be defined as:

$$A = 1 - R = 1 - \left| \frac{Z - Z_0}{Z + Z_0} \right|^2$$

Electromagnetic absorbers are specifically chosen or designed materials that can inhibit the reflection or transmission of electromagnetic radiation. The particular absorption frequencies, thickness, component arrangement and configuration of the materials also determine capabilities and uses. In addition materials such as metamaterials are being used to improve performances and diversity of applications.

An illustration of EM emissions and applications of EM absorbers are depicted in the Fig. 2.12.

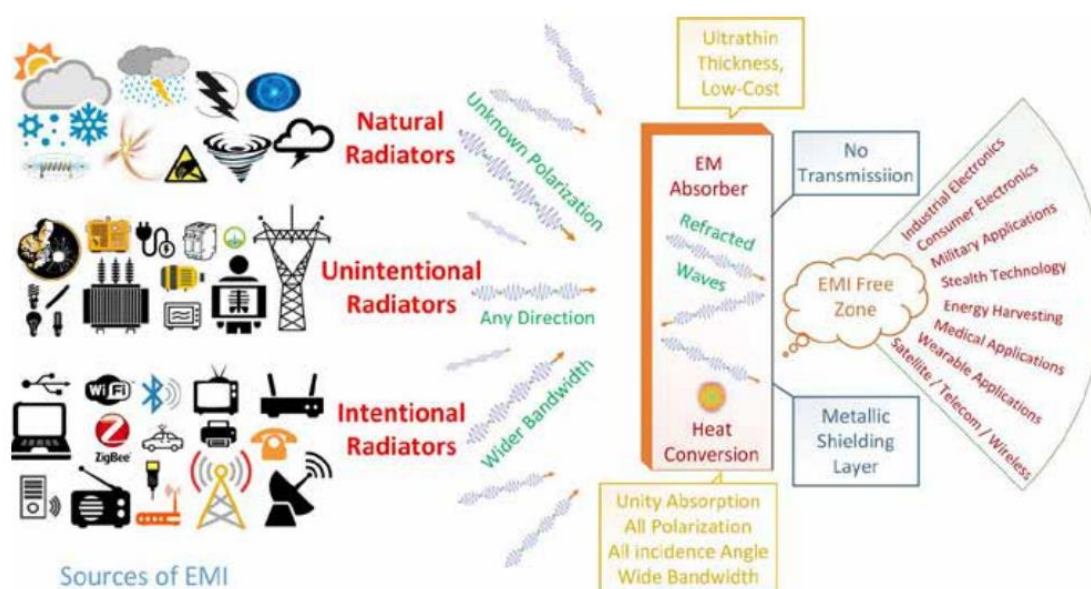


Fig. 2.12 Illustration of EM radiation and absorption in the current scenario.

2.6 Metamaterial-based solution discussed in the paper “Design and Evaluation of Radiated Emission Metamaterial Absorbers”^[16]

In the paper [36], a new solution for the mitigation of unwanted radiated emissions from high-speed systems was developed, metamaterial Frequency Selective Surface (FSS) is used as a screen to pass or suppress certain frequency.

EMC failures can happen at different frequencies, they depend of the data rate and type of the high speed interfaces in the system. In this paper the system contained a PCIe Gen 3 board, the illustration of it is in the Fig. 2.13, and it has been scanned for radiated emission. The report shown a strong frequency component at 8 GHz.

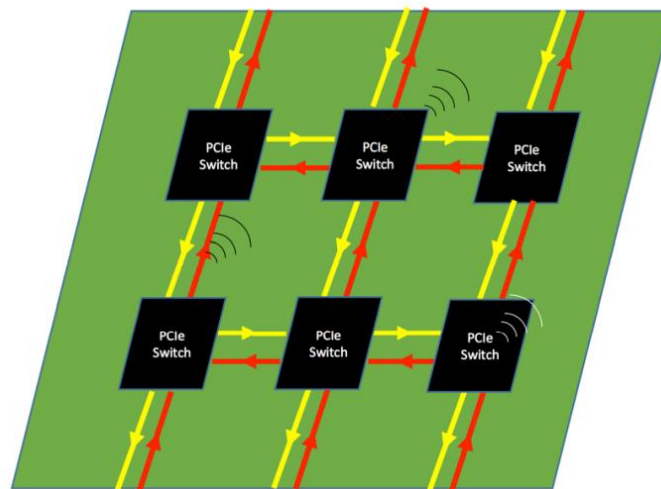


Fig. 2.13 PCIe switch.

2.6.1 Source of Radiation.

In this system the causes of the radiated emission were analysed. Basic emission waveform theory identifies four types of waveforms as possible sources for unwanted

radiations: square wave, sinusoidal wave, damped oscillation, and spike. When emission is traced back to its source waveform, layout and operational specifications can be adjusted to alleviate the problem.

Unwanted radiation spikes are expected to occur at the Nyquist frequency in radiated emission tests of digital systems such as PCIe boards, half of the data rate in Hz. However, there have been cases that emission spikes were observed at twice the Nyquist frequency instead, and this was one of them.

These simulations on the report demonstrated that one possible source of the radiated emission spikes in an 8 Gbps PCIe Gen 3.0 interface, is the delay differences between differential lines.

The rise time and differential delay on the power of the common mode signal at 8 GHz had a big impact. It was shown that faster edge rate for differential signals and larger skew between positive and negative traces result in stronger harmonics in the spectrum of the common mode signal, which contribute to the radiated emissions from these traces. Therefore, 8 GHz is the fundamental frequency of the unwanted emissions.

The studied in the paper proposed solution targets suppressing 8 GHz emissions generated by a mock-up system board replicating an enterprise storage unit with a PCIe Gen 3.0 interface. The system considered for evaluation of this approach was based on a data center's storage box containing PCIe Gen 3 switch fabric board which failed FCC compliance testing at 8 GHz.

2.6.2 Solution: Impedance Matching Metamaterial Absorber.

The solution proposed is based on the design of an impedance matching surface that acts as an absorber at the frequency of EMC failure. To do that a material with complex

dielectric and magnetic properties was introduced to match the surface impedance at the frequency of EMC failure with the free space impedance. This metamaterial was used in the simulations to evaluate the effectiveness of frequency selective surfaces (FSS) in reducing radiated emissions.

The metamaterial designs had the form of planar, periodic metal-dielectric arrays in two-dimensional space (squared). Frequency behaviour of an FSS is entirely determined by the geometry of the surface in one period (unit cell) provided that the surface size is infinite. One advantage of this FSS design is its two-dimensional (2-D) symmetry. For the square patches with the same gap and width on all four sides, the inductance, capacitance, and resistance of the impedance-matching network are the same for both E_y and E_x field directions.

The matching network was implemented by the 2-layer geometry shown in Fig. 2.14. Each dielectric layer is considered as a transmission line with its length equal to the layer thickness.

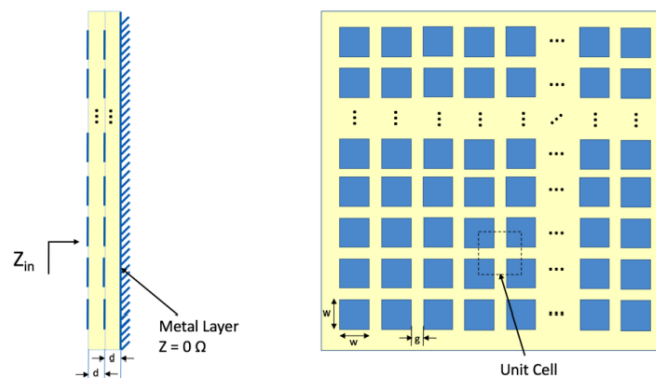


Fig. 2.14 Side and top views of the two-layer metamaterial absorber.

The substrate material was FR406 and its features are a thickness $d = 1.5748$ mm, $\epsilon_r = 3.93$, and $\tan \delta$ (tangent loss) = 0.0167. The metallic patch is of nickel-phosphorus with a conductivity

of 99000 S/m. To define the dimensions of the metal patch and the dimensions of the unit cell, some parametric simulations were carried out in [36].

In Figures 2.15 - 2.18, we can see the effect of the different parameters on the reflection coefficient. Analysing all these simulations the paper concluded that the best performance of the absorber (-46dB) will be with the following features:

- Dimension of unit cell: 4.7 mm x 4.7 mm
- Dimension of metallic patch: 3.7 mm x 3.7 mm
- Metallic patch thickness: 0.1 μm

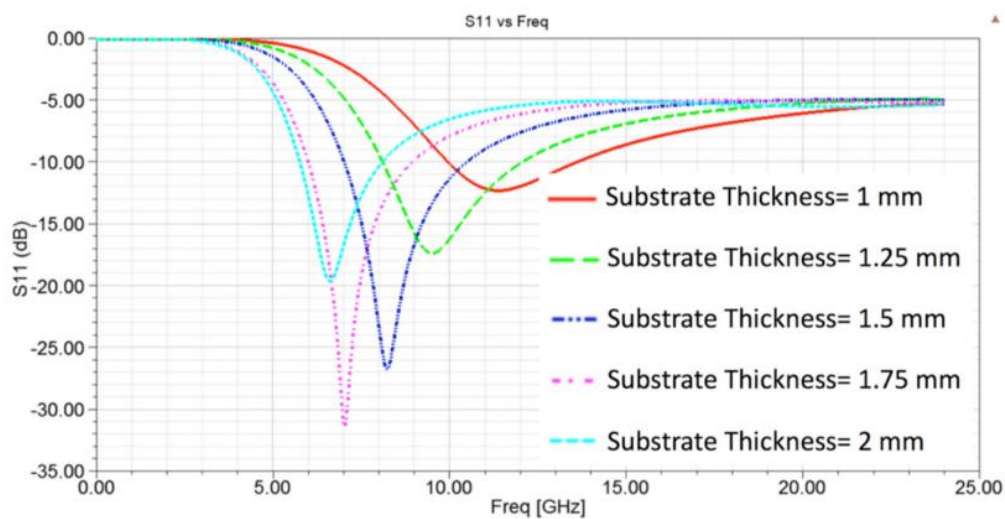


Fig. 2.15 Effect of the dielectric substrate thickness on the reflection coefficient.

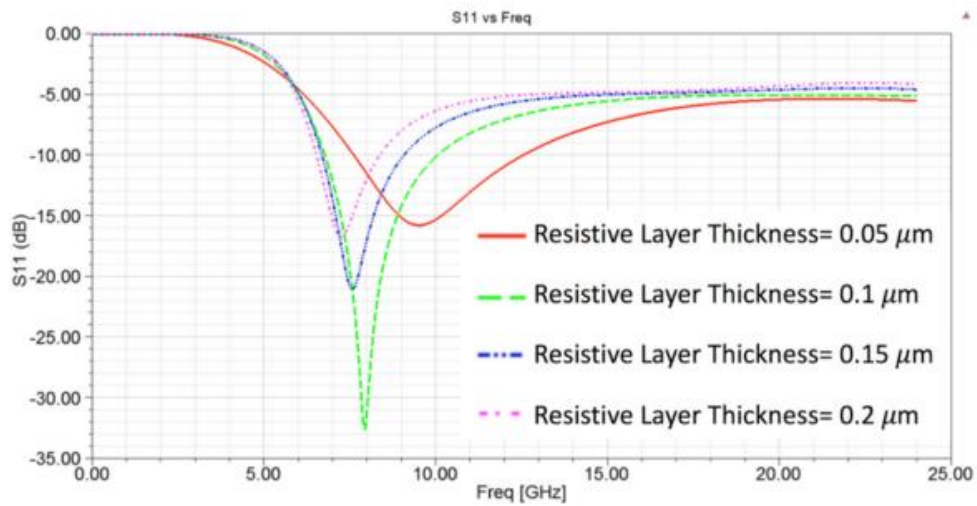


Fig. 2.16 Effect of the metallic patch thickness on the reflection coefficient.

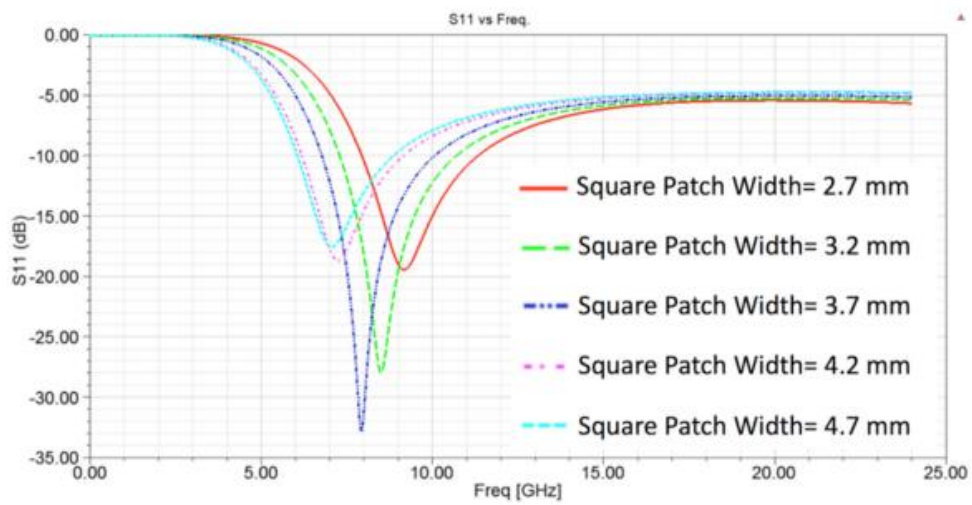


Fig. 2.17 Effect of the square metallic patch width on the reflection coefficient.

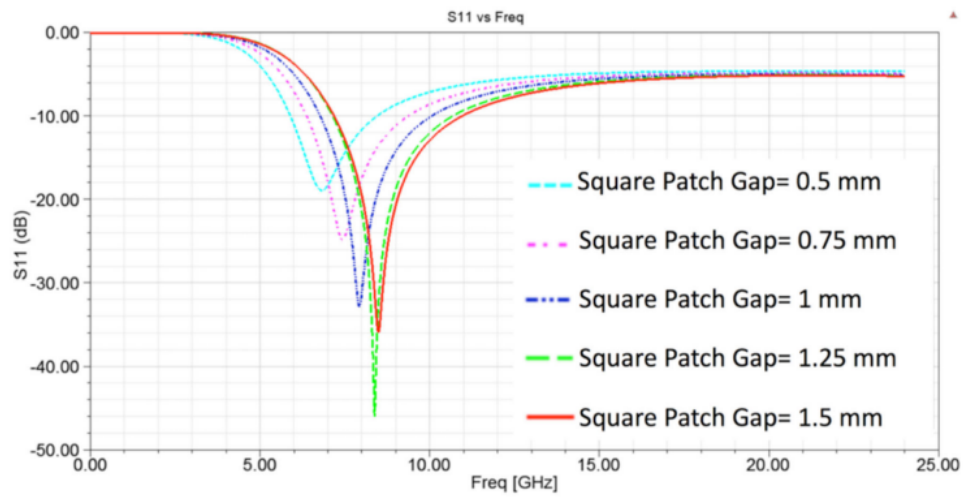


Fig. 2.18 Effect of the gap (for a fixed patch width of 3.7 mm) on the reflection coefficient.

CHAPTER III

ANALYSIS AND SIMULATION OF A SINGLE LAYER METAMATERIAL UNIT CELL FOR THE REDUCTION OF RADIATED EMISSIONS

3.1 Introduction

In this chapter, an in-depth parametric analysis of metamaterial unit cells for radiated emission reduction is performed. In the industrial sector, it is very important that an effective solution can be implemented in the last stages of product development, in order to prevent EMI. The ideal solution must have a low profile and a small size. It must also be inserted into the system or module without requiring substantial changes in the mechanical design of the enclosures. For these reasons, metamaterial absorbers represent the best choice.

The process of designing and optimizing a metamaterial absorber is faster if numerical simulations are used. In addition, simulators provide a quicker tool for tuning the design parameters to find the best surface impedance that gives a smaller amount of radiation emission. The software adopted in this work is Ansoft Designer V3.

The parameters considered in the following analysis are the loss tangent, the thickness of the metal layer and the conductivity of the metal patch.

3.2 Unit cell geometry

The basic structure considered in this paragraph is a metamaterial unit cell adopted for designing a frequency selective surface (FSS) absorber (this structure is similar to the structure used in the paper “Design and Evaluation of Radiated Emission Metamaterial Absorbers” [36]). The operating frequency is 8 GHz.

The aim of the analysis is to understand the effects of the geometric and electrical parameters of the unit cell on the absorber performance. Furthermore, the idea is to use the results of the analysis to simplify the unit cell proposed in [37], by properly optimizing a structure composed of a single layer of a periodic metal pattern instead of the two-layer structure illustrated in [36] and discussed in chapter II.

The dielectric substrate is FR4_epoxy having permittivity $\epsilon_r=4.4$, loss-tangent=0.02, while the metal initially used for the patch is the copper having conductivity $\sigma=5.8e7$ S/m.

This basic structure has the same thickness used in the metamaterial structure of the paper [36], namely 3.2mm.

In Fig. 3.1 we can see a 3D illustration of the unit cell and in Fig. 3.2 there are the materials and the thickness of the layers composing the cell.

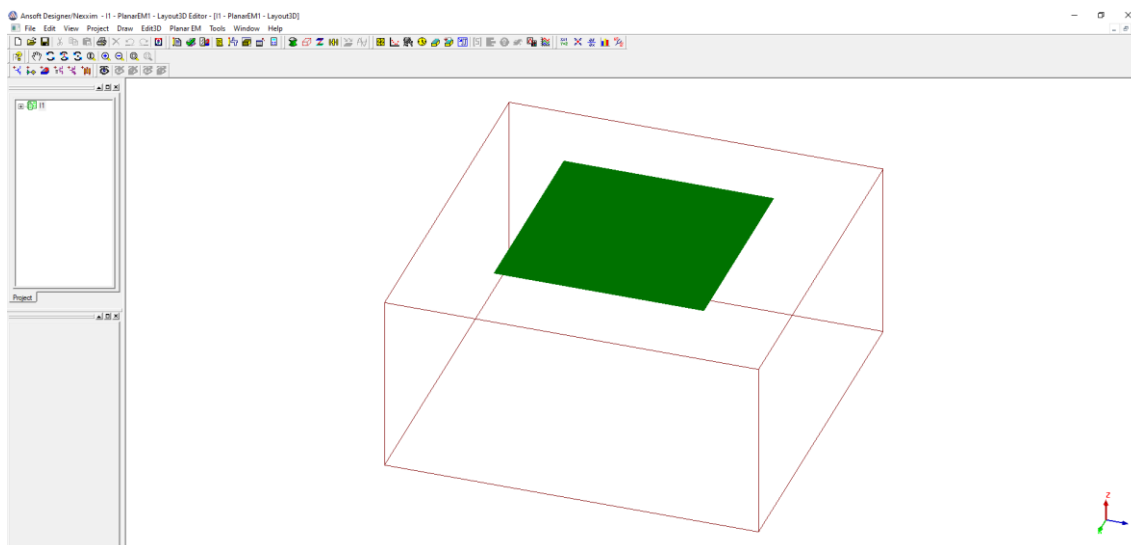


Fig. 3.1 Illustration 3D view of the unit cell.

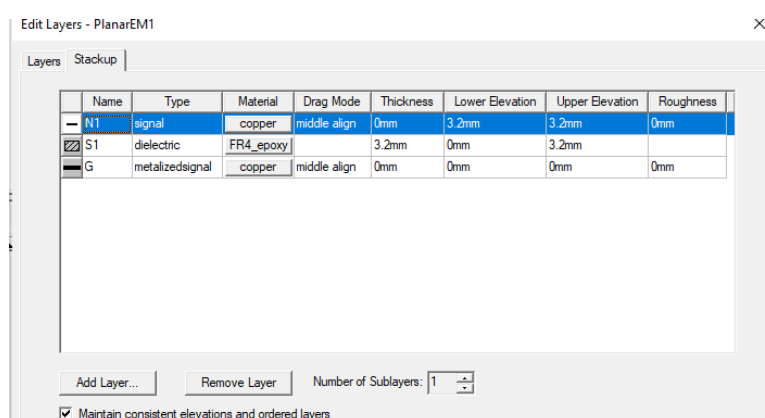


Fig. 3.2 Layers of the unit cell.

There are three layers: the ground plane layer, the substrate layer and the conductor layer hosting the periodic metallic pattern (at this time we will consider copper as conductor with a thickness equal to zero).

3.3 Design of resonant metamaterial unit cells

Defined the size of the unit cell, we must look for the length of the side of the patch (L) to have the resonant frequency at 8GHz.

We choose four unit cell dimensions ($D \times D$):

- 4.7 mm x 4.7 mm ,
- 4.2 mm x 4.2 mm,
- 7.5 mm x 7.5 mm,
- 9.4 mm x 9.4mm.

The frequency range for the analysis is set from 6 GHz to 11 GHz.

- D=4.7mm: Parametric simulation versus the patch side length (L).

Fig. 3.3 shows how the peak of the impedance (real part) of the unit cell varies when the patch side length (L) changes. Fig. 3.4 shows the cross of zero of the impedance (imaginary part) when the patch side length (L) changes from 2 mm to 3.6 mm. After this preliminary analysis, we set L in order to have the resonance frequency at 8GHz.

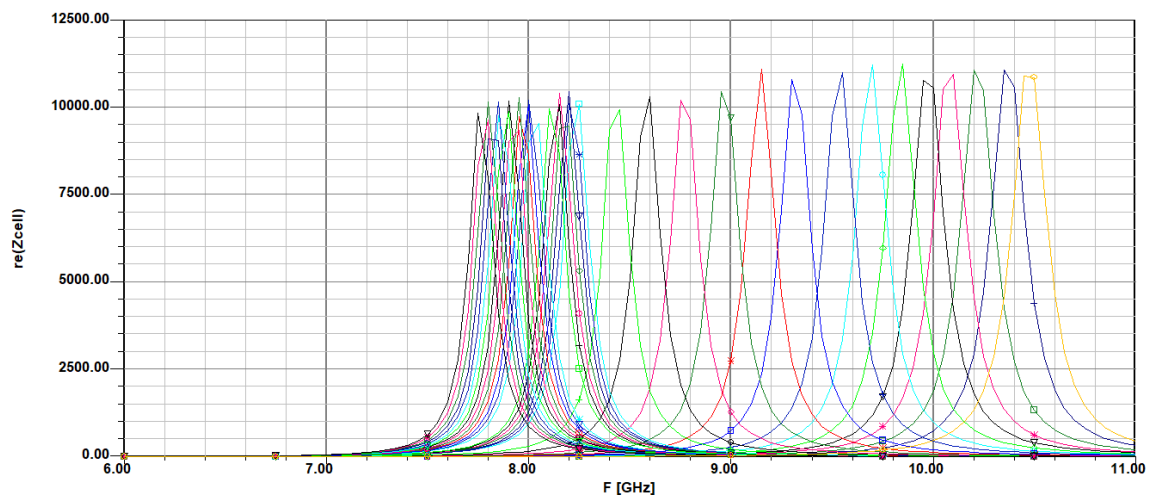


Fig. 3.3 Plot of the real part of the cell impedance for different values of L ($D=4.7\text{mm}$).

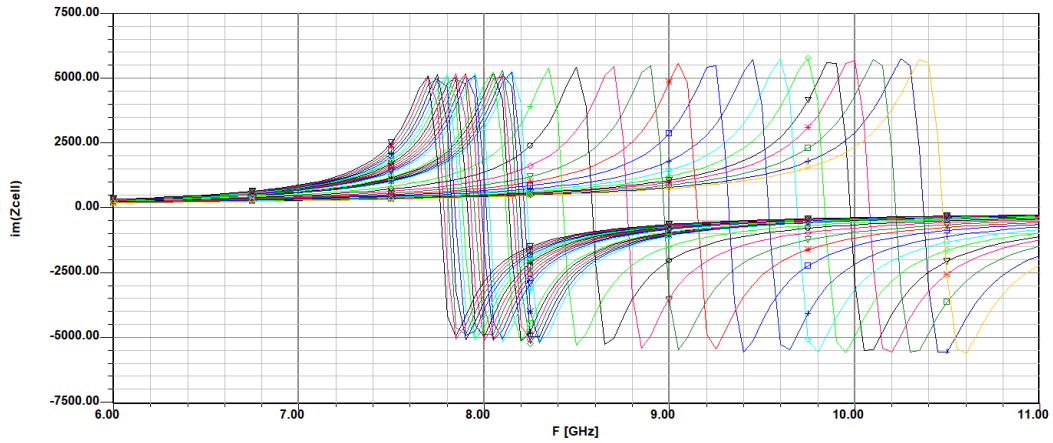


Fig. 3.4 Plot of the imaginary part of the cell impedance for different values of L ($D=4.7\text{mm}$).

As in Fig. 3.3 there are many values of L , the data has been processed using MATLAB, with few values of L to better see the impedance behavior. It can be observed the real part of the impedance in Fig. 3.5 (a) and the imaginary part of the impedance in Fig. 3.5 (b).

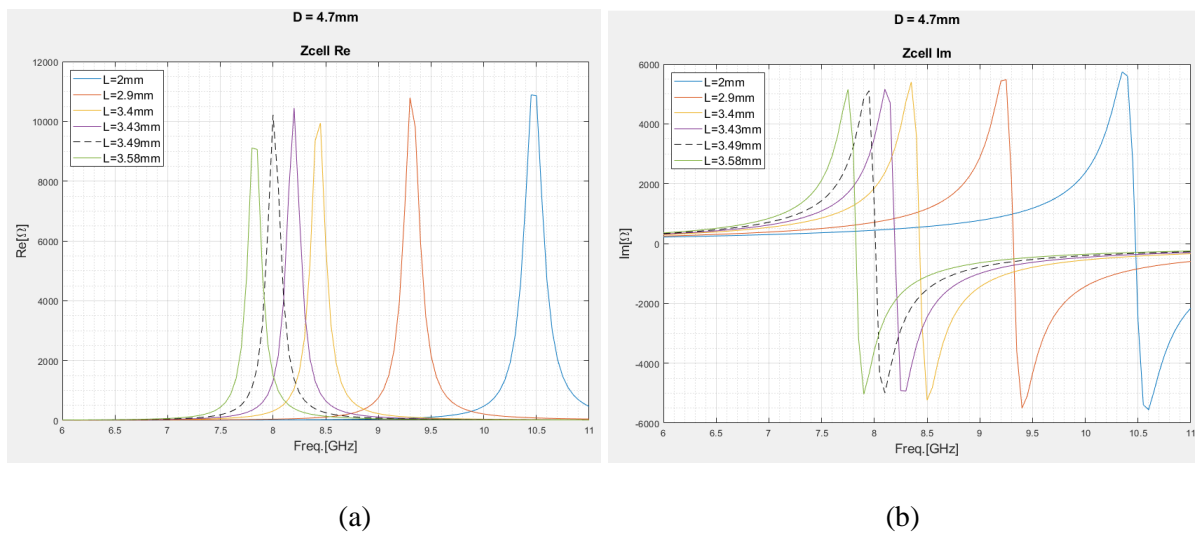


Fig. 3.5 Behavior of the impedance for different values of L ($D=4.7\text{mm}$): (a) Real part; (b) Imaginary part.

We can see that when the value of L increases, the resonance frequency decreases. With L=3.49mm the resonance frequency is 7.986GHz, so it is very closer to our target.

Now we can obtain the reflection coefficient of our structure that is given by the relationship between the impedance of the unit cell (Z_L) and the impedance of the free space (Z_0):

$$\Gamma = \frac{Z_L - Z_0}{Z_L + Z_0}$$

An absorber must have a reflection coefficient near to zero at the frequency target. To obtain a low value of the reflection coefficient the cell impedance must be closer to the value of 377Ω (impedance of the free space).

In Fig. 3.6, we can see the traces of the unit cell reflection coefficient for different values of L.

The reflection coefficient in correspondence of a few values of L is shown in Fig. 3.7:

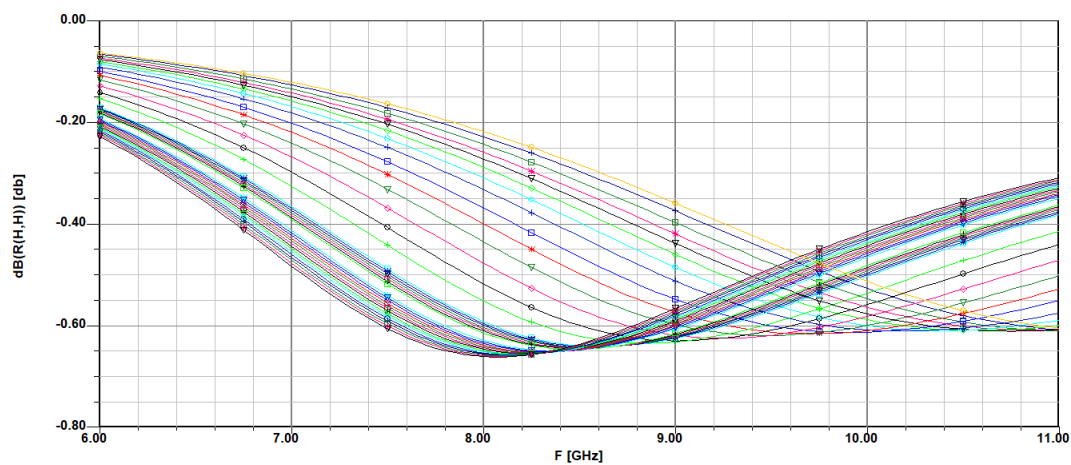


Fig. 3.6 Reflection coefficient for different values of L (D=4.7mm).

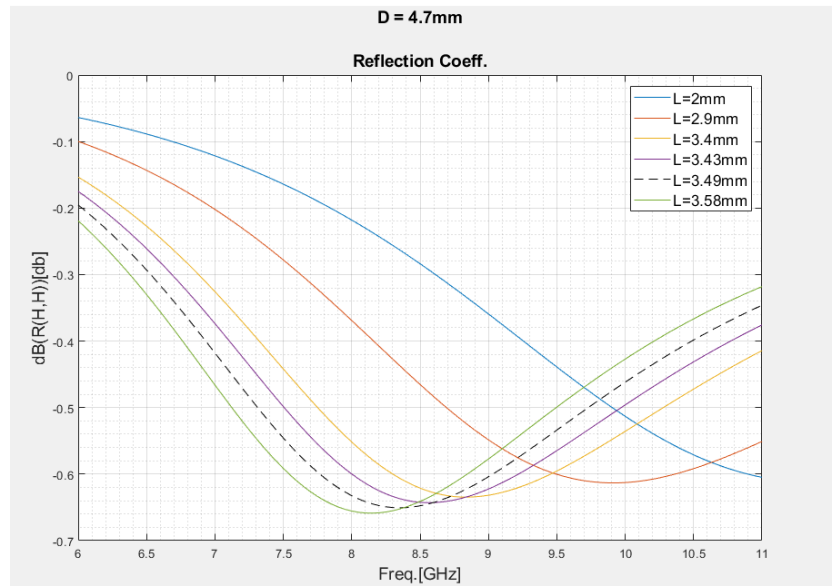


Fig. 3.7 Reflection coefficient for different values of L (D=4.7mm) (processing in Matlab).

For this case the value of the reflection coefficient is very high (near to 1), we can confirm that when we see the plot of the cell's impedance (Fig. 3.5), it has values too high with respect to free space impedance, causing a mismatching.

Another important parameter is the absorption coefficient defined as:

$$A = 1 - R - T$$

where R is the power reflection coefficient whilst T is the transmission coefficient. In a metamaterial absorber, the parameter T will be equal to zero (due to the ground plane), so the absorption is equal to:

$$A = 1 - R$$

and R is defined as:

$$R = |\Gamma|^2 = \left| \frac{Z - Z_0}{Z + Z_0} \right|^2 ;$$

So:

$$A = 1 - R = 1 - \left| \frac{Z - Z_0}{Z + Z_0} \right|^2$$

The absorption coefficient (%) for different values of L is reported in Fig. 3.8.

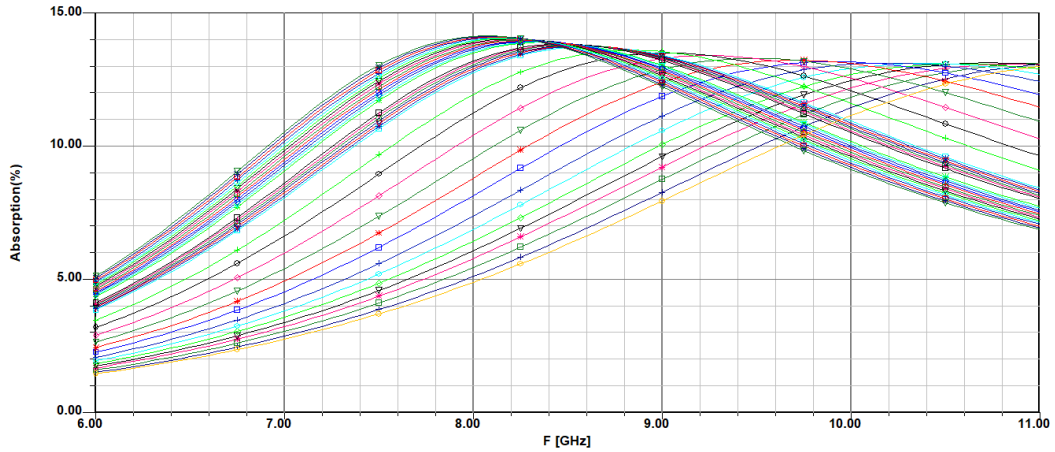


Fig. 3.8 Absorption of the unit cell for different values of L (D=4.7mm).

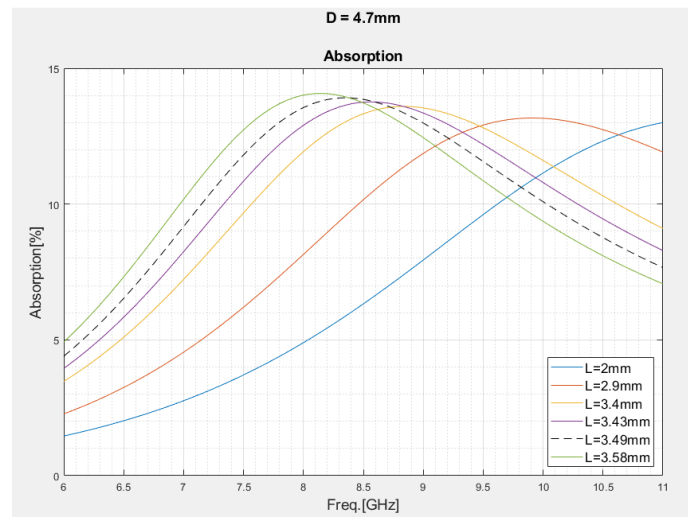


Fig. 3.9 Absorption of the unit cell for different values of L (D=4.7mm) (processing in Matlab).

In Fig. 3.9, we can confirm that the value of the absorption is very low; a good absorber must have at least 90% of absorption at the frequency target. For the above reason the structure

must be optimized in order to reduce the unit cell impedance and then to achieve a zero reflection coefficient and a unitary absorption.

- ***D=4.2mm: Parametric simulation versus the patch side length (L).***

The same analysis has been developed for the unit cell length equal to 4.2mm, in order to set the value of L giving the resonance frequency at 8 GHz.

Fig. 3.10 (a) shows the real part of the impedance and Fig. 3.10 (b) the imaginary part of the impedance processed in Matlab. We can observe a resonance frequency equal to 7.991GHz for $L=3.23$ mm.

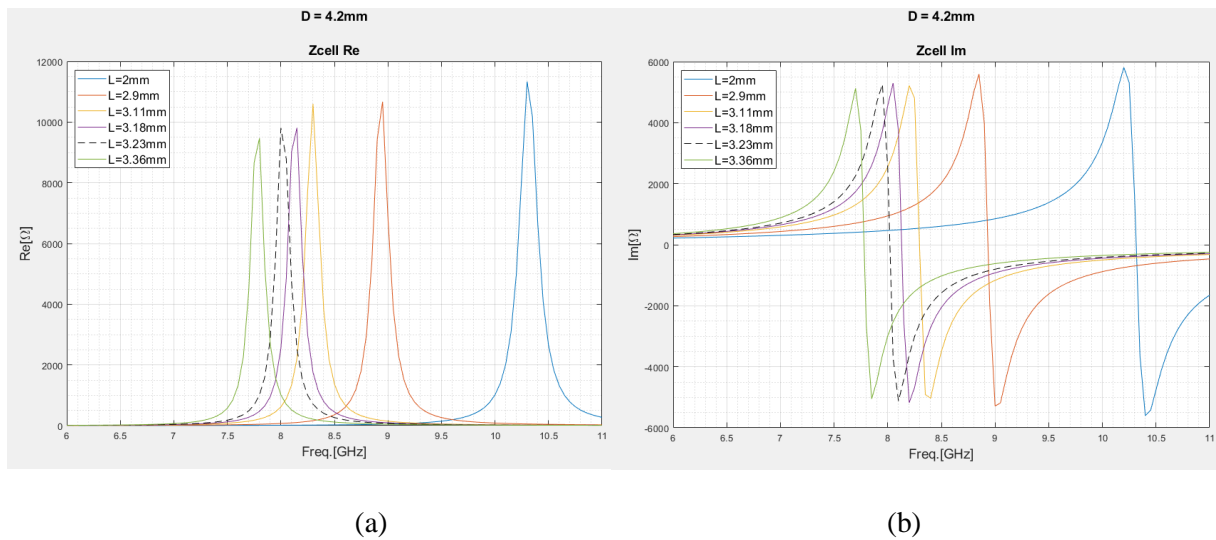


Fig. 3.10 Behavior of the impedance for different values of L ($D=4.2$ mm) : (a) Real part; (b) Imaginary part

- ***D=7.5mm: Parametric simulation versus the patch side length (L).***

Observing the results depicted in Fig. 3.11 (a) and in Fig. 3.11 (b), we can obtain the resonance frequency 7.992GHz with $L=4.69$ mm when $D=7.5$ mm.

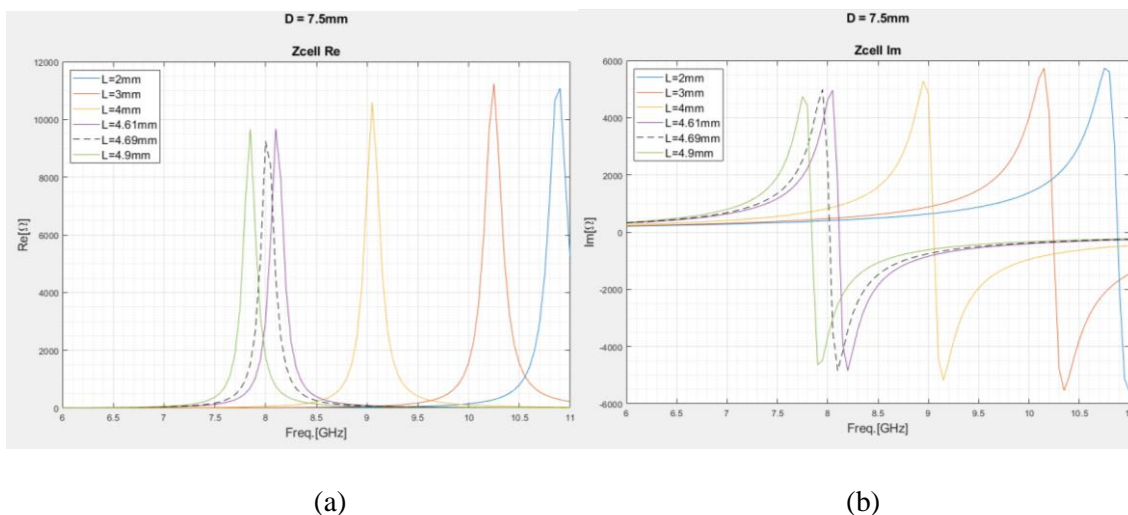


Fig. 3.11 Behavior of the impedance for different values of L ($D=7.5\text{mm}$): (a) Real part; (b) Imaginary part

- $D=9.4\text{mm}$: Parametric simulation respects to the patch side length (L).

Finally, Fig. 3.12 (a) and Fig. 3.12 (b) show that with $L=5.32\text{mm}$ the resonance frequency is 7.998GHz , when $D=9.4\text{mm}$.

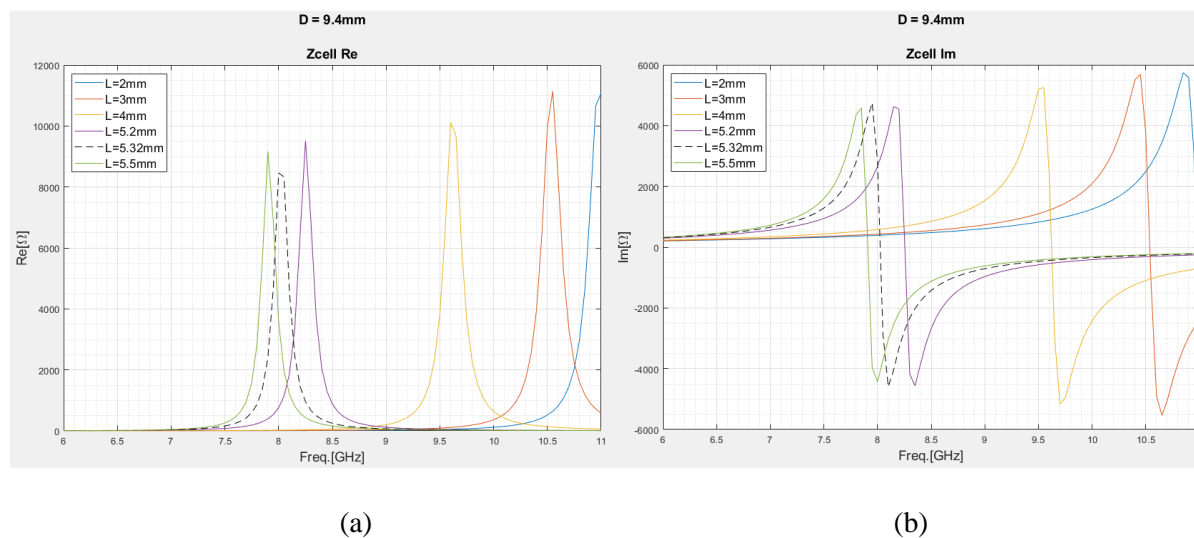


Fig. 3.12 Behavior of the impedance for different values of L ($D=9.4\text{mm}$): (a) Real part; (b) Imaginary part

Analyzing all the above cases, we can conclude that when we reduce the unit cell (D) we have to reduce the patch size L to fix the resonance to a value close to 8 GHz.

In addition, the biggest value of L means a lowest value of the impedance, and it means that the reflection coefficient will be lowest and the absorption will be highest.

Anyway in all cases, the structure must be optimized in order to reduce the unit cell impedance and then to achieve a zero reflection coefficient and a unitary absorption.

3.4 Unit cell behavior vs dielectric loss tangent

In this paragraph, we will see the effects of dielectric loss tangent on the behavior of unit cell impedance. The ϵ_r is still equal to 4.4, whilst the LossTan factor is varied from 0.02 up to 0.1 for the cases of $D=4.7\text{mm}$ and $D=4.2\text{mm}$.

- $D=4.7\text{mm}$ and $L=3.49\text{mm}$.

Fig. 3.13 (a) and Fig. 3.13 (b) confirm that the resonance frequency is 8GHz for all considered values of the LossTan parameter. The figures also show that if the LossTan increases, the impedance of the cell decreases.

Fig. 3.14 (a) shows that the reflection coefficient decreases when the loss tan increases, because the impedance of the cell is a little closer to the impedance of the free space.

In Fig. 3.14 (b) we can see that with the highest loss tangent value we obtain the lowest impedance of the cell (closer to impedance of the free space) and it is better for the absorption.

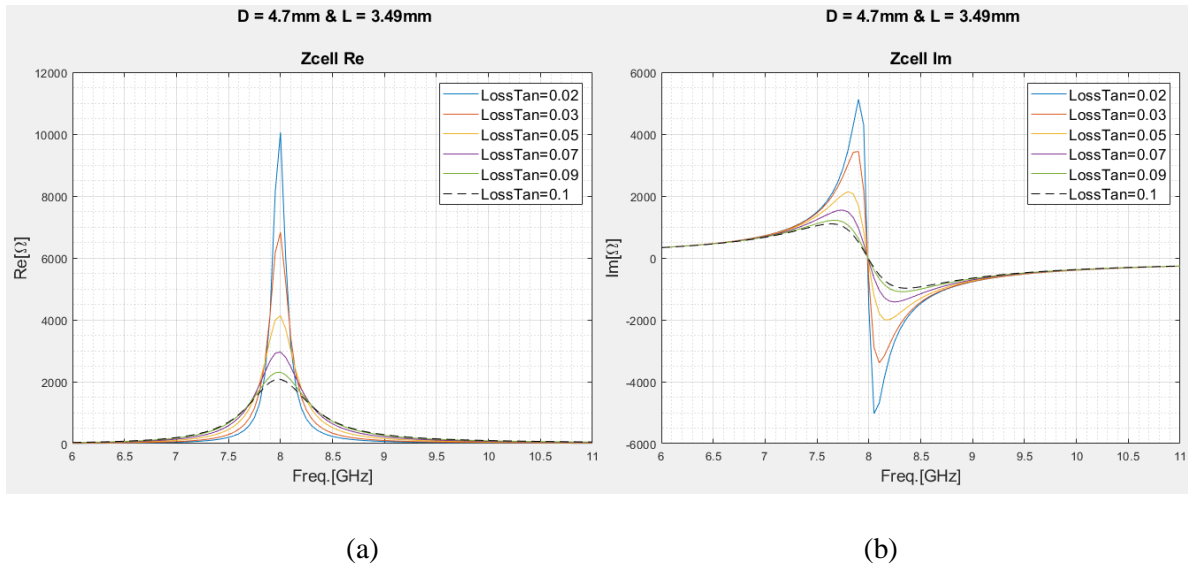


Fig. 3.13 Behavior of the impedance for different values of loss tangent ($D=4.7\text{mm}$ $L=3.49\text{mm}$):

(a) Real part; (b) Imaginary part.

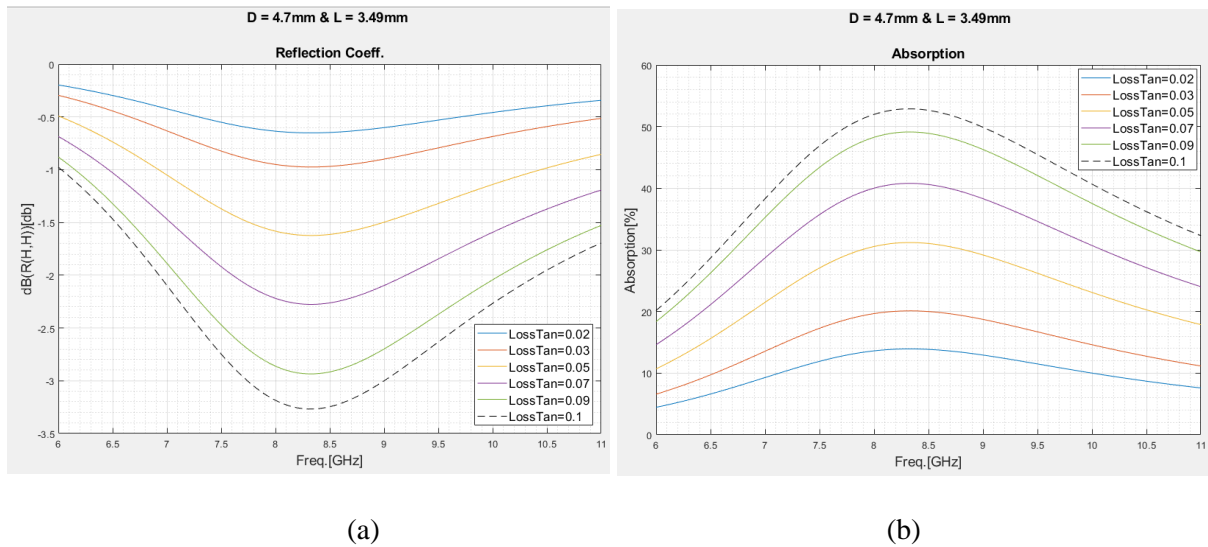


Fig. 3.14 (a) Reflection coefficient for different values of loss tangent; (b) Absorption for different values of loss tangent. ($D=4.7\text{mm}$ $L=3.49\text{mm}$)

Fig. 3.15 (a) illustrates the relationship between the impedance of the cell and the loss tan at the resonance frequency. If the loss tangent increases, the impedance of the cell decreases similar to an exponential decay.

The graph in Fig. 3.15 (b) shows the relationship between absorption of the cell and the loss tan at the resonance frequency. If the loss tan increases, the value of the absorption increases too, almost linearly.

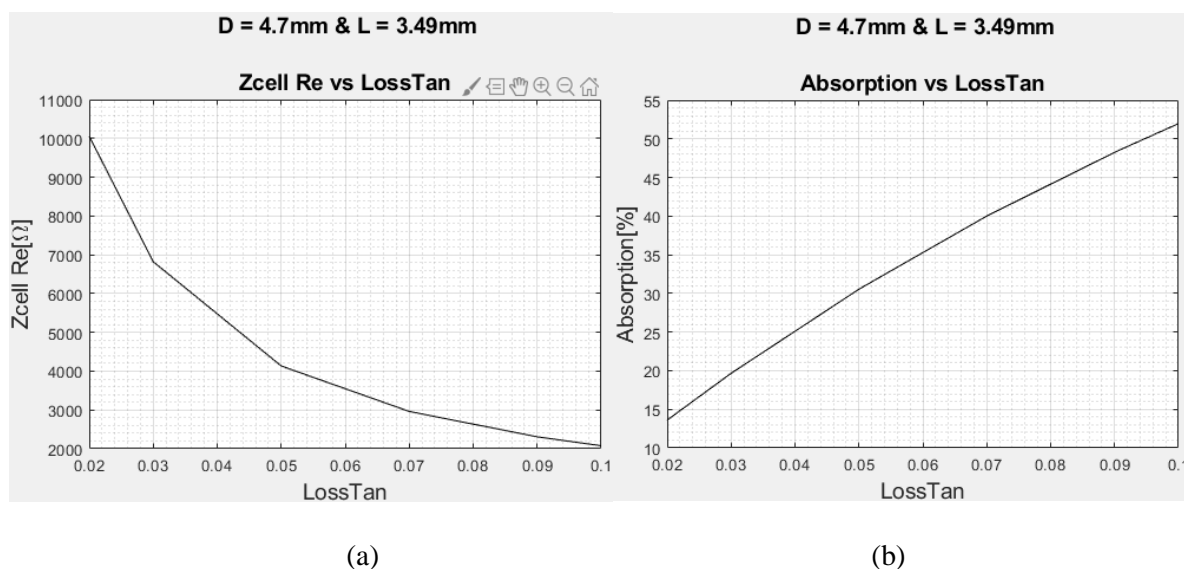


Fig. 3.15 (a) Behavior of the impedance for different values of loss tan at the resonance frequency; (b) Absorption for different values of loss tangent at the resonance frequency.

(D=4.7mm L=3.49mm)

- ***D=4.2mm and L=3.23mm.***

Fig. 3.16 (a) and Fig. 3.16 (b) show that the resonance frequency is 8 GHz for all considered values of the LossTan. The behavior of the impedance is similar to the previous case. In fact, the impedance of the cell is inversely proportional to the loss tangent value. Fig. 3.17 (a) and Fig. 3.17 (b) show similar results of reflection coefficient and absorption to those illustrated in Fig. 3.14 for the cell having D=4.7mm and L=3.49mm.

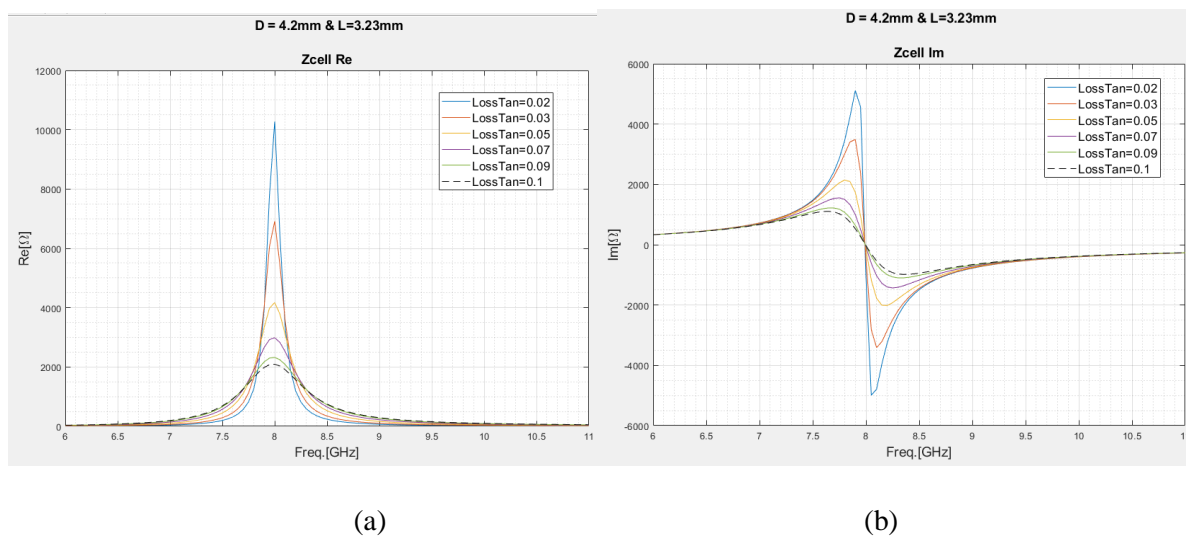


Fig. 3.16 Impedance for different values of loss tangent ($D=4.2\text{mm}$ $L=3.23\text{mm}$):

(a) Real part; (b) Imaginary part.

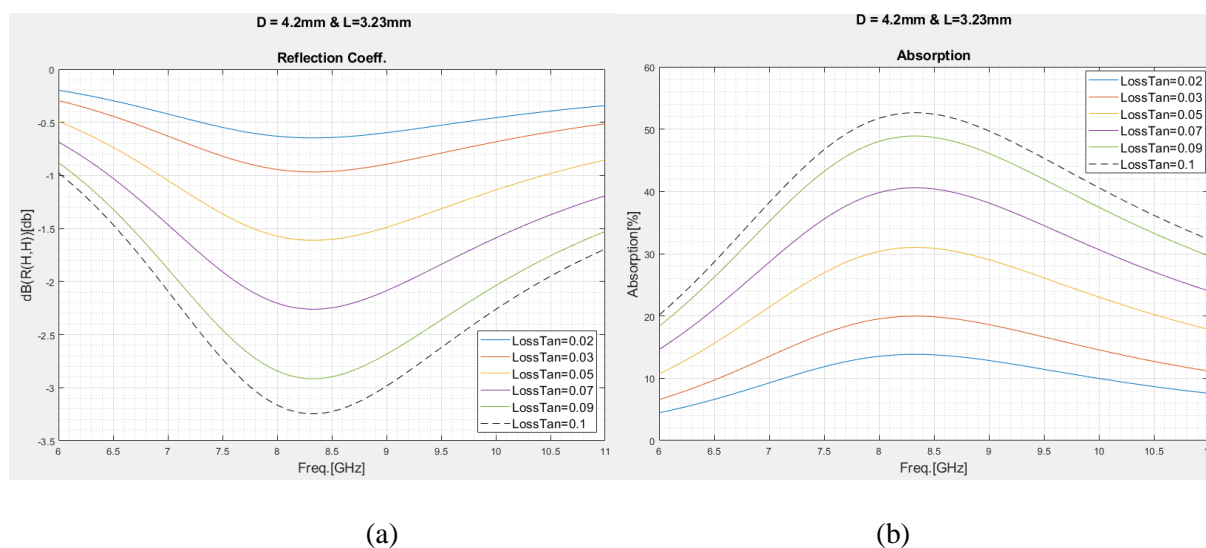


Fig. 3.17 (a) Behavior of the reflection coefficient for different values of loss tangent;
(b) Behavior of the absorption for different values of loss tangent. ($D=4.2\text{mm}$ $L=3.23\text{mm}$)

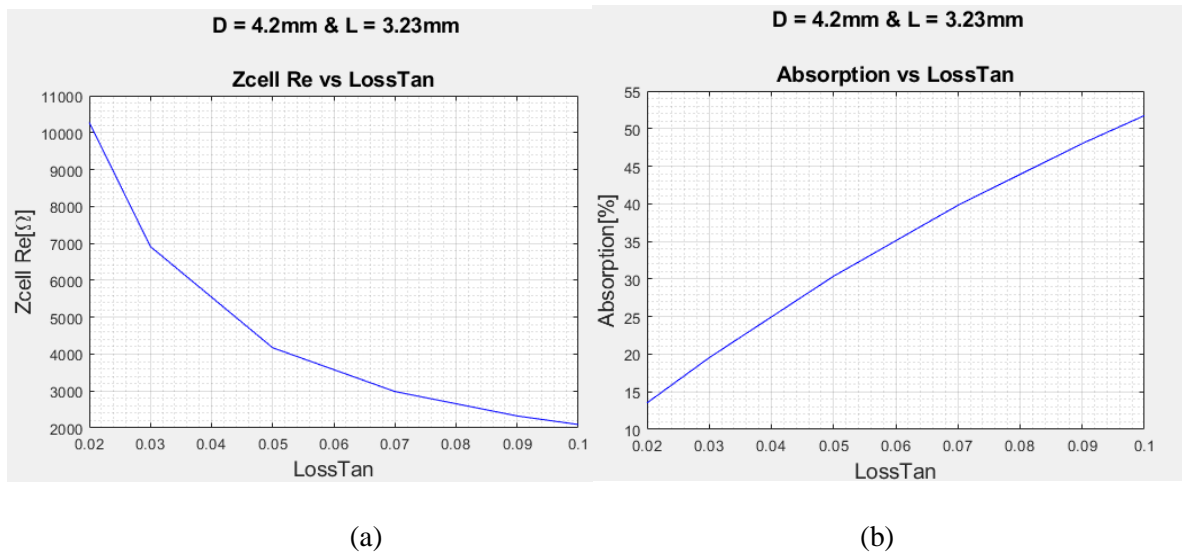


Fig. 3.18 (a) Behavior of the impedance for different values of loss tan at the resonance frequency; (b) Absorption for different values of loss tangent at the resonance frequency.

(D=4.2mm L=3.23mm)

Fig. 3.18 (a) and Fig. 3.18 (b) show the relationship between the impedance and the absorption of the cell versus the loss tan at the resonance frequency. The results are very similar to those illustrated in the previous section. The impedance of the cell falls exponentially while the absorption increases almost linearly as the loss tan increases.

3.5 Unit cell behavior vs thickness of the metal layer

In this paragraph, we will see the effects of the thickness of the metal layer (MT) on the behavior of unit cell impedance. The features of the substrate FR4_epoxy are $\epsilon_r=4.4$, loss-tangent=0.02, whilst the metal considered is copper having $\sigma=5.8e7$ S/m.

The discrete points considered for MT are 1e-2mm, 1e-3mm, 1e-4mm, 1e-5mm, 1e-6mm and 2e-7mm. The simulations have been performed with Ansoft Designer and the data processed in Matlab.

- $D=4.7\text{mm}$ and $L=3.49\text{mm}$.

We can see in Fig. 3.19 (a) and Fig. 3.19 (b) that the thickness of the conductor affects the resonance frequency; when the thickness of the conductor decreases the impedance of the unit cell decreases too. How it is shown in Fig. 3.20 (b), the absorption at the required frequency (8GHz) is not enough, but it is good at the higher frequencies.

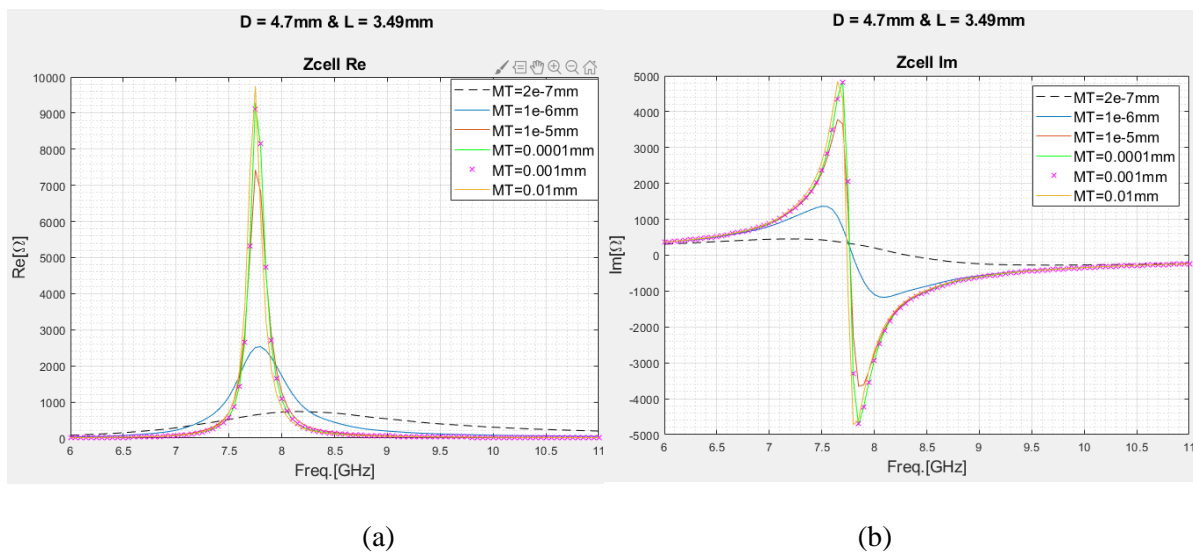
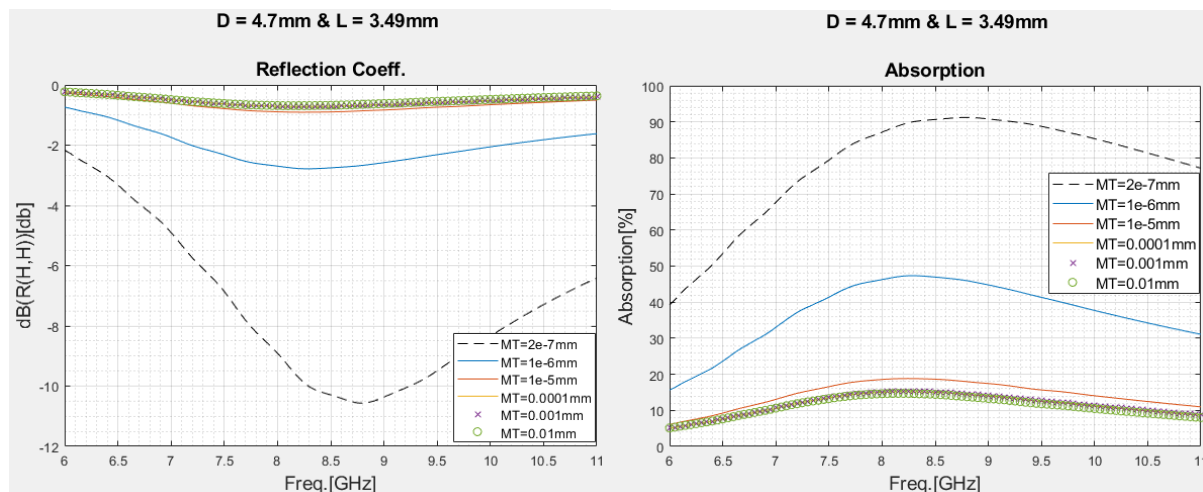


Fig. 3.19 Impedance for different values of metal thickness ($D=4.7\text{mm}$ $L=3.49\text{mm}$):

(a) Real part; (b) Imaginary part.

Fig. 3.21 (a) and Fig. 3.21 (b) respectively show the behavior of the impedance and the absorption versus the thickness of the conductor, at the resonance frequency.

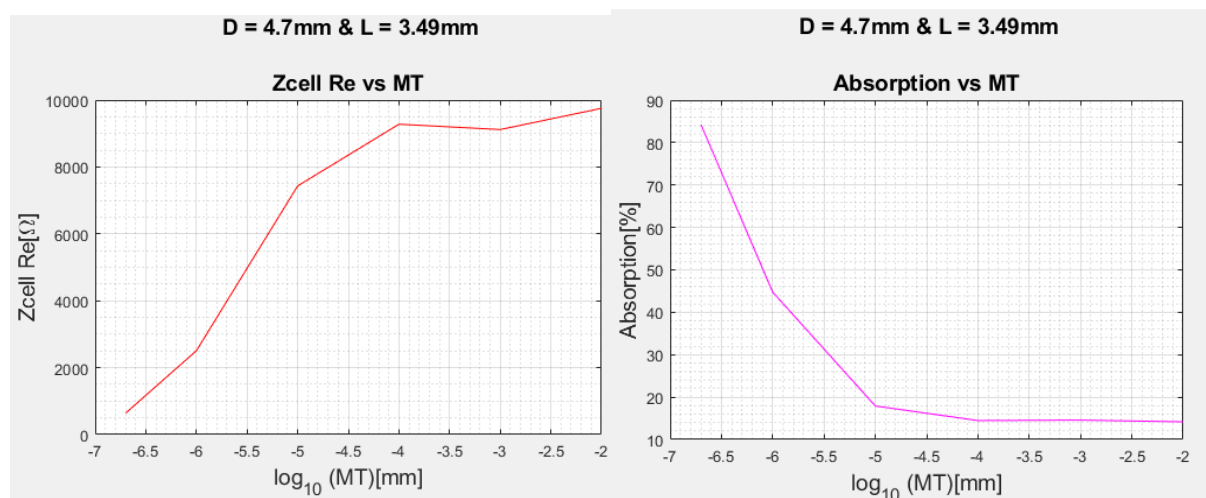
In general, the impedance of the unit cell increases when the thickness of the metal increases, and the best absorption is achieved in the case of the lowest thickness of the conductor. Anyway, a MT equal to $2e-7\text{mm}$ is physically infeasible, and then this result is purely theoretical.



(a)

(b)

Fig. 3.20 (a) Reflection coefficient for different values of metal thickness; (b) Absorption for different for different values of metal thickness. ($D=4.7\text{mm}$ $L=3.49\text{mm}$)



(a)

(b)

Fig. 3.21 (a) Behavior of the impedance for different values of metal thickness at the resonance frequency; (b) Absorption for different values of metal thickness at the resonance frequency.

($D=4.7\text{mm}$ $L=3.49\text{mm}$)

- $D=4.2\text{mm}$ and $L=3.23\text{mm}$.

Fig. 3.22 (a) and Fig. 3.22 (b) show that the behavior of the unit cell impedance is very similar to the previous case. We obtain an impedance of the cell closer to impedance of the free space for the lowest value of the thickness. The reflection coefficient shown in the Fig. 3.23(a) is slightly greater than the previous case due the dimension of the unit cell, in this case the dimension is small than the previous case.

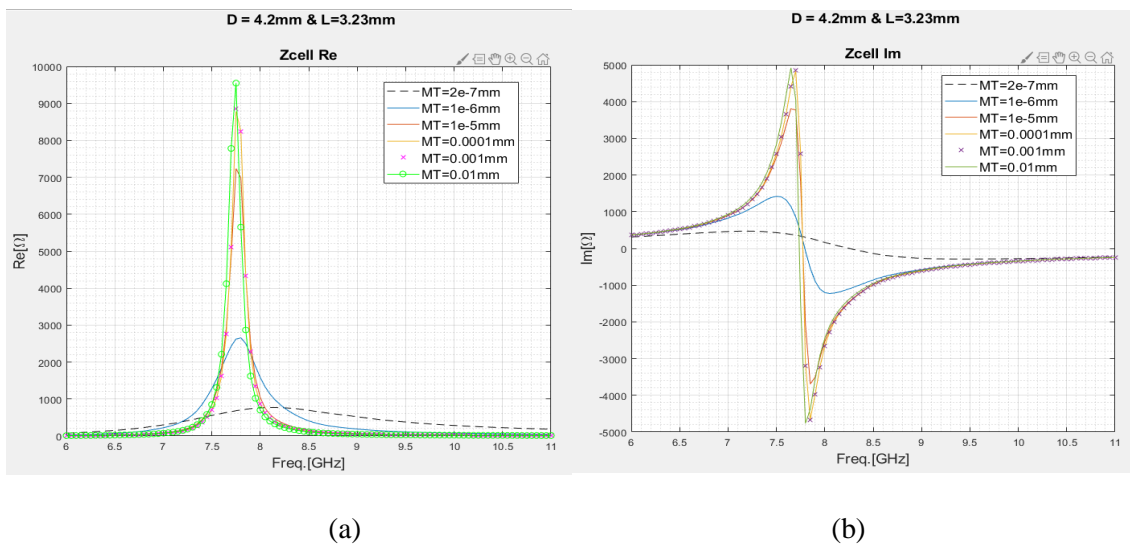


Fig. 3.22 Behavior of the impedance for different values of metal thickness ($D=4.2\text{mm}$ $L=3.23\text{mm}$): (a) Real part; (b) Imaginary part.

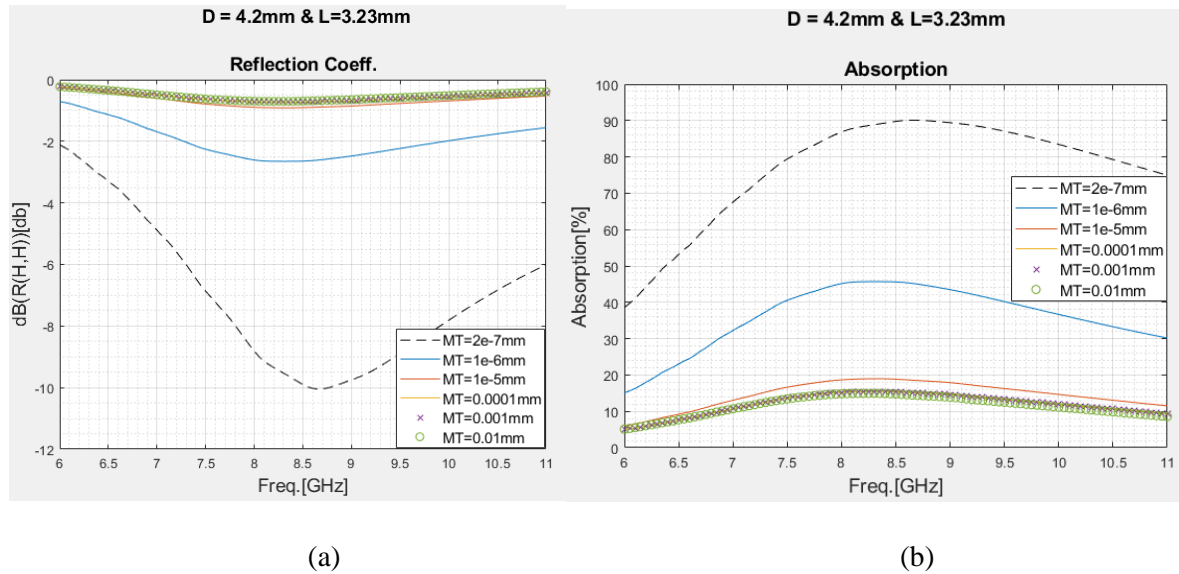


Fig. 3.23 (a) Behavior of the reflection coefficient for different values of loss tangent; (b) Absorption for different values of loss tangent. ($D=4.2\text{mm}$ $L=3.23\text{mm}$)

The behavior of the impedance and the absorption of the cell (at the resonance frequency) versus the metal thickness are shown in Fig. 3.24 (a) and Fig. 3.24 (b), respectively.

As in the previous case, the resonance frequency is equal to 7.75GHz and the impedance of the unit cell increases when the thickness of the metal increases.

In the case of a metal layer made of copper, the best absorption is achieved in the case of the lowest thickness of the conductor.

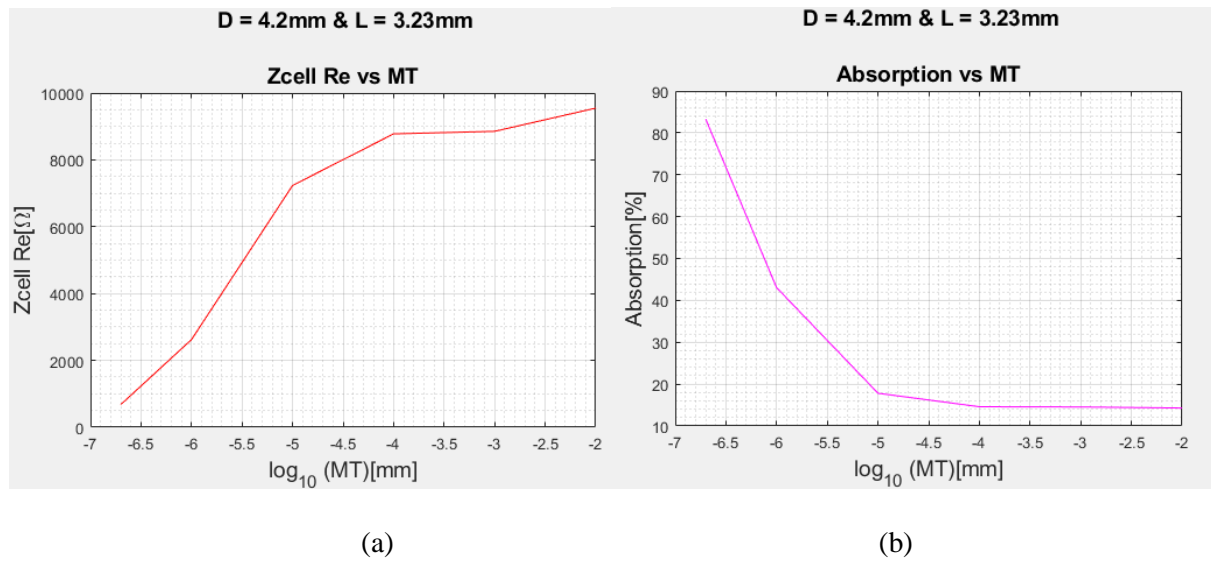


Fig. 3.24 (a) Behavior of the impedance for different values of metal thickness at the resonance frequency; (b) Absorption for different values of metal thickness at the resonance frequency.

(D=4.2mm L=3.23mm)

3.6 Unit cell behavior vs conductivity of the metal patch

In this paragraph, we will see the effects of the conductivity (σ) of the metal layer on the behavior of unit cell impedance, for different thickness. The conductivity values considered in the analysis are in some discrete points comprised between 99000 S/m and $5.8e7$ S/m.

3.6.1 D=4.7mm and L=3.49mm - substrate is FR4_epoxy: $\epsilon_r=4.4$, loss-tangent=0.02.

- **Case 1: Thickness of the conductor = 0.01mm.**

In this case, we can see in Fig. 3.25 (a) that if the conductivity increases the impedance of the cell increases too.

In Fig. 3.25 (b), we can observe that the absorption is too low for each considered conductivity value, but the lower conductivity value produces a higher absorption value. The absorption

peak is close to the frequency target, but for all conductivity values, the absorption coefficient is too small for a good absorber

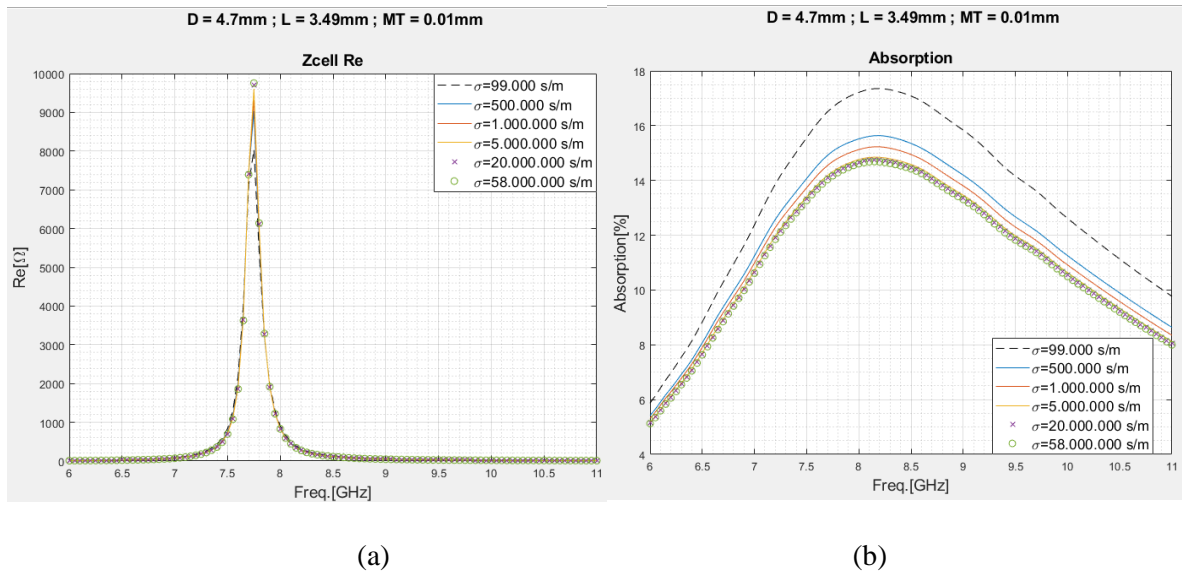


Fig. 3.25 (a) Behavior of the real part of the impedance for different values of metal conductivity;
(b) Behavior of the absorption for different values of metal conductivity. ($MT = 0.01\text{mm}$)

- **Case 2: Thickness of conductor = 0.001mm.**

In this case (Fig. 3.26 (a)), by decreasing the value of the thickness, the impedance decreases for all values of the conductivity. In particular, the lowest value of the conductivity produces the best value of the impedance. The lowest impedance of the cell corresponds to the highest value of the absorption. The absorption is still too low, for all values of the conductivity, as illustrated in Fig. 3.26 (b).

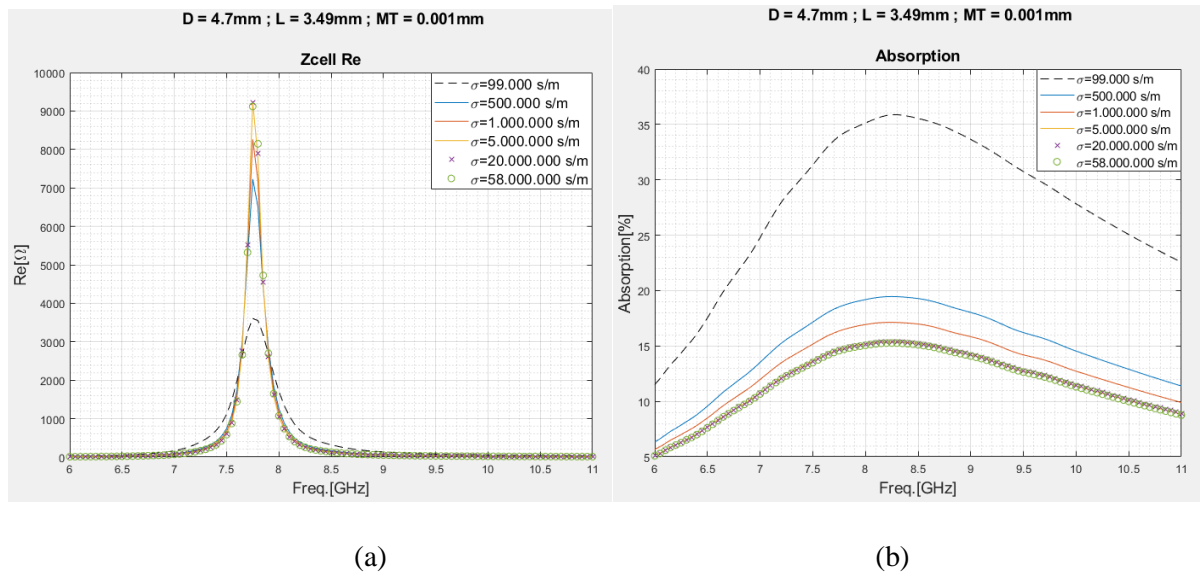


Fig. 3.26 (a) Behavior of the real part of the impedance due conductivity of the metal layer.

(b) Behavior of the absorption due conductivity of the metal layer. ($MT = 0.001\text{mm}$)

- **Case 3: Thickness of conductor = 0.0001mm.**

As in the previous cases, the plot in Fig. 3.27 (a) shows that the lowest value of the conductivity produces the lowest value of the unit cell impedance. Furthermore, Fig. 3.27 (b) shows a better absorption, but the peak is in correspondence of a higher frequency with respect to our frequency target, and the value of the absorption in our frequency target is about 80%.

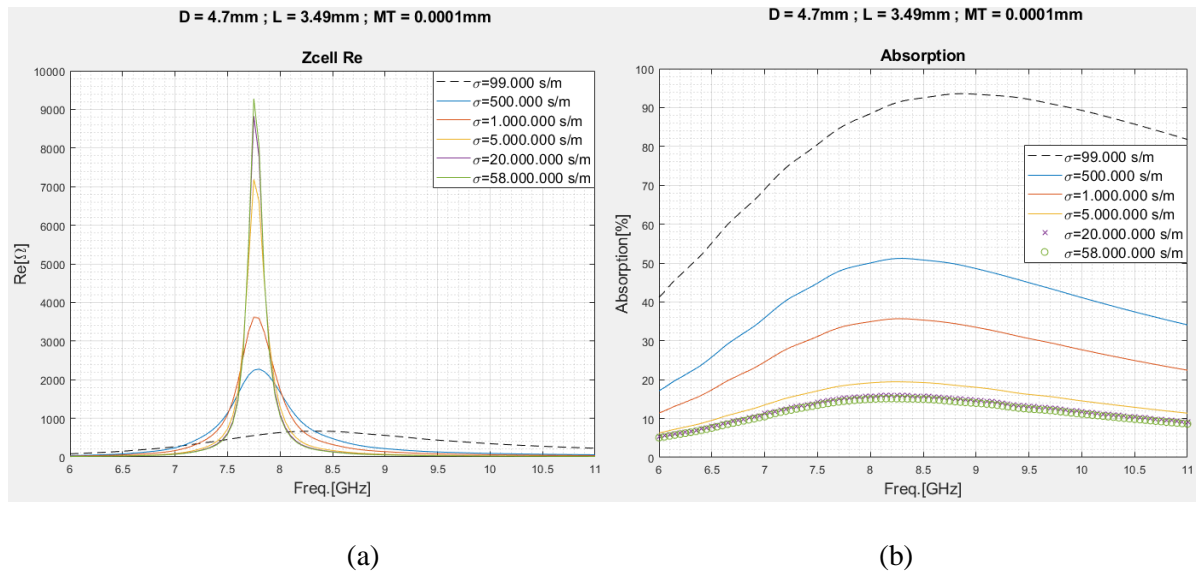


Fig. 3.27 (a) Behavior of the real part of the impedance due conductivity of the metal layer;
 (b) Behavior of the absorption due conductivity of the metal layer. ($MT = 0.0001\text{mm}$)

- **Case 4: Thickness of conductor = $1 \times 10^{-5}\text{ mm}$.**

Fig.3.28 (a) shows that, by further reducing the thickness of the conductor, the resonance frequency changes more rapidly with the conductivity variations. Furthermore, the impedance of the unit cell decreases when the conductivity decreases, except for the lowest value $\sigma=99000\text{ S/m}$. For this last value, in fact, the resonance frequency moves up to a greater value whilst the impedance increases a little.

In Fig. 3.28 (b), the absorption coefficient has the best performance in correspondence of the conductivity value equal to 500000 S/m , but the absorption peaks are in correspondence of higher frequencies than our frequency target.

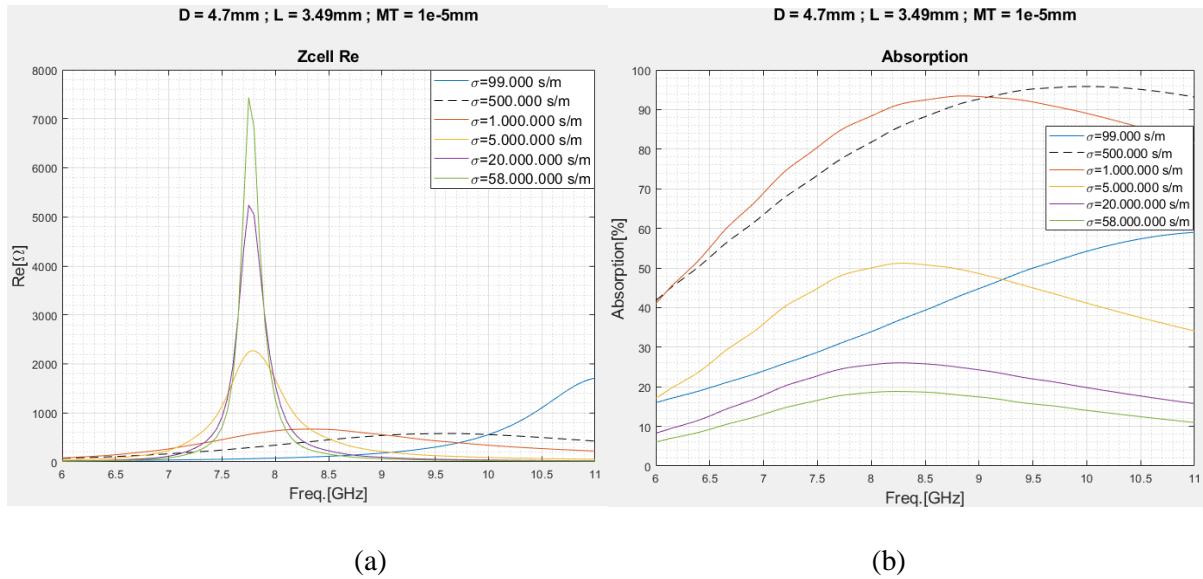


Fig. 3.28 (a) Behavior of the real part of the impedance due conductivity of the metal layer.

(b) Behavior of the absorption due conductivity of the metal layer. ($MT = 1 \times 10^{-5}\text{ mm}$)

- **Case 5: Thickness of conductor = $1 \times 10^{-6}\text{ mm}$.**

Fig. 3.29 (a) shows that by further decreasing the thickness of the conductor the behavior of the cell is quite different with respect to the previous cases. Fig. 3.29 (b) shows that the highest value of the absorption is at 10 GHz, which is far to the required frequency. The absorption in 8 GHz is not good for anyone of the values of the conductivity.

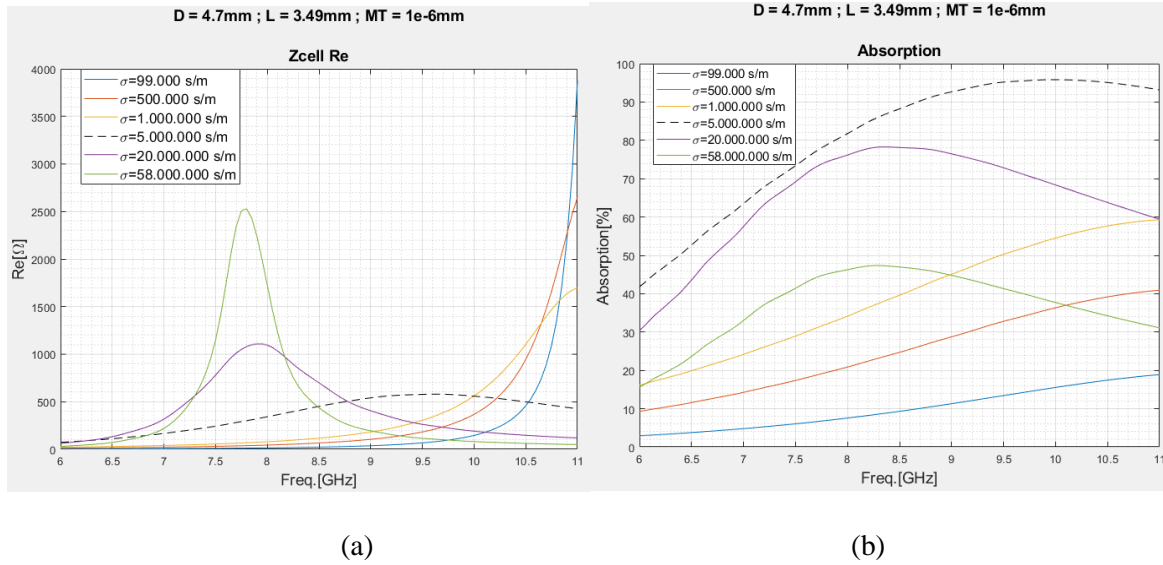


Fig. 3.29 (a) Behavior of the real part of the impedance due conductivity of the metal layer.

(b) Behavior of the absorption due conductivity of the metal layer. ($MT = 1 \times 10^{-6}$ mm)

- **Case 6: Thickness of conductor = 2×10^{-7} mm.**

In Fig. 3.30 (a), we can see that at the lowest value of the conductor thickness the two major values of conductivity produce the lowest values of the unit cell impedance and a good absorption value (Fig. 3.30 (b)). Anyway, this thickness value is too small thus it is physically infeasible.

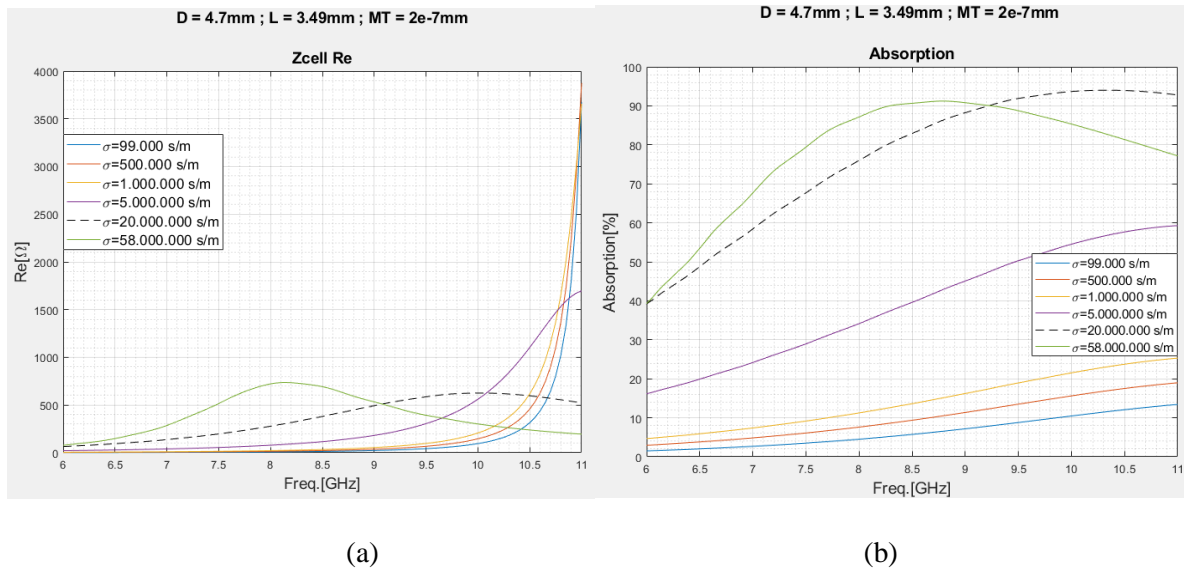


Fig. 3.30 (a) Behavior of the real part of the impedance due conductivity of the metal layer.

(b) Behavior of the absorption due conductivity of the metal layer. ($MT = 2 \times 10^{-7}\text{ mm}$)

Finally, Fig. 3.31 (a) and Fig. 3.31 (b) respectively show the behavior of the impedance and the absorption of the cell (at the resonance frequency) when we change the conductivity of the metal, for different metal thickness values. In particular, we consider the following different values of conductor's thickness that are physically feasible:

- $D=4.7\text{ mm}$, $L=3.49\text{ mm}$, $MT=0.01\text{mm}$
- $D=4.7\text{ mm}$, $L=3.49\text{ mm}$, $MT=0.001\text{mm}$
- $D=4.7\text{ mm}$, $L=3.49\text{ mm}$, $MT=0.0001\text{mm}$

In general, the impedance of the cell increases when the conductivity increases. In addition, to obtain the same value of the impedance in correspondence of a greater thickness value, the conductivity must be lower.

The best value of absorption at the resonance frequency (7.75GHz) is with the lowest value of the conductivity.

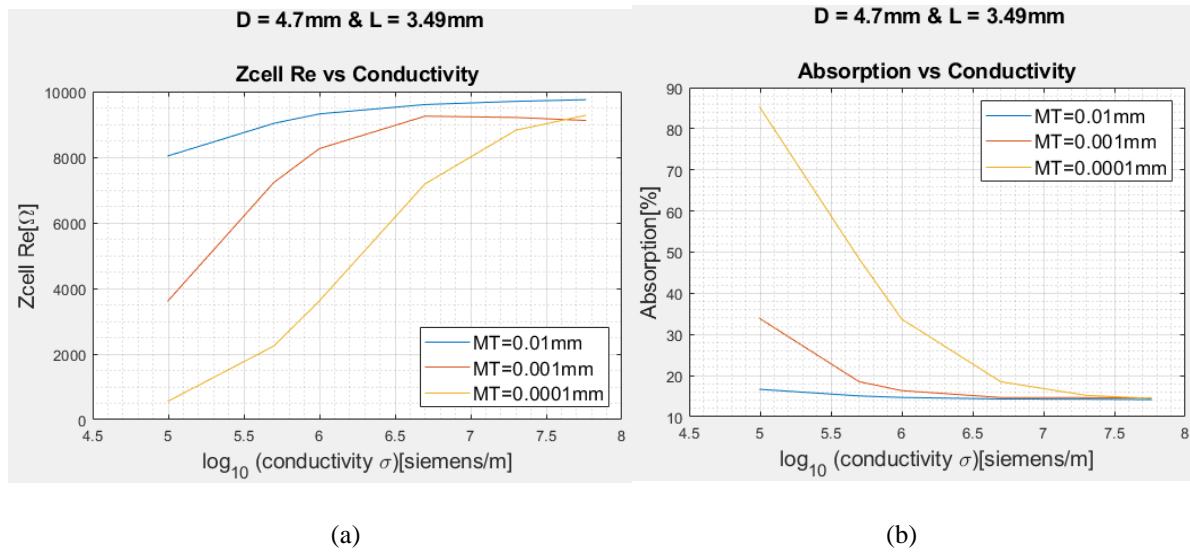


Fig. 3.31 (a) Behavior of the impedance for different values of conductivity for each metal thickness at the resonance frequency; (b) Absorption for different values of conductivity for each metal thickness at the resonance frequency. (D=4.7 mm, L=3.49 mm)

3.6.2 D=4.2mm and L=3.23mm - substrate is FR4_epoxy: $\epsilon_r=4.4$, loss-tangent=0.02.

As described below, in the case of D=4.2 mm, we get results similar to the previous case and for this reason we perform a faster analysis. In particular, we show the behavior of the impedance and the absorption of the cell (at the resonance frequency) when we change the conductivity of the metal, for different metal thickness values. As for the previous unit cell (D=4.7mm), we consider the following different values of conductor's thickness that are physically feasible:

- D=4.2 mm L=3.23 mm, MT=0.01mm
- D=4.2 mm L=3.23 mm, MT=0.001mm
- D=4.2 mm L=3.23 mm, MT=0.0001mm

The resonance frequency is 7.75GHz. Fig. 3.32 shows that the impedance of the cell increases when the conductivity increases. The highest value of absorption corresponds to the lowest value of the conductivity.

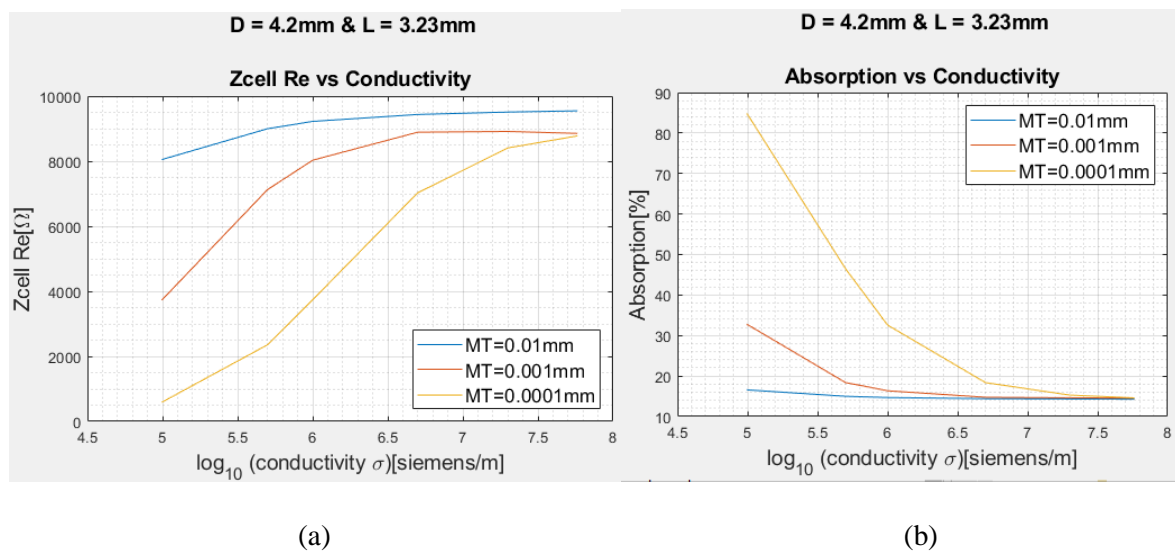


Fig. 3.32 (a) Behavior of the impedance for different values of conductivity for each metal thickness at the resonance frequency; (b) Absorption for different values of conductivity for each metal thickness at the resonance frequency. ($D=4.2\text{ mm}$, $L=3.23\text{ mm}$)

3.7 Final considerations

Analyzing the results obtained in sections 3.6.1 and 3.6.2, we can conclude that there is a relationship between the thickness of the conductor and its conductivity to achieve good performances in terms of absorption. In particular, if the conductor has a higher conductivity, the thickness must be very small, and if the conductivity is small, the thickness must be larger. For example, in the case of a metal layer made of nickel phosphorus, having conductivity

equal to 99000 S/m, a thickness equal to $1e-4$ mm is necessary to achieve an absorption greater than 80%. Whilst in the case of the copper, having a conductivity equal to $5.8e7$ S/m, the thickness must be $2e-7$ mm or less to have a good performances absorber.

Fig. 3.33 (a) and Fig. 3.33 (b) show the relationship between the impedance of the cell and the absorption of the cell ($D=4.7\text{mm}$) versus the loss tan at the resonance frequency (7.75 GHz), for the following thickness values:

- $D=4.7$ mm, $L=3.49$ mm, $MT=0.01\text{mm}$
- $D=4.7$ mm, $L=3.49$ mm, $MT=0.001\text{mm}$
- $D=4.7$ mm, $L=3.49$ mm, $MT=0.0001\text{mm}$

The impedance of the cell falls exponentially while the absorption increases almost linearly as the loss tan increases.

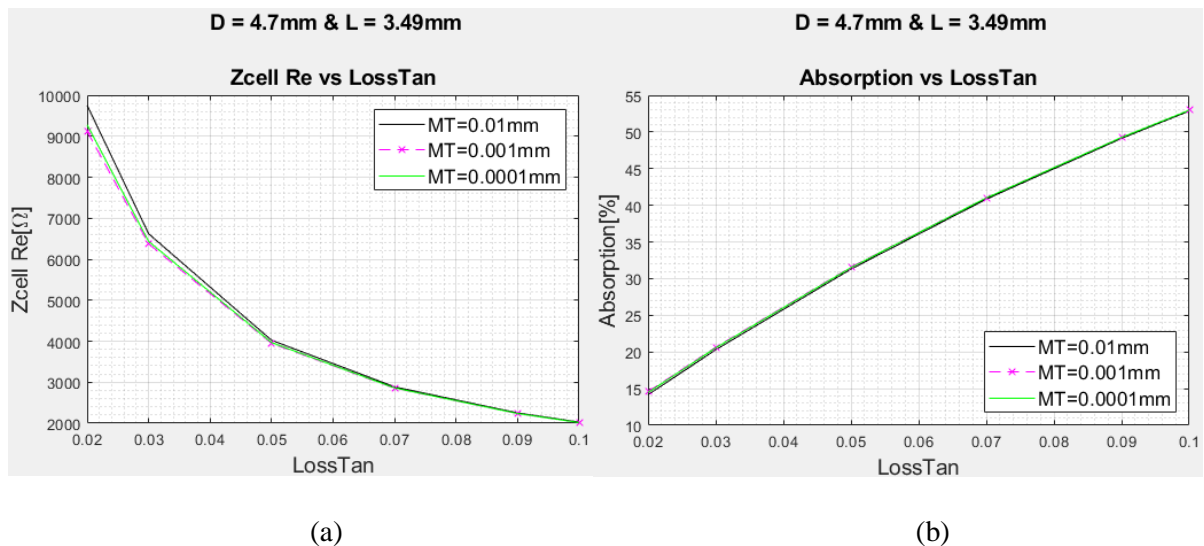


Fig. 3.33 (a) Behavior of the impedance for different values of conductivity for each metal thickness at the resonance frequency; (b) Behavior of the absorption for different values of conductivity for each metal thickness at the resonance frequency. ($D=4.7$ mm, $L=3.49$ mm)

In Fig. 3.34(a) and Fig. 3.34(b) are shown the behavior of the impedance and the absorption of the cell ($D=4.2\text{mm}$) versus the loss tan at the resonance frequency (7.75GHz), for the following thickness values:

- $D=4.2\text{ mm}$, $L=3.23\text{ mm}$, $MT=0.01\text{mm}$
- $D=4.2\text{ mm}$, $L=3.23\text{ mm}$, $MT=0.001\text{mm}$
- $D=4.2\text{ mm}$, $L=3.23\text{ mm}$, $MT=0.0001\text{mm}$

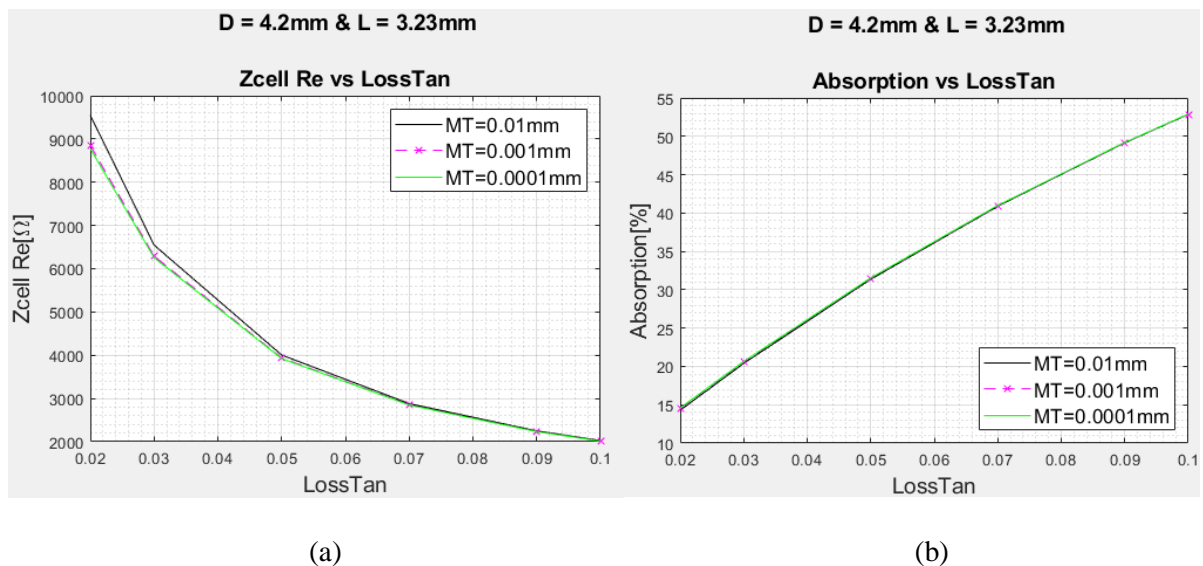


Fig. 3.34 (a) Behavior of the impedance for different values of conductivity for each metal thickness at the resonance frequency; (b) Behavior of the absorption for different values of conductivity for each metal thickness at the resonance frequency. ($D=4.2\text{ mm}$, $L=3.23\text{ mm}$)

If the loss tangent increases, the impedance of the cell decreases. In addition, if the loss tan increases the value of the absorption increases too. For this reason, we can improve the absorption of the unit cell by increasing the value of the loss tan, a variation of 0.1 in the value of the loss tan represents an increase of 5% in the absorption of the unit cell. The problem at

this point is to get a dielectric material with high loss tan. In conclusion, the main parameters to be exploited to improve the absorption of the unit cell are the conductivity and the thickness of the metal patch.

3.8 Design of a single layer metamaterial unit cell for the reduction of radiated emissions

Taking into account the results achieved in the parametric analysis, we design a single layer unit cell with good performances in terms of absorption. We fix the metal's thickness and the conductivity and we looking for the size of the patch to obtain a resonance frequency at 8 GHz.

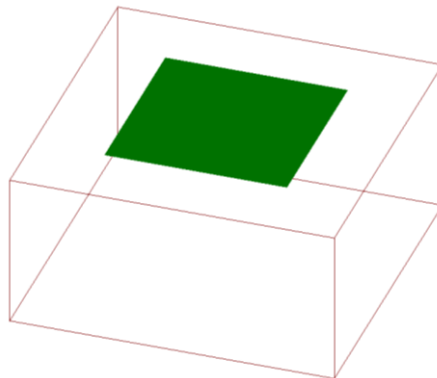


Fig. 3.35 Illustration 3D of the unit cell.

	Name	Type	Material	Drag Mode	Thickness	Lower Elevation	Upper Elevation	Roughness
—	patch	signal	Nickel Phosphorus	middle align	0.0001mm	3.19995mm	3.20005mm	0mm
▨	sub	dielectric	FR4_epoxy		3.2mm	0mm	3.2mm	
■	groundplane	metalizedsignal	copper	middle align	0mm	0mm	0mm	0mm

Fig. 3.36 Edit layers of the unit cell.

Fig. 3.35 shows the unit cell design in the software Ansoft Design V3. Fig. 3.36 shows the layers structure of the unit cell. The metallic layer is of nickel-phosphorus material (conductivity $\sigma=99000$ S/m) with a thickness of 0.0001 mm.

The dielectric substrate is FR4_epoxy: permeability $\epsilon_r=4.4$, loss-tangent=0.02. The thickness of the dielectric substrate is equal to 3.2mm. Parametric simulations with respect to the patch size (L) are performed to move the resonance down to 8 GHz, for different unit cell sizes (D x D).

- **D×D=4.7mm×4.7mm.**

Fig. 3.37(a) and Fig. 3.37(b) show that when the value of L increases, the resonance frequency decreases. Fig. 3.38(a) shows the reflection coefficient computed in correspondence of each considered value of L. We can observe that the cell resonates at 8 GHz when L is equal to 3.9mm. Fig. 3.38(b) shows that the absorber has a good behavior at our frequency target and around it. When L is equal to 3.9mm, the resonance frequency is very close to our target (8GHz) and the absorption is very high (99%).

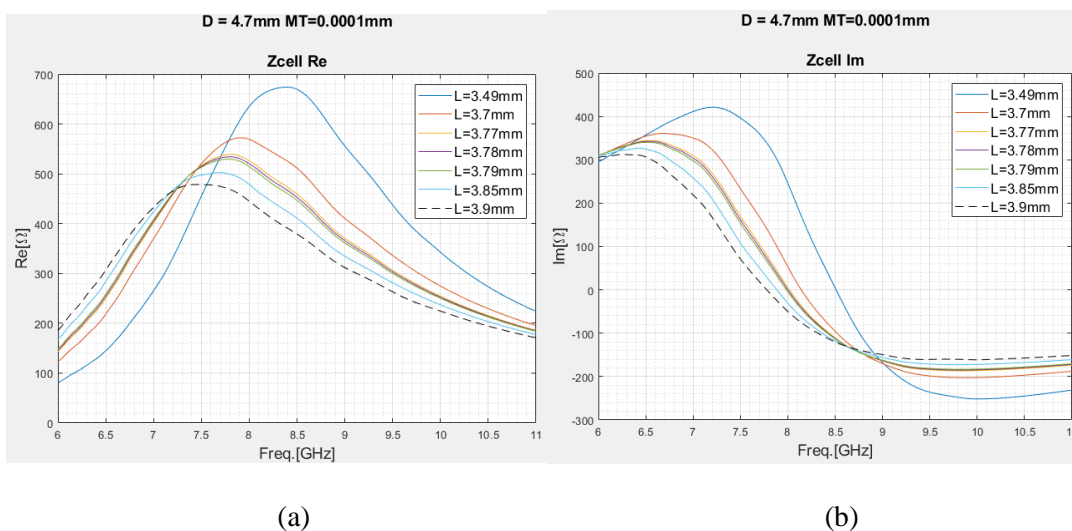


Fig. 3.37 Behavior of the impedance for different values of L (D=4.7 mm, MT=0.0001 mm): (a) Real part; (b) Imaginary part.

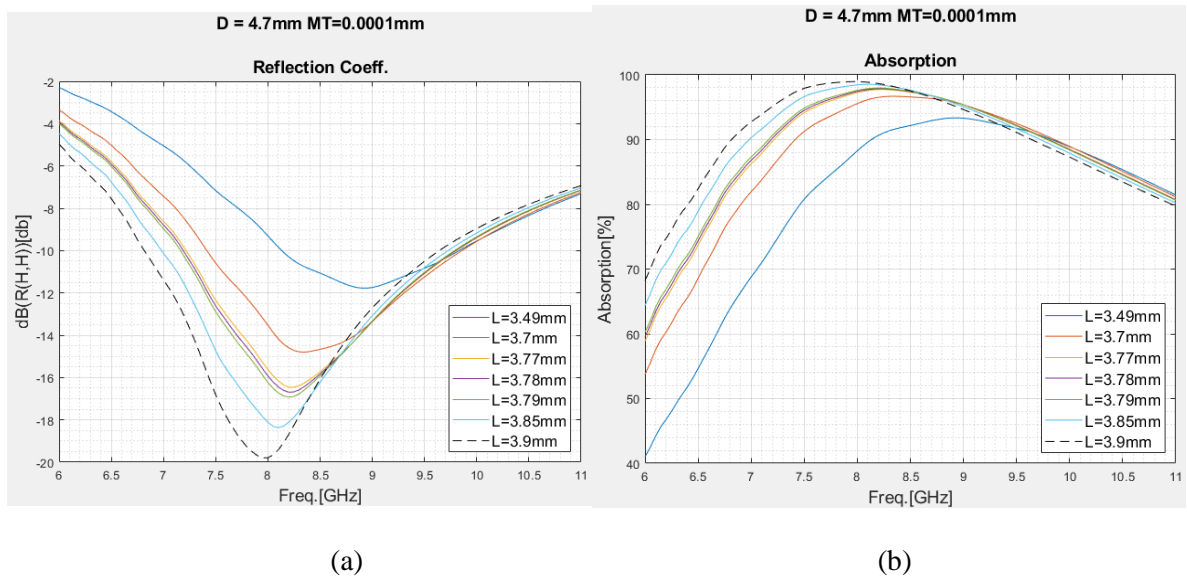


Fig. 3.38 (a) Reflection coefficient; (b) Absorption coefficient. ($D=4.7$ mm, $MT=0.0001$ mm)

- **$D \times D = 4.2\text{mm} \times 4.2\text{mm}$**

Fig. 3.39(a) and Fig. 3.39(b) show that when the value of L increases, the resonance frequency decreases. Fig. 3.40(a) shows the reflection coefficient computed in correspondence of each considered value of L . We can observe that the cell resonates at 8 GHz when L is equal to 3.55mm. Fig. 3.40(b) shows that the absorber has a good behavior at our frequency target and around it, but with $L=3.6\text{mm}$ the resonance frequency is lower than 8GHz, but the absorption is the best.

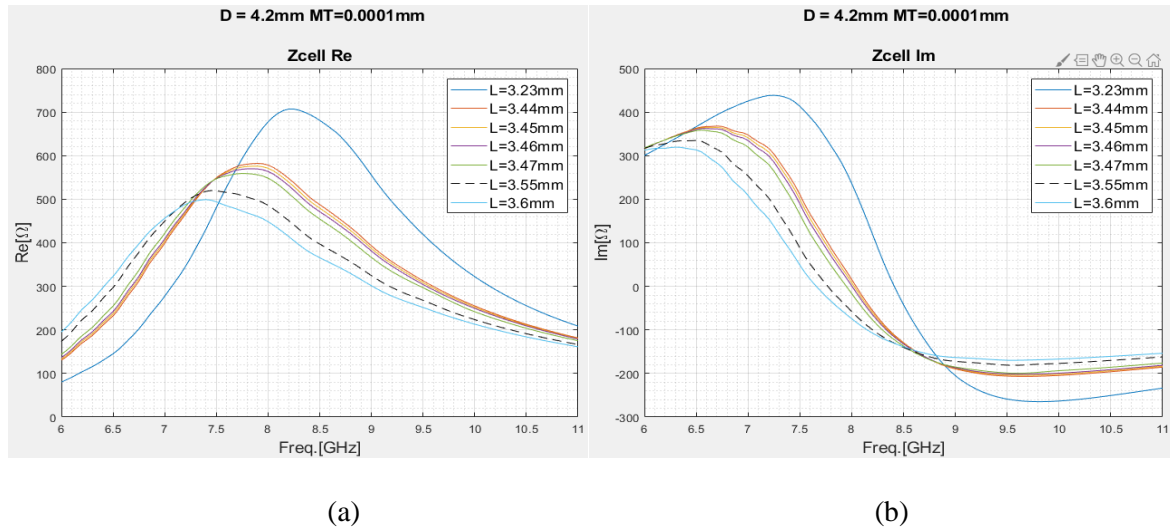


Fig. 3.39 Behavior of the impedance for different values of L ($D=4.2$ mm, $MT=0.0001$ mm): (a) Real part; (b) Imaginary part.

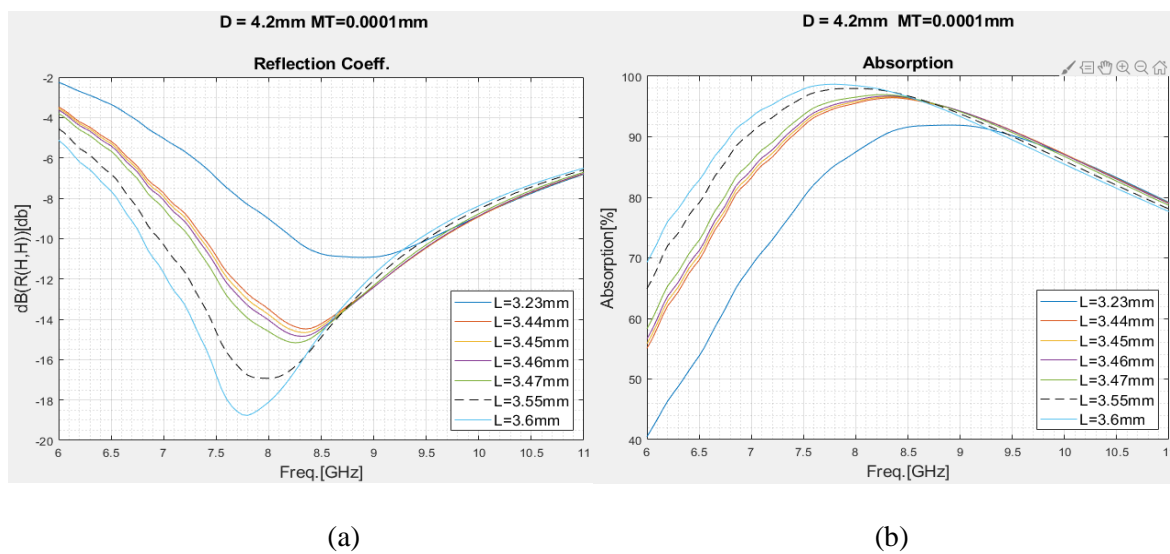


Fig. 3.40 (a) Reflection coefficient; (b) Absorption coefficient. ($D=4.2$ mm, $MT=0.0001$ mm)

Analyzing all the cases, we can conclude that when we reduce the unit cell (D) we have to reduce the patch size to fix the resonance to 8 GHz, and the same in the reverse way. The absorption is better in the case of the larger size length of the unit cell than the small one.

CHAPTER IV

ANALYSIS AND DESIGN OF MINIATURIZED ABSORBER CELLS FOR RADIATED EMISSION REDUCTION

4.1 Introduction

In the previous chapter, we analyzed the effects of several unit cell parameters. We have seen that there is a relationship between some parameters and the absorption, such as the thickness of the metal patch and its conductivity. The results obtained from the parametric analysis have been exploited to design a unit cell with dimensions similar to those of the paper taken as a reference [36], but with the great advantage of having a structure composed by a single layer of a periodic metal pattern instead of the two-layer structure illustrated in [36] and discussed in chapter II.

This simpler single-layer structure avoids assembly and alignment problems, making the manufacturing step easier and cheaper.

The aim of this chapter is to exploit fractal geometries to reduce the dimensions of the unit cell.

The use of smaller cells, in fact, allows to put more elements in the same area, improving the performance of the absorber and making more accurate the assumption based on the use of a periodic and infinite array, usually adopted for the analysis of metamaterials.

In the following paragraphs an accurate analysis of the unit cell was performed, with the aim of obtaining a perfect absorber with unit cell dimensions much lower than 4.7 mm x 4.7 mm (Basic structure).

4.2 Fractal Structure ^[37]

The proposed absorber scheme is shown in Fig. 4.1. It is composed of a surface formed by metallic fractal patches printed on a dielectric substrate, which is placed on a ground plane.

Fractal patches, in general, have the advantage of being miniaturized. In particular, with a Minkowski patch of size $L \times L$ and scale factor S it is not necessary to have a very large length L to obtain a small resonance frequency, because fixed the length of the patch L , we can obtain the resonance frequency by varying the value of the scale factor S .

In this case, the resonance length is not determined only by the dimension L , but it also depends on the scale factor S , so the effective resonance length is greater and is equal to:

$$L_{eff} = (1 + 2S)L$$

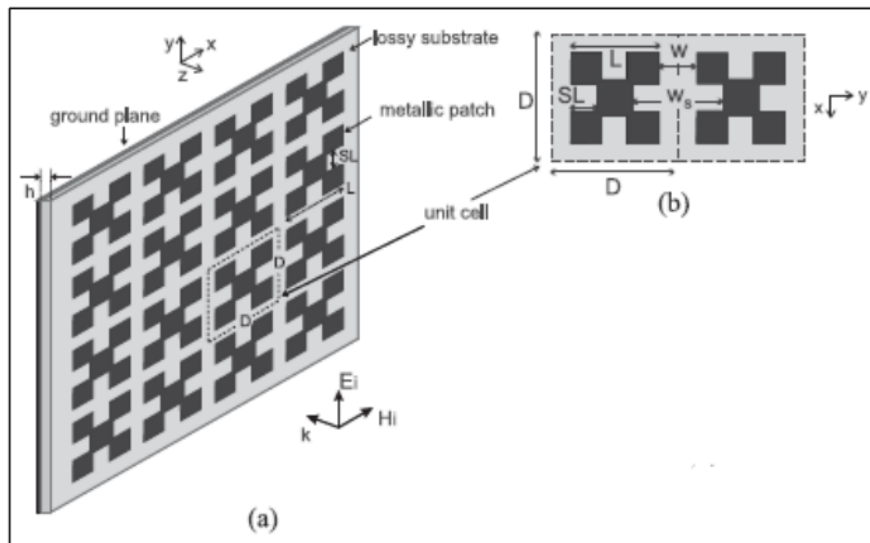


Fig. 4.1 Structure of the fractal metamaterial absorber a) Image 3D b) Unit cell geometry.

The configuration of the metamaterial unit cell proposed in this chapter is illustrated in Fig. 4.2. The layers and the materials used are shown in Fig. 4.3. The metallic layer is of nickel-phosphorus material (conductivity $\sigma=99.000$ siemens/m) with a thickness of 0.0001 mm. The dielectric substrate is FR4_epoxy: permeability $\epsilon_r=4.4$, loss-tangent=0.02. The thickness of the dielectric substrate is equal to 3.2mm. The scalar factor S can vary between 0 up to $1/3$.

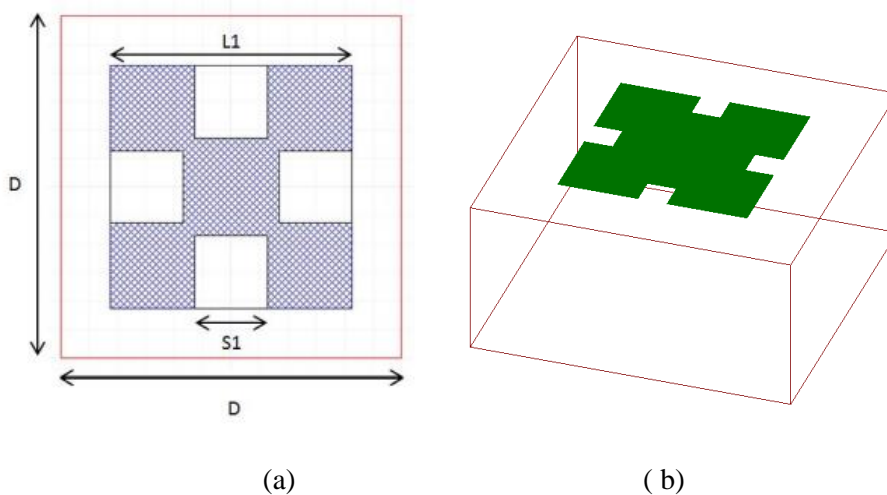


Fig. 4.2 Geometry of the unit cell: (a) View 2D; (b) View 3D

	Name	Type	Material	Drag Mode	Thickness	Lower Elevation	Upper Elevation	Roughness
—	patch	signal	Nickel Phosphorus	middle align	0.0001mm	3.19995mm	3.20005mm	0mm
▨	sub	dielectric	FR4_epoxy		3.2mm	0mm	3.2mm	
■	groundplane	metalizedsignal	copper	middle align	0mm	0mm	0mm	0mm

Fig. 4.3 Layers of Fractal structure in Ansoft Designer V3.

In the next section the parametric simulations of the cell are performed, by varying S and reducing the size of the unit cell.

4.3 Analysis versus the scaling factor S

In this section a parametric analysis versus the scaling factor S is performed, for different dimensions of the unit cell ($D \times D$) and different dimensions of the metallic patch (L).

4.3.1 Unit Cell $D \times D = 4.7 \text{ mm} \times 4.7 \text{ mm}$.

In section 3.8 we choose $L = 3.9 \text{ mm}$ to get the resonance frequency at 8GHz, with a square metallic patch. With that value, we begin the parametric analysis for a fractal patch. The considered discrete values of S are 0.1, 0.15 and 0.2.

- $D=4.7\text{mm} - L=3.9\text{mm}$.

In Fig. 4.4, we can see that when S increases the resonance frequency increases too.

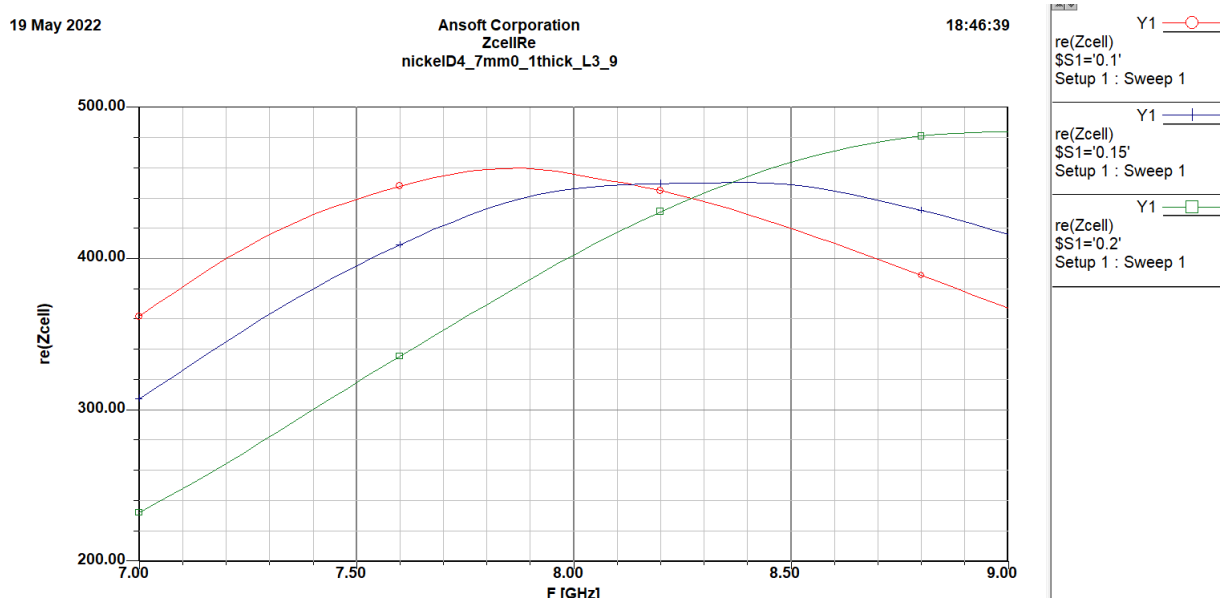


Fig. 4.4 Real part of the unit cell impedance for different values of S ($D=4.7$ mm, $L=3.9$ mm).

Fig. 4.5 shows the behavior of the absorption for each value of S . In correspondence of the target frequency, the absorption decreases when S increases. By analyzing the behavior of the resonant frequency, we conclude that, for a fixed size of D , we can increase the value of L to reduce the resonant frequency and at the same time we can increase S to achieve a near-perfect absorption at our target frequency.

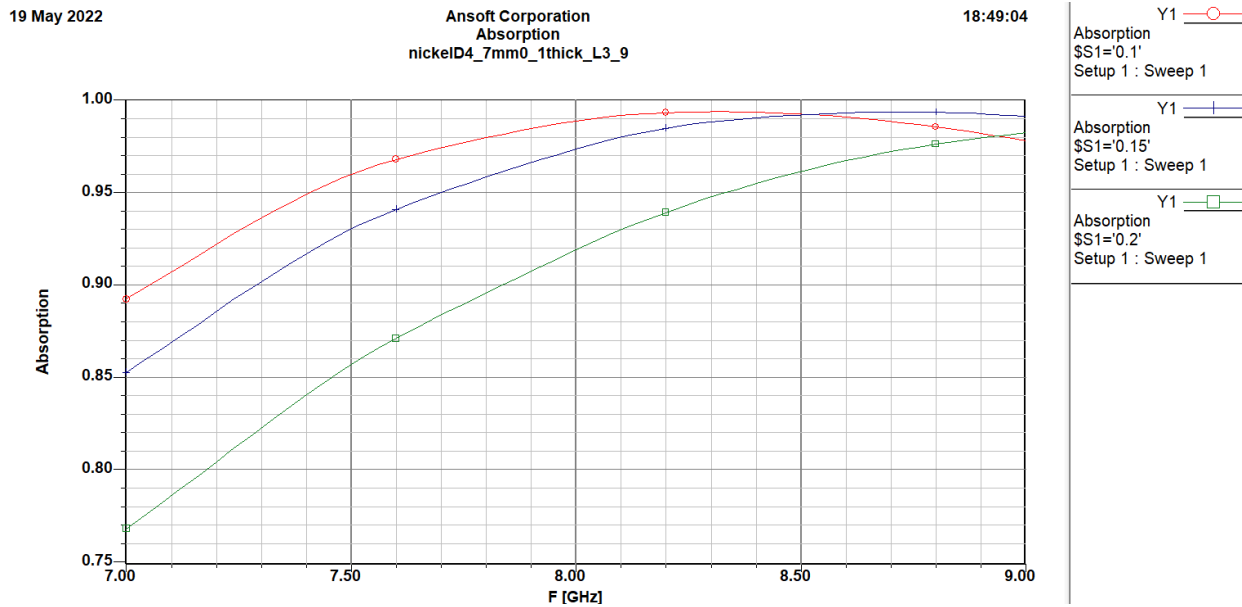


Fig. 4.5 Absorption of the unit cell for different values of S ($D=4.7$ mm, $L=3.9$ mm).

In the next analysis, L will be increased until obtaining a practically unitary absorption (perfect absorber) at 8GHz.

- **$D=4.7mm$ $L=4mm$.**

Fig. 4.6 illustrates the impedance (real part) of the unit cell; we can see that the impedance is lower than the previous case. Fig. 4.7 shows the absorption of the unit cell for each value of S, in this case when $S=0.1$ the absorption is near to 1 at 8 GHz, but is not a perfect absorber yet.

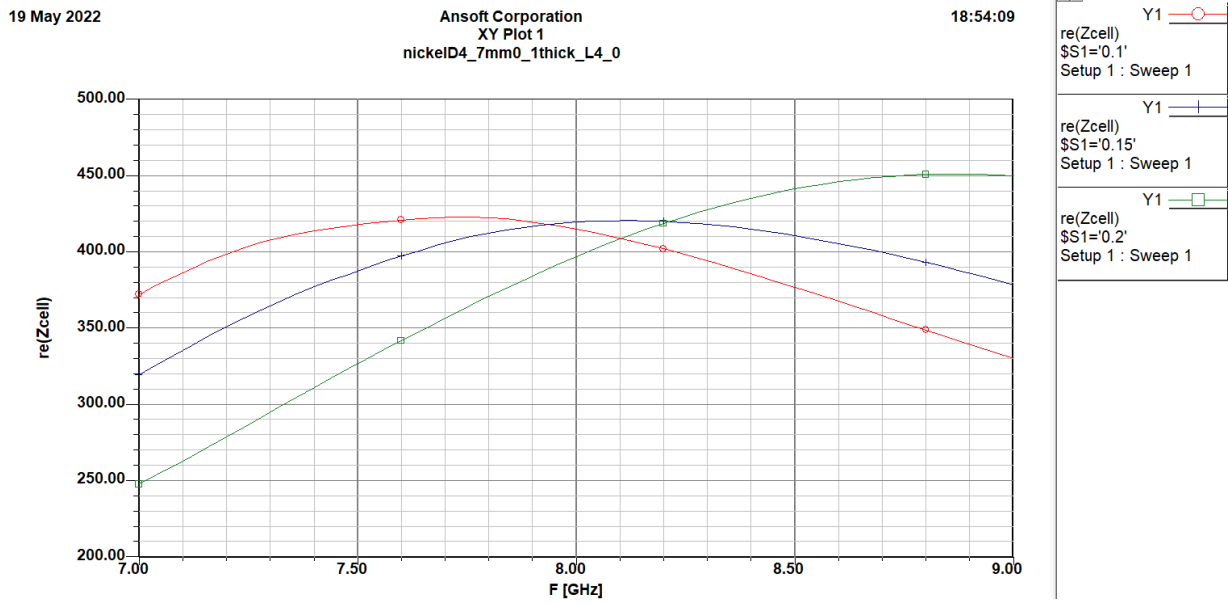


Fig. 4.6 Real part of the unit cell impedance for different values of S (D=4.7 mm, L=4 mm).

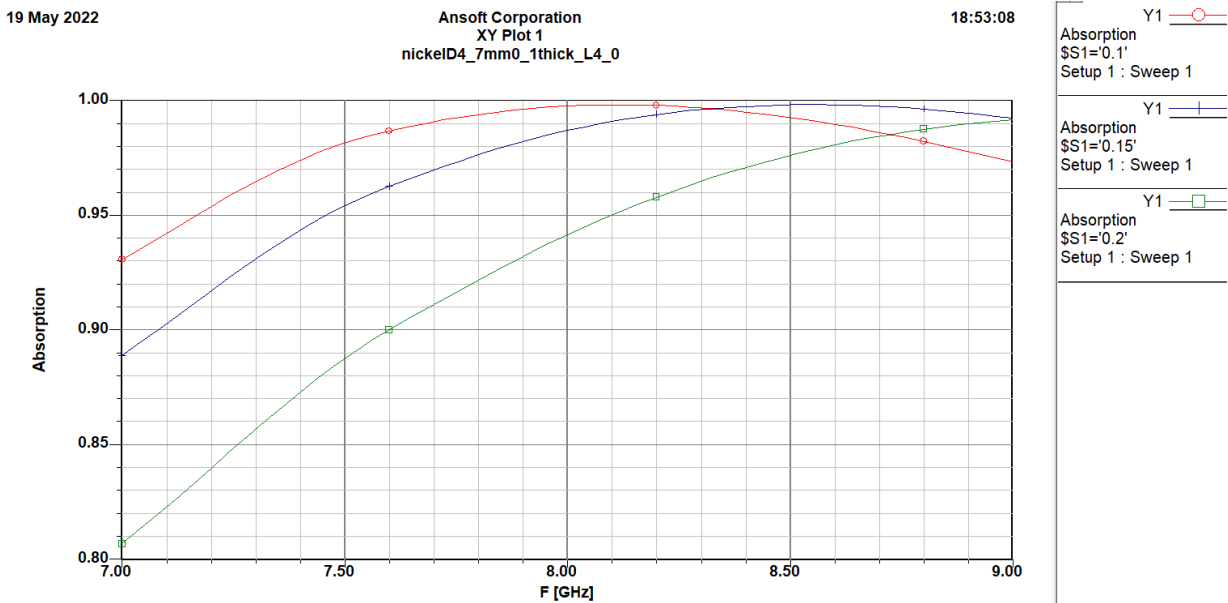


Fig. 4.7 Absorption of the unit cell for different values of S (D=4.7 mm, L=4 mm).

- $D=4.7\text{mm}$ $L=4.1\text{mm}$.

Fig. 4.8 shows that by increasing L the impedance decreases. Fig. 4.9 shows the absorption of the unit cell for each value of S, in this case with $S=0.1$ the absorption is very near to 1 at 8 GHz.

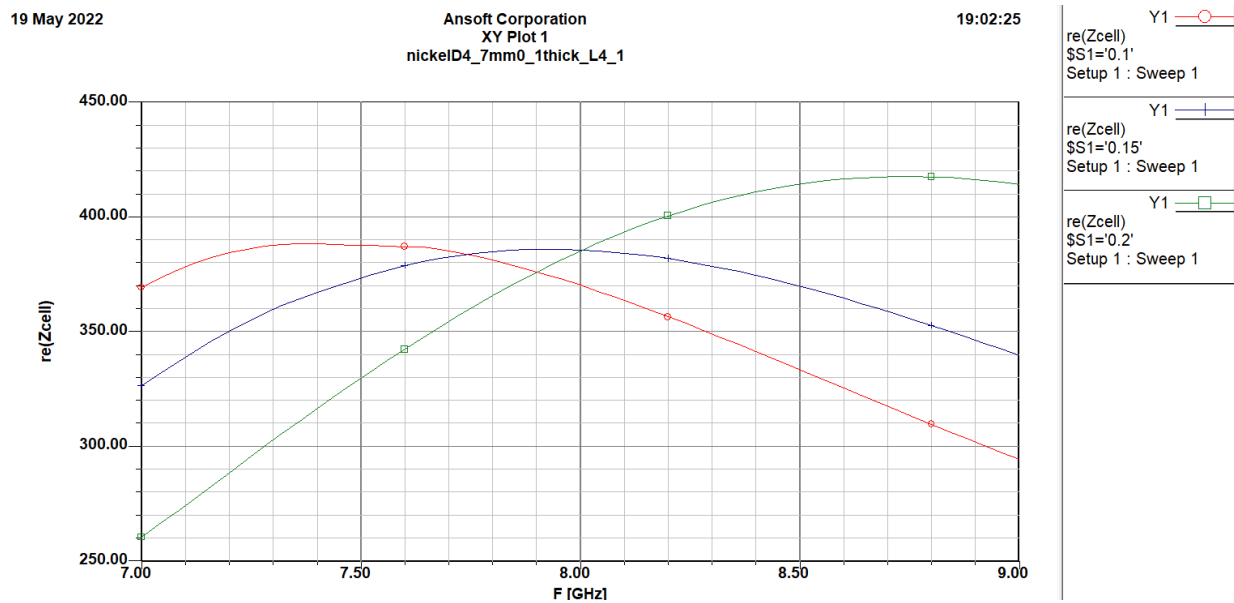


Fig. 4.8 Real part of the unit cell impedance for different values of S ($D=4.7$ mm, $L=4.1$ mm).

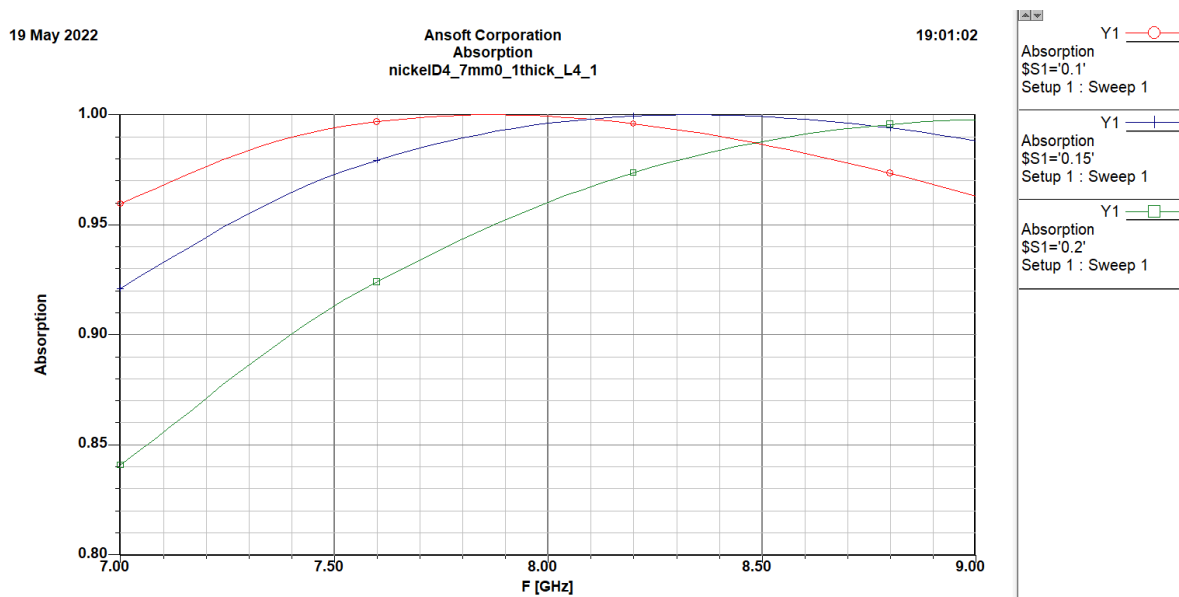


Fig. 4.9 Absorption of the unit cell for different values of S ($D=4.7$ mm, $L=4.1$ mm).

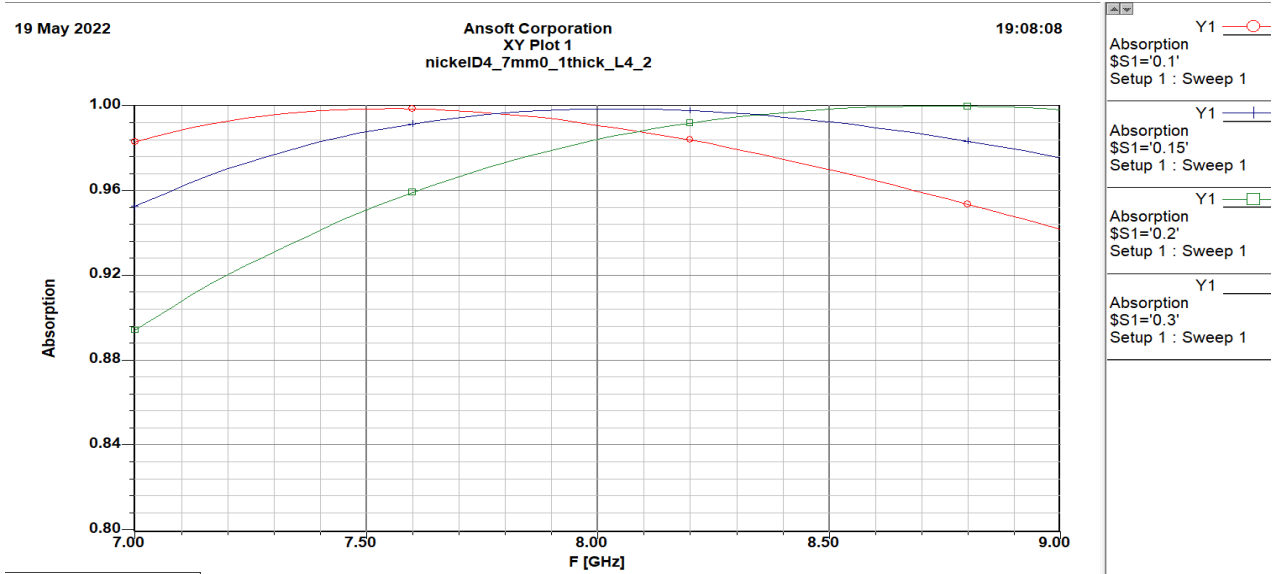


Fig. 4.11 Absorption of the unit cell for different values of S (D=4.7 mm, L=4.2 mm).

In Fig. 4.12, we can see the behavior of the impedance of the unit cell with a scaling factor equal to 0.15, for different values of L. It is evident that when the patch length increases the impedance of the unit cell decreases. Fig. 4.13 illustrates that for a fixed a scalar factor equal to 0.15 the best absorption is achieved for L equal to 4.2mm.

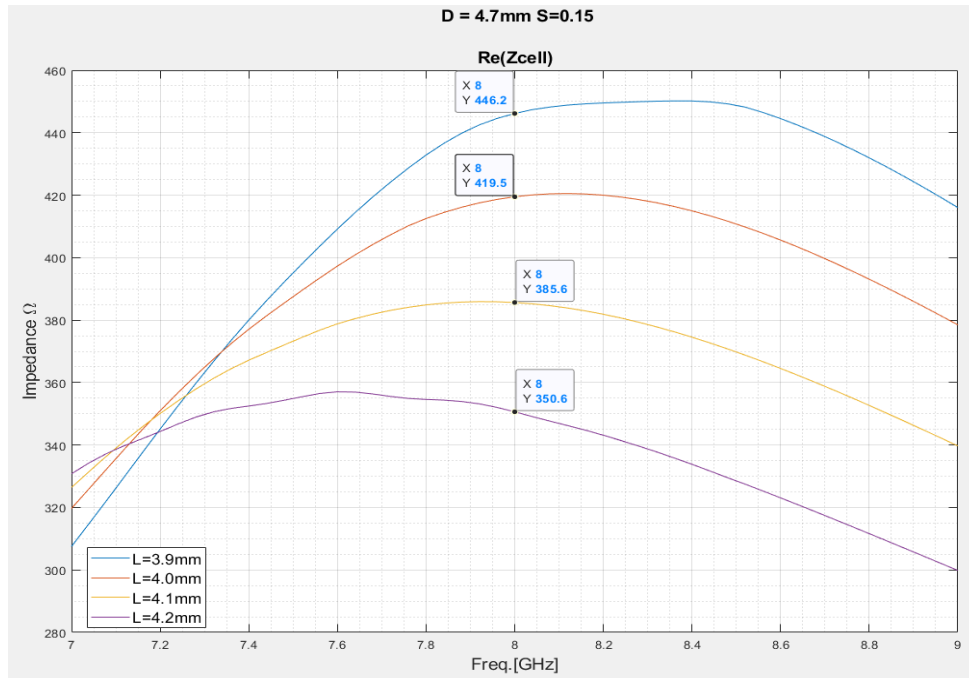


Fig. 4.12 Unit cell impedance for different values of L and S=0.15 (D=4.7 mm).

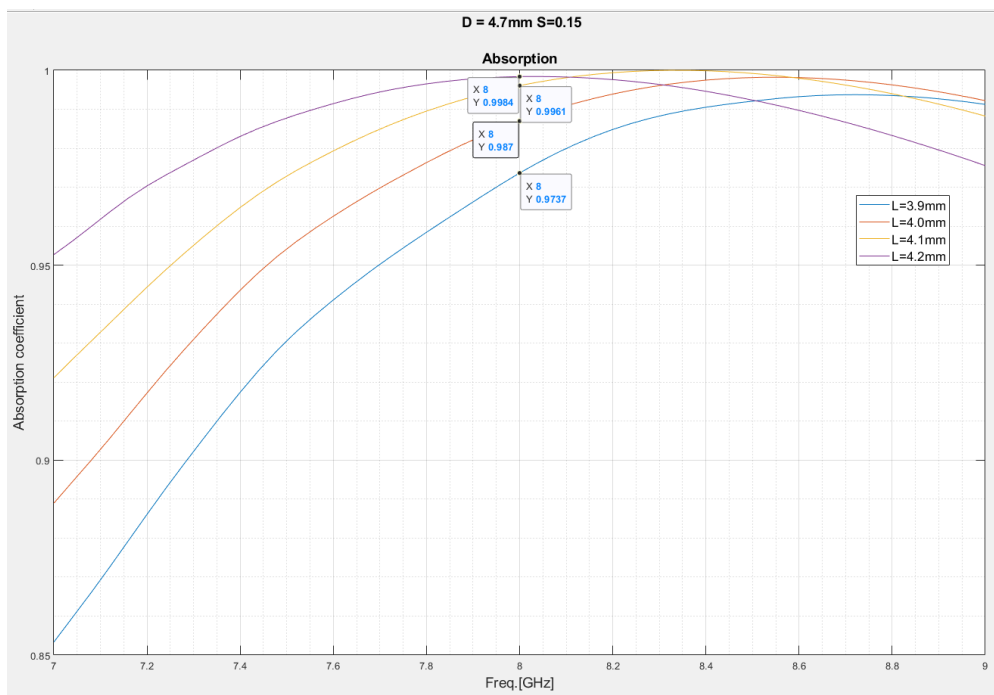


Fig. 4.13 Absorption of the unit cell for different values of L and S=0.15 (D=4.7 mm).

Now we know the behavior of the impedance and absorption of the unit cell due to the different parameters, in particular the size of the metallic patch, L , and the fractal-scaling factor, S .

The previous analysis is replicated for smaller unit cells and the results of the best absorption will be shown below.

4.3.2 Unit Cell $D \times D = 4.2 \text{ mm} \times 4.2 \text{ mm}$.

In Fig. 4.14 is illustrated the behavior of the impedance of the unit cell with a scaling factor equal to 0.15, for different values of L . We can see that when the L increases the impedance of the unit cell decreases.

For the different values of L , we can obtain different values of the absorption. Fig. 4.15 shows that in this case the best option is the second bigger value of L (3.8mm).

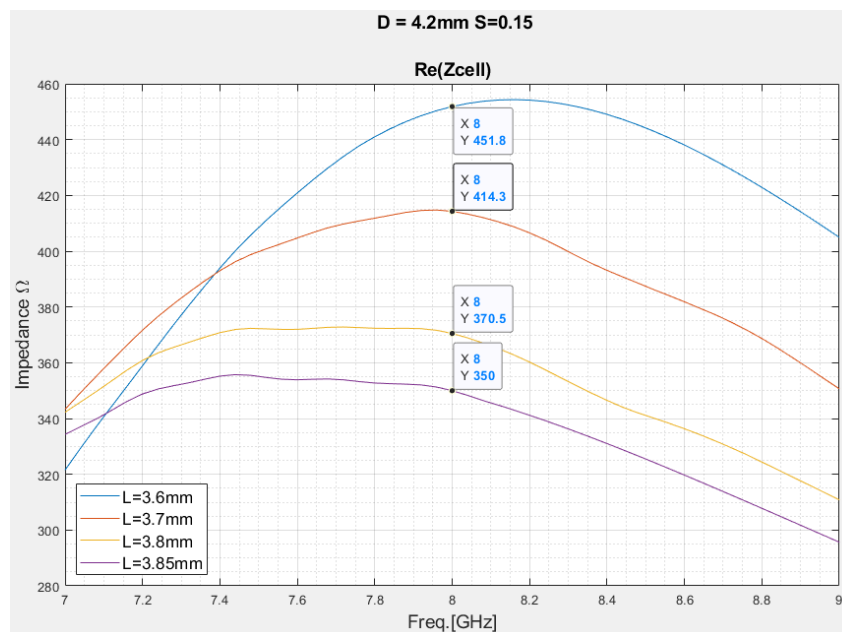


Fig. 4.14 Unit cell impedance for different values of L and $S=0.15$ ($D=4.2 \text{ mm}$).

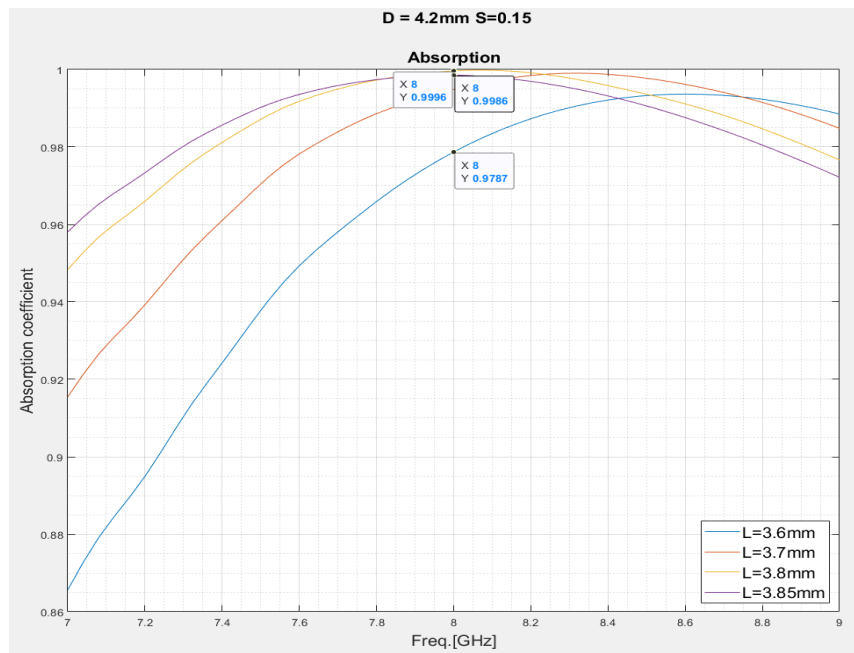


Fig. 4.15 Absorption of the unit cell for different values of L and S=0.15 (D=4.2 mm).

4.3.3 Unit Cell $D \times D = 3.8 \text{ mm} \times 3.8 \text{ mm}$.

In this case, the first value of L is set to 3.18mm. In Fig. 4.16, we can see the behavior of the impedance of the unit cell with S equal to 0.15, for different values of L. As in the previous cases, when the patch dimension increases the impedance of the unit cell decreases.

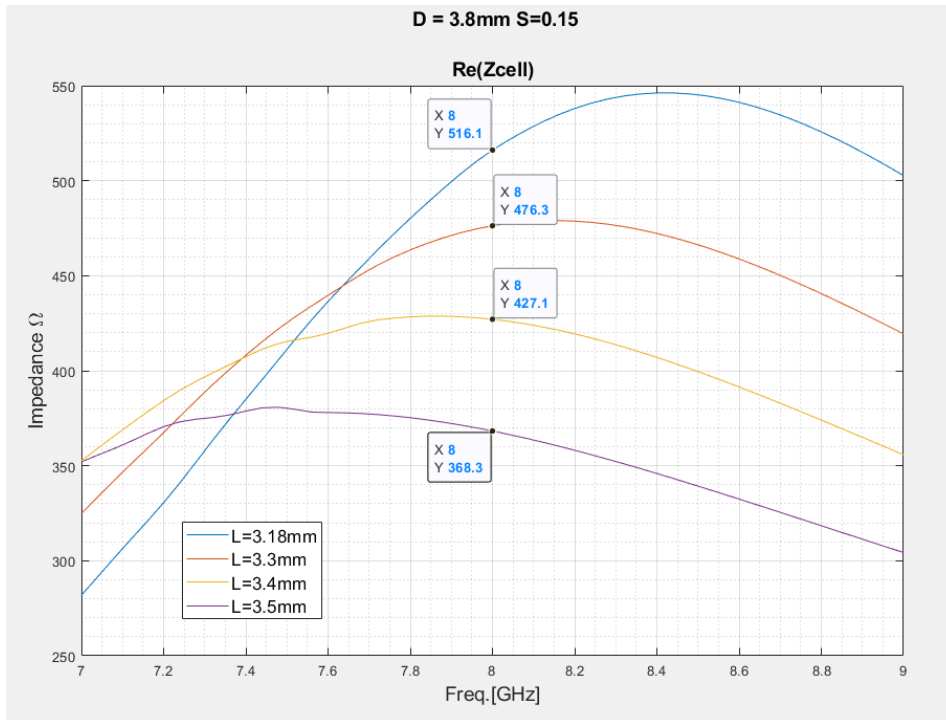


Fig. 4.16 Unit cell impedance for different values of L and S=0.15 (D=3.8 mm).

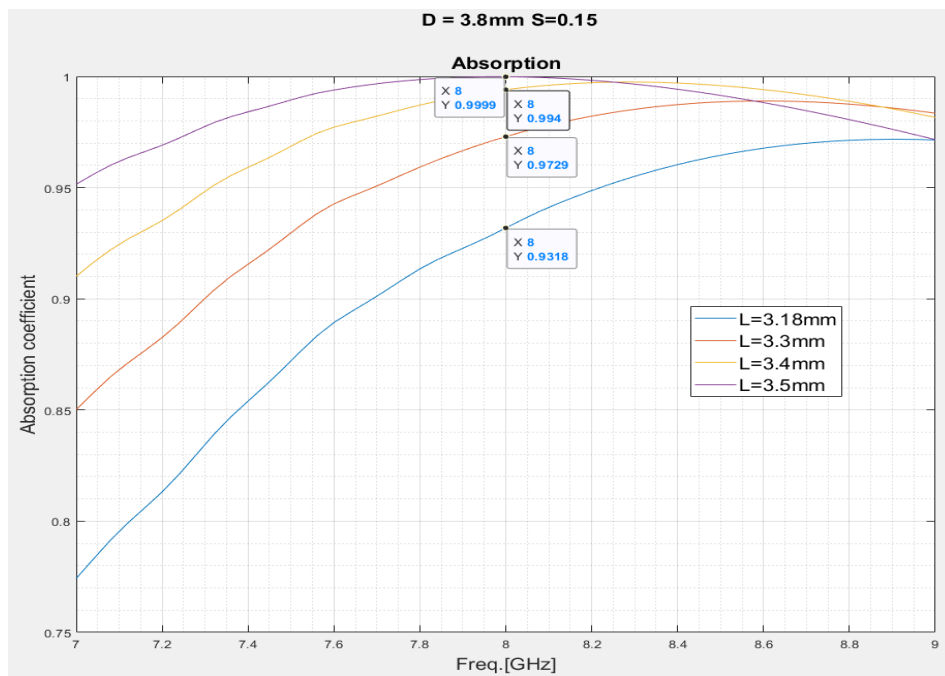


Fig. 4.17 Absorption of the unit cell for different values of L and S=0.15 (D=3.8 mm).

In Fig. 4.17, we can observe that the best absorption at our frequency target is achieved when L is equal to 3.5mm. Analyzing the results of all unit cells, we can obtain a relationship between the ratio of the area of the metallic path and the unit cell area and the unit cell impedance.

By considering the area of the metallic patch equal to $A_p = (L \times L) - 4(S \times L)^2$, and the area of the unit cell equal to $A_c = D \times D$, we define the ratio:

$$\frac{\text{Metallic Patch Area}}{\text{Unit Cell Area}} = \frac{A_p}{A_c} = \frac{(L \times L) - 4(S \times L)^2}{D \times D}$$

Table 4.1 shows the relationship between the ratio $\frac{A_p}{A_c}$ and the impedance of the unit cell for different resonant cells. Furthermore, Fig. 4.18 shows that, for all considered cases, the traces have a similar behavior. When the ratio $\frac{A_p}{A_c}$ increases the value of the impedance decreases. However, a smaller unit cell has a higher impedance than larger unit cells for the same value of the ratio $\frac{A_p}{A_c}$

D	S	L	area	MetallicPatchArea/CellArea	Impedance
4.7	0.15	3.9	13.8411	0.626577637	446.2
4.7	0.15	4	14.56	0.659121775	419.5
4.7	0.15	4.1	15.2971	0.692489814	385.6
4.7	0.15	4.2	16.0524	0.726681756	350.6
4.2	0.15	3.6	11.7936	0.668571429	451.8
4.2	0.15	3.7	12.4579	0.706230159	414.3
4.2	0.15	3.8	13.1404	0.744920635	370.5
4.2	0.15	3.85	13.488475	0.764652778	350
3.8	0.15	3.18	9.202284	0.637277285	516.1
3.8	0.15	3.3	9.9099	0.686281163	476.3
3.8	0.15	3.4	10.5196	0.728504155	427.1
3.8	0.15	3.5	11.1475	0.771987535	368.3

Table 4.1 Unit cells behaviors versus the ratio $\frac{A_p}{A_c}$

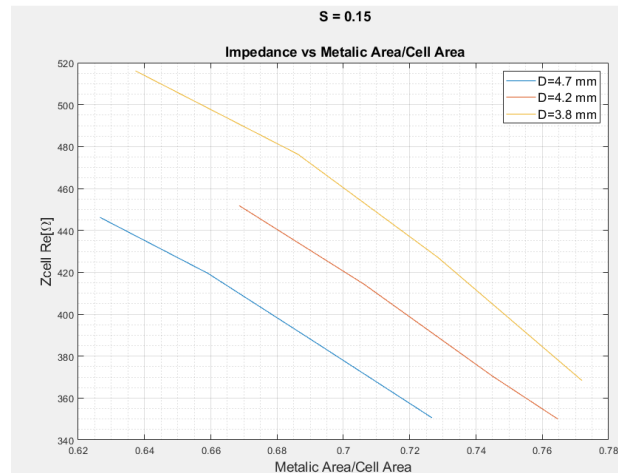


Fig. 4.18 Unit cell impedance versus the ratio $\frac{A_p}{A_c}$ for different values of D

4.3.4 Unit Cell $D \times D = 3.2 \text{ mm} \times 3.2 \text{ mm}$.

In this case, the first value of L is set to 2.75mm. The considered discrete values of S are 0.1, 0.11, 0.15 and 0.2. A new value of S is added to see if there is a significant change with a small step of S.

- $D=3.2\text{mm}$ $L=2.75\text{mm}$.

In Fig. 4.19 we can see how changes the peak of the real part of the unit cell impedance, when S increases the resonance frequency increases too. The behavior is equal than the previous cases.

Fig. 4.20 shows the behavior of the absorption for each value of S. The absorption decreases when S increases at the target frequency. How we saw in the previous analysis, we can get a perfect absorption by increasing L and realizing the matching condition with a proper value of S.

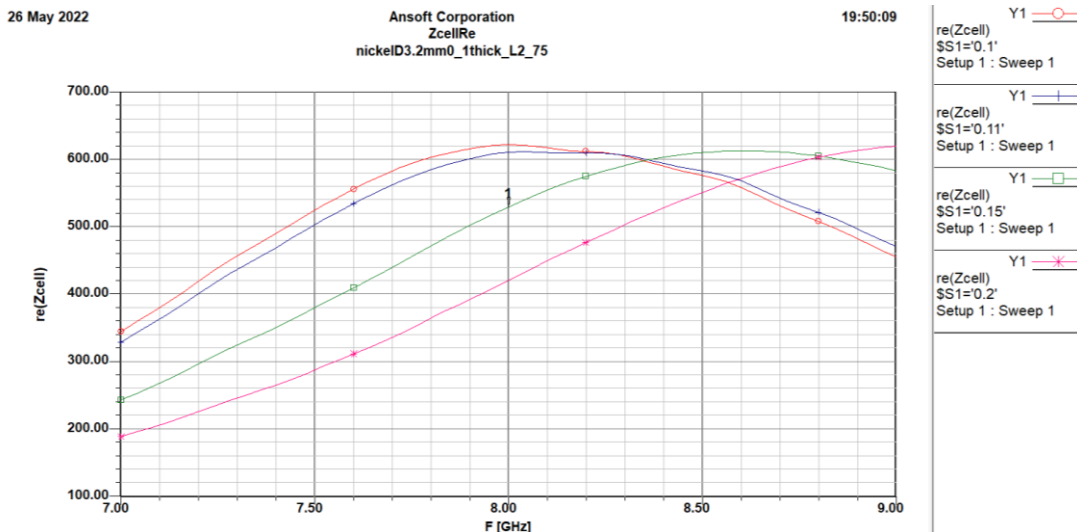


Fig. 4.19 Real part of the unit cell impedance for different values of S (D=3.2 mm L=2.75 mm).

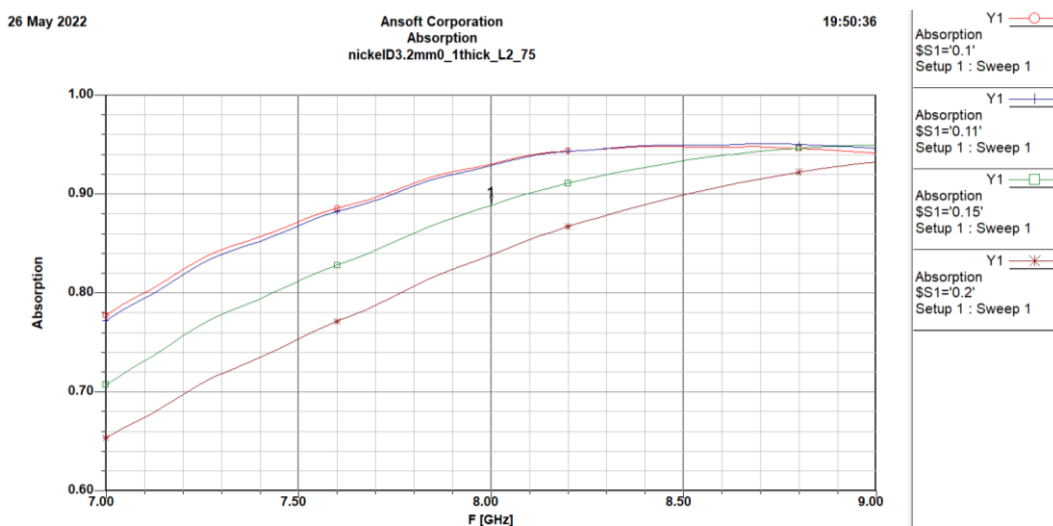


Fig. 4.20 Absorption of the unit cell for different values of S (D=3.2 mm L=2.75 mm).

- **D=3.2mm L=2.8mm.**

In Fig. 4.21 is illustrated the impedance (real part) of the unit cell; we can see that the impedance is lower than the previous case.

Fig. 4.22 shows the absorption of the unit cell for each value of S. In the case of S=0.1, the absorption is near to 1 at 8 GHz, but is not a perfect absorber yet.

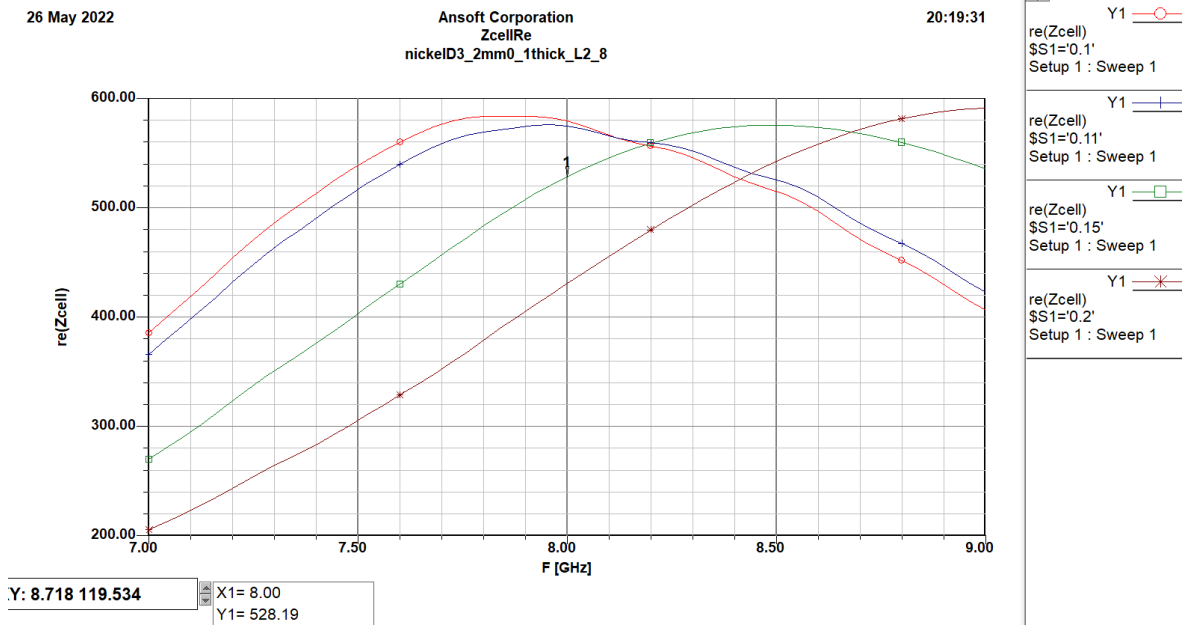


Fig. 4.21 Real part of the unit cell impedance for different values of S (D=3.2 mm L=2.8 mm).

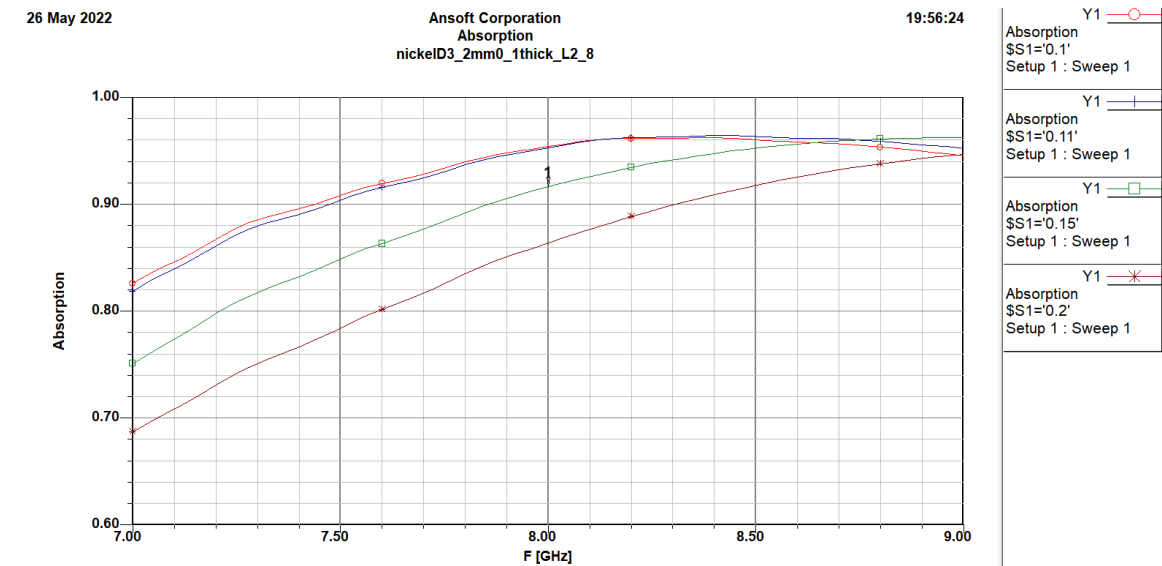


Fig. 4.22 Absorption of the unit cell for different values of S (D=3.2 mm L=2.8 mm).

- $D=3.2\text{mm}$ $L=2.9\text{mm}$.

In Fig. 4.23, the impedance results to be smaller due to the increase of the value of L. Fig. 4.24 shows the absorption of the unit cell for each value of S, in this case with S=0.1 the absorption is very near to 1 at 8 GHz.

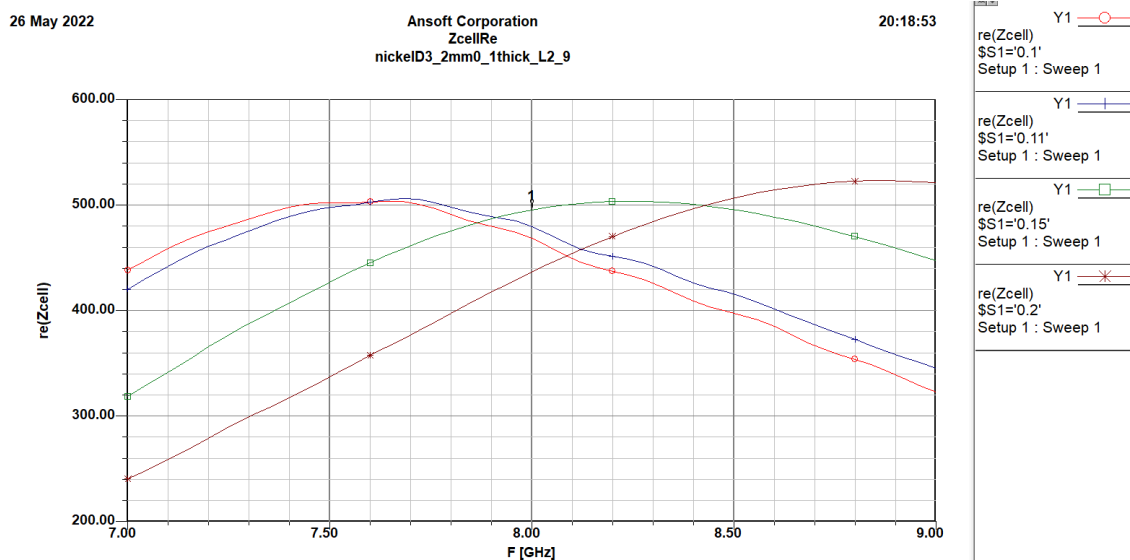


Fig. 4.23 Real part of the unit cell impedance for different values of S ($D=3.2$ mm $L=2.9$ mm).

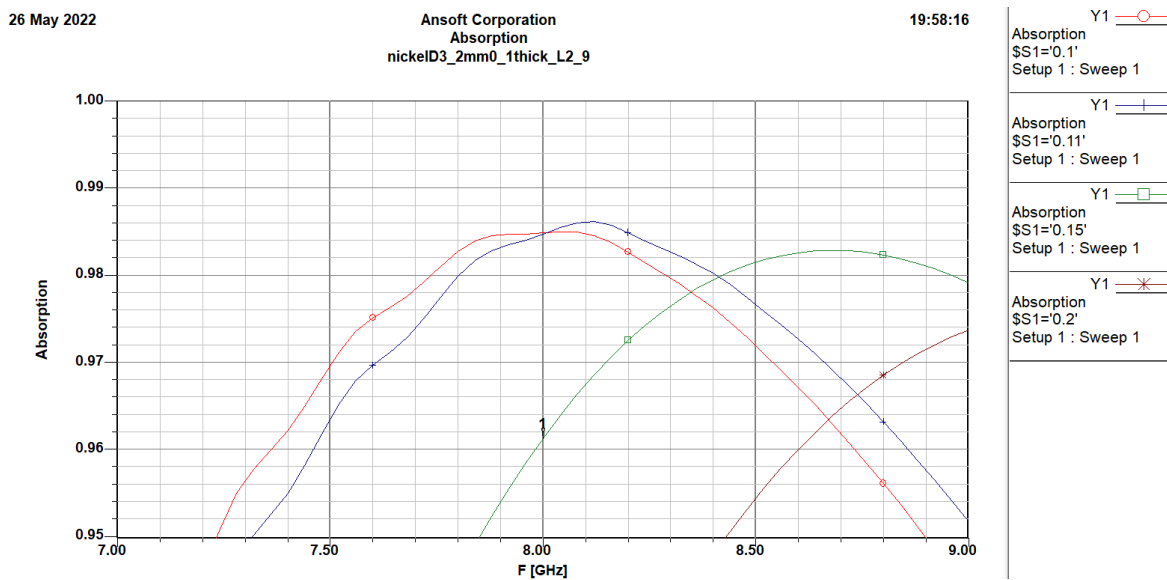


Fig. 4.24 Absorption of the unit cell for different values of S ($D=3.2$ mm $L=2.9$ mm).

- $D=3.2\text{mm}$ $L=3\text{mm}$.

Fig. 4.25 shows that the impedance (real part) of the unit cell is near to the impedance of the free space, but the behavior begins to be weird so we must not increase more the value of L. In this case, the absorption has the best value when the scalar factor S is equal to 0.15 (Fig. 4.26). The absorber developed in this point has de best performance.

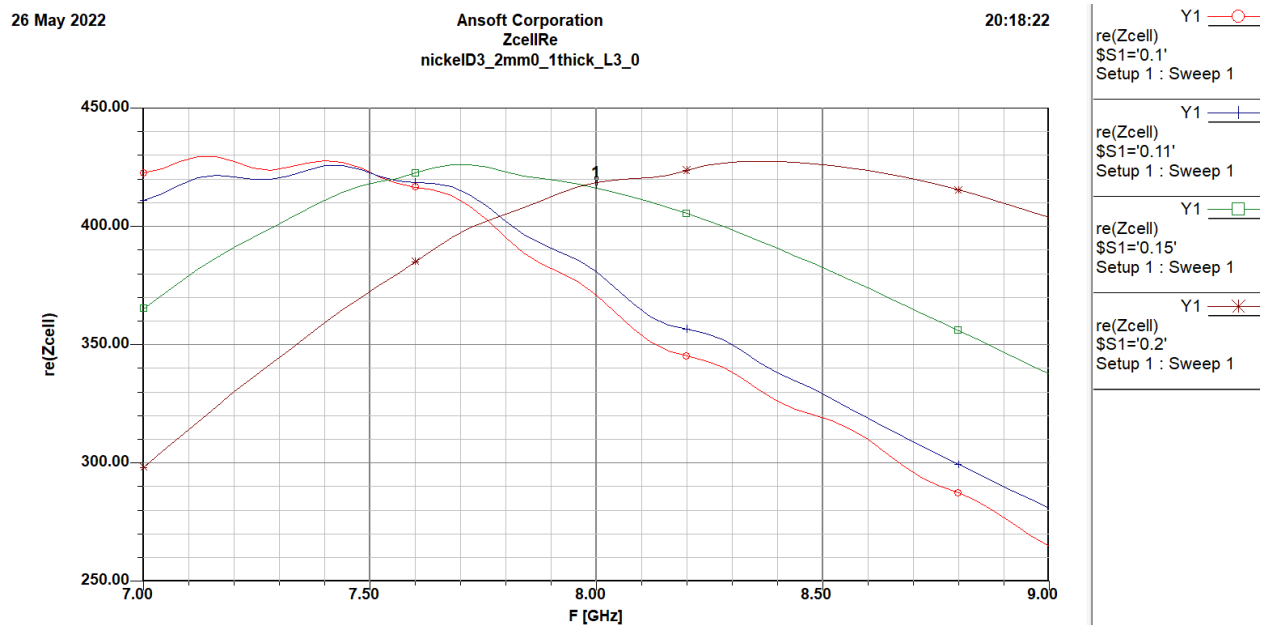


Fig. 4.25 Real part of the unit cell impedance for different values of S ($D=3.2$ mm $L=3$ mm).

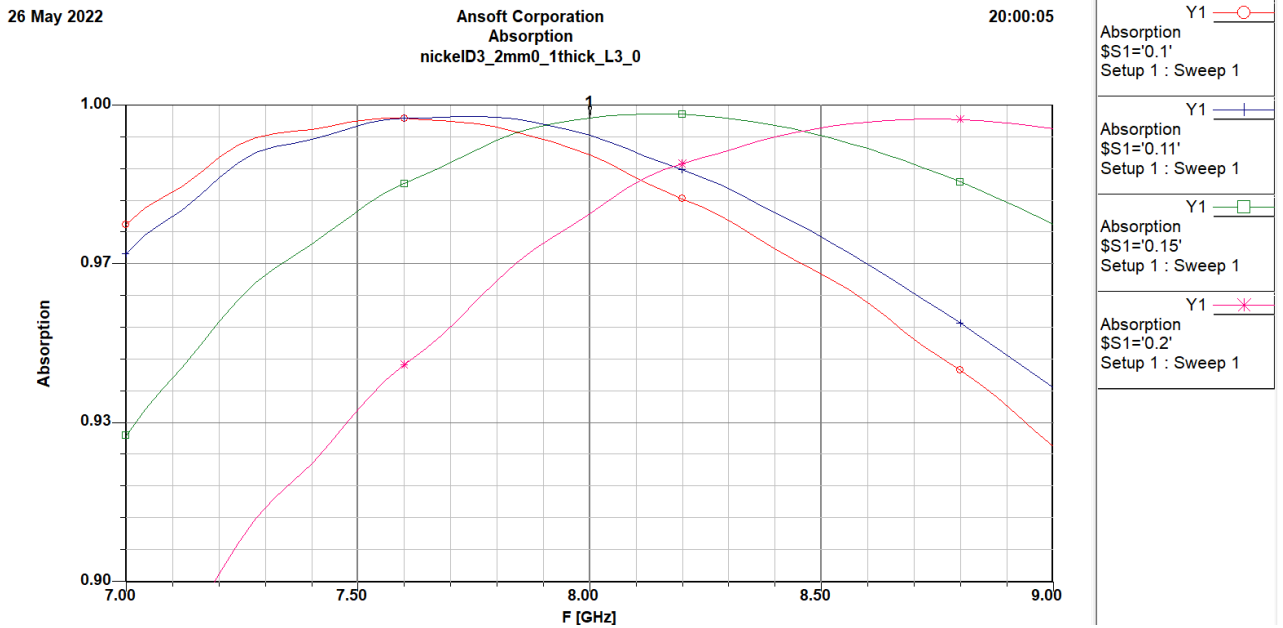


Fig. 4.26 Absorption of the unit for different values of S (D=3.2 mm L=3 mm).

In Fig. 4.27, we can see the behavior of the impedance of the unit cell for a scaling factor equal to 0.15, for different values of L. If the patch length increases the impedance of the unit cell decreases. Fig. 4.28 illustrates the absorption for different values of L and S=0.15. The quasi perfect absorption is achieved when L is equal to 3 mm.

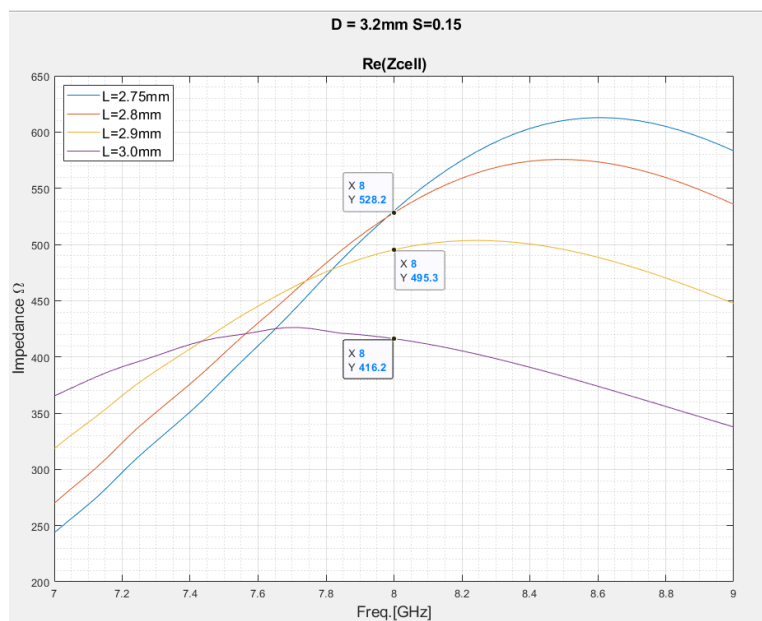


Fig. 4.27 Unit cell impedance for different values of L and S=0.15 (D=3.2 mm).

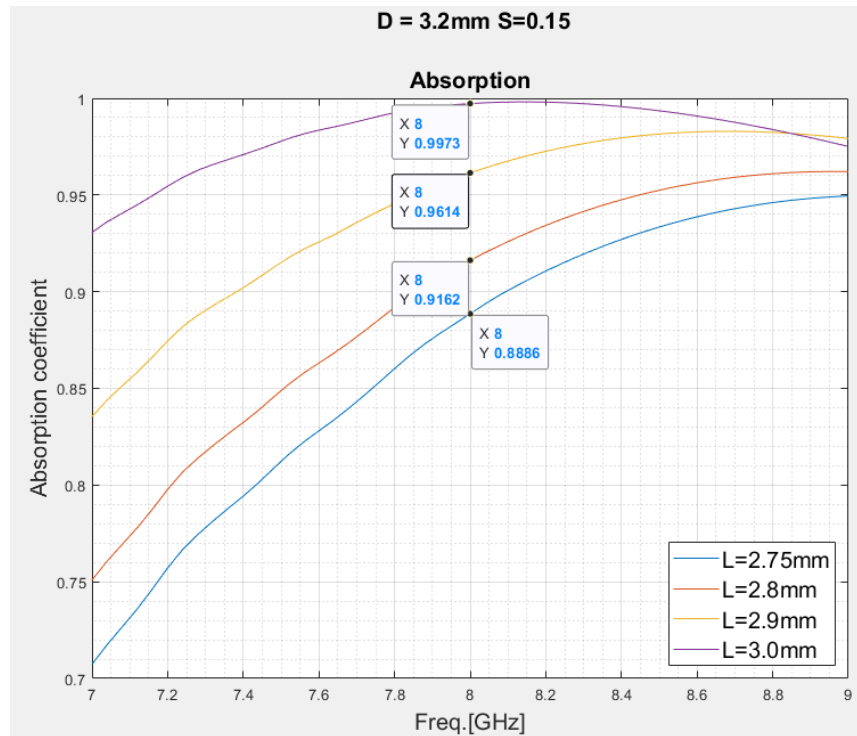


Fig. 4.28 Absorption of the unit cell for different values of L and S=0.15 (D=3.2 mm).

A similar analysis was performed for smaller unit cells whenever the behavior could be considered stable. The smallest unit cell analysis is presented below.

4.3.5 Unit Cell $D \times D = 2.5 \text{ mm} \times 2.5 \text{ mm}$.

- $D=2.5\text{mm}$ $L=2.2\text{mm}$.

The first value of L is fixed to 2.2mm. In Fig. 4.29, we observe that when S increases the resonance frequency increases too. The impedance in these cases is too high. Fig. 4.30 illustrates the behavior of the absorption for each value of S. The absorption is not enough good, also the absorption decreases when S increases at the target frequency.

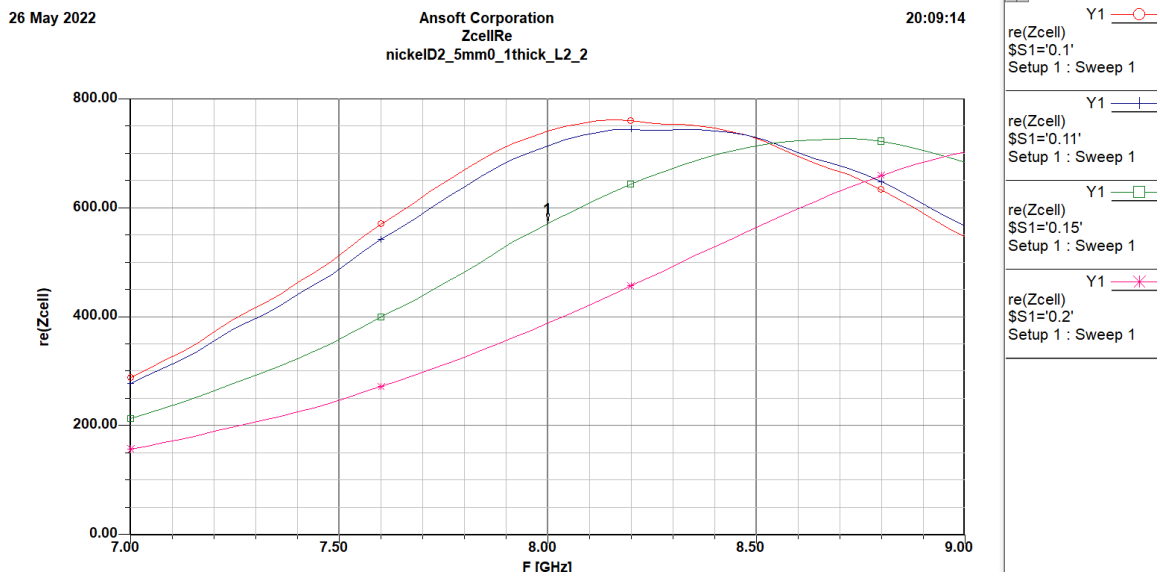


Fig. 4.29 Real part of the unit cell impedance for different values of S (D=2.5 mm L=2.2 mm).

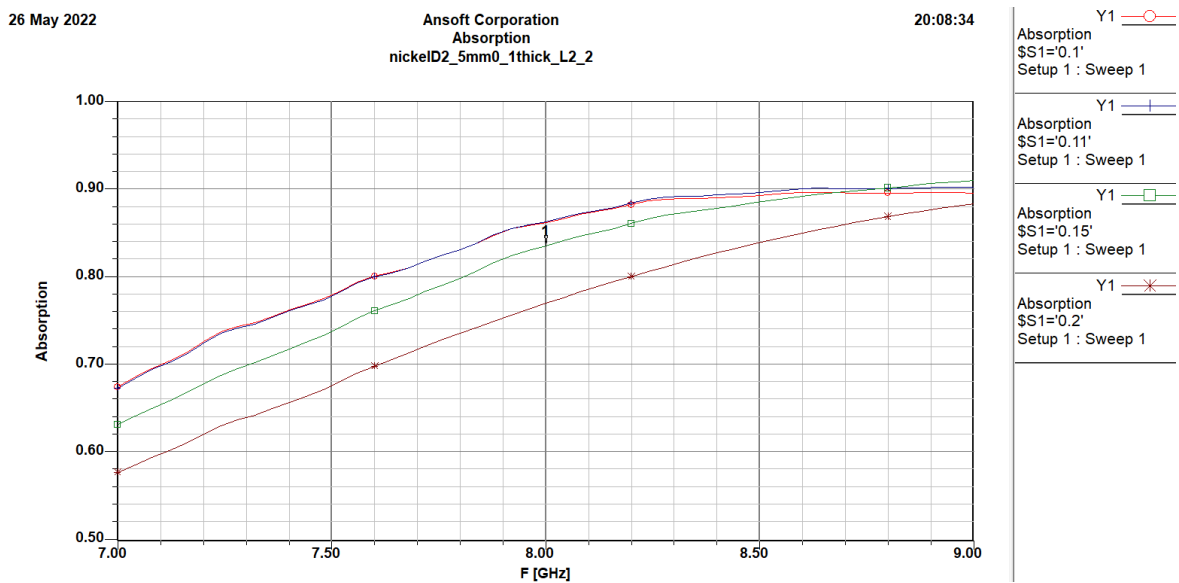


Fig. 4.30 Absorption of the unit cell for different values of S (D=2.5 mm L=2.2 mm).

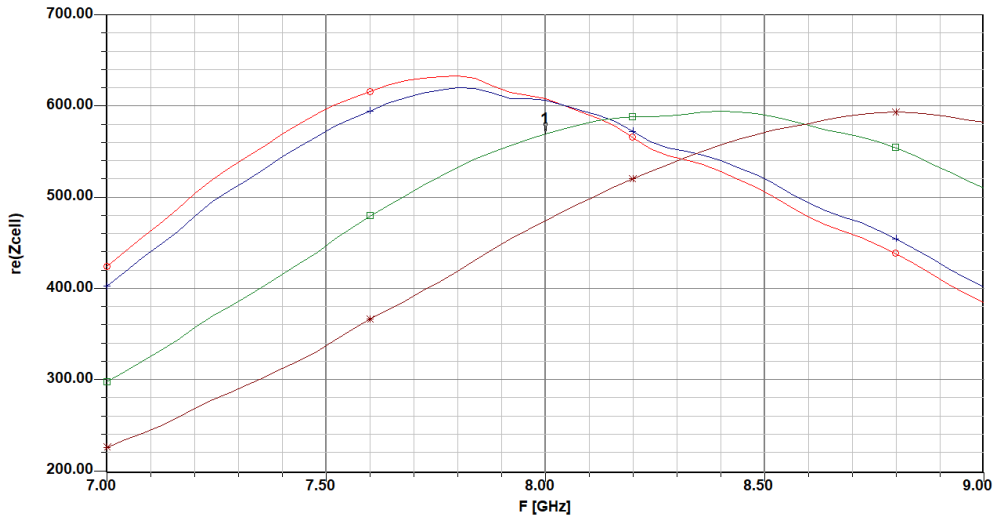
- **D=2.5mm L=2.3mm.**

In the Fig. 4.31 is illustrated the impedance (real part) of the unit cell, we can see that the impedance is lower than the previous case, but is still high. Fig. 4.32 shows the absorption of the unit cell for each value of S, in this case when S=0.1 the absorption is near to 1 at 8 GHz.

26 May 2022

Ansoft Corporation
ZcellRe
nickelD2_5mm0_1thick_L2_3

20:17:14



Y1

re(Zcell)
\$S1=0.1'
Setup 1 : Sweep 1

Y1

re(Zcell)
\$S1=0.11'
Setup 1 : Sweep 1

Y1

re(Zcell)
\$S1=0.15'
Setup 1 : Sweep 1

Y1

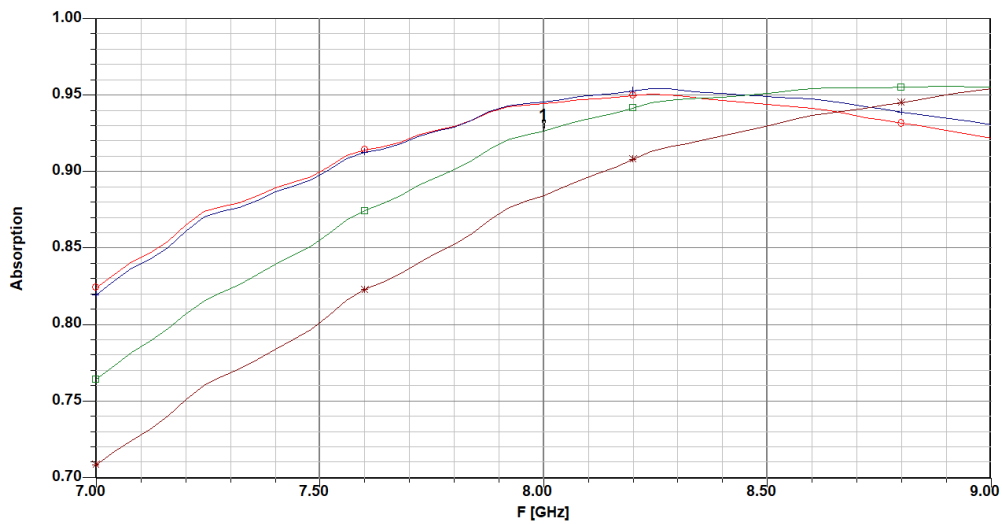
re(Zcell)
\$S1=0.2'
Setup 1 : Sweep 1

Fig. 4.31 Real part of the unit cell impedance for different values of S (D=2.5 mm L=2.3 mm).

26 May 2022

Ansoft Corporation
Absorption
nickelD2_5mm0_1thick_L2_3

20:11:09



Y1

Absorption
\$S1=0.1'
Setup 1 : Sweep 1

Y1

Absorption
\$S1=0.11'
Setup 1 : Sweep 1

Y1

Absorption
\$S1=0.15'
Setup 1 : Sweep 1

Y1

Absorption
\$S1=0.2'
Setup 1 : Sweep 1

Fig. 4.32 Absorption of the unit cell for different values of S (D=2.5 mm L=2.3 mm).

- $D=2.5\text{mm}$ $L=2.4\text{mm}$.

In Fig. 4.33, the impedance has been reduced by increasing the value of L , but the behavior begins to be weird. Fig. 4.34 shows the absorption of the unit cell for each value of S , in this case for $S=0.15$ the absorption is very near to 1 at 8 GHz.

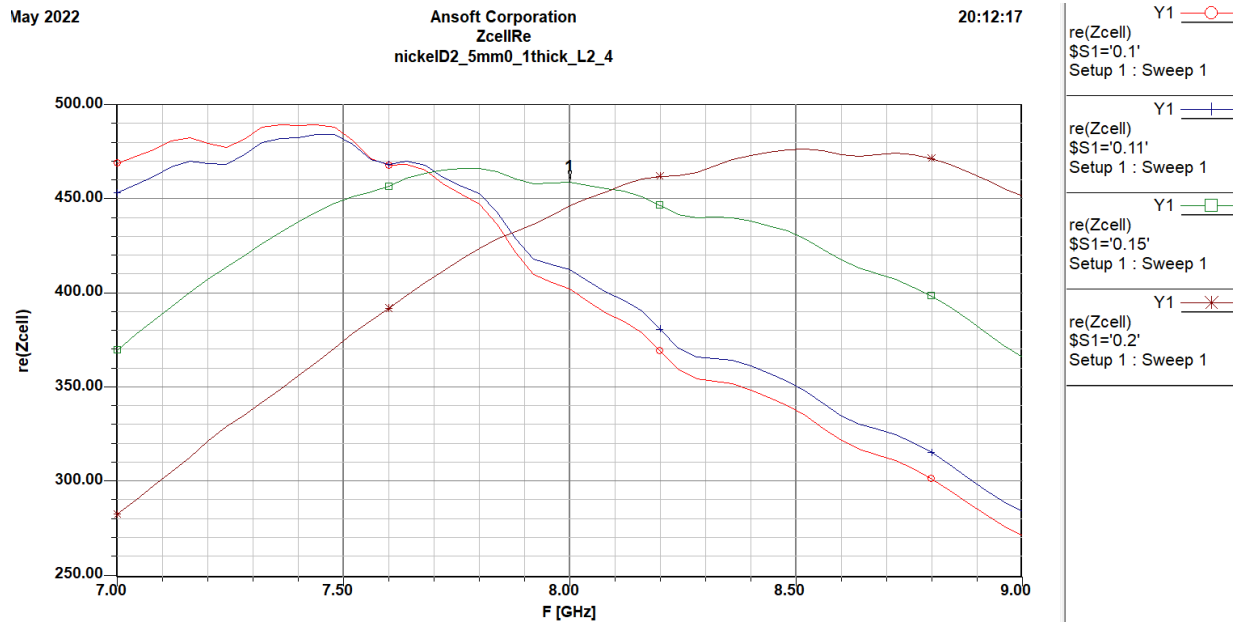


Fig. 4.33 Real part of the unit cell impedance for different values of S ($D=2.5$ mm $L=2.4$ mm).

26 May 2022

Ansoft Corporation
Absorption
nickelD2_5mm0_1thick_L2_4

20:13:38

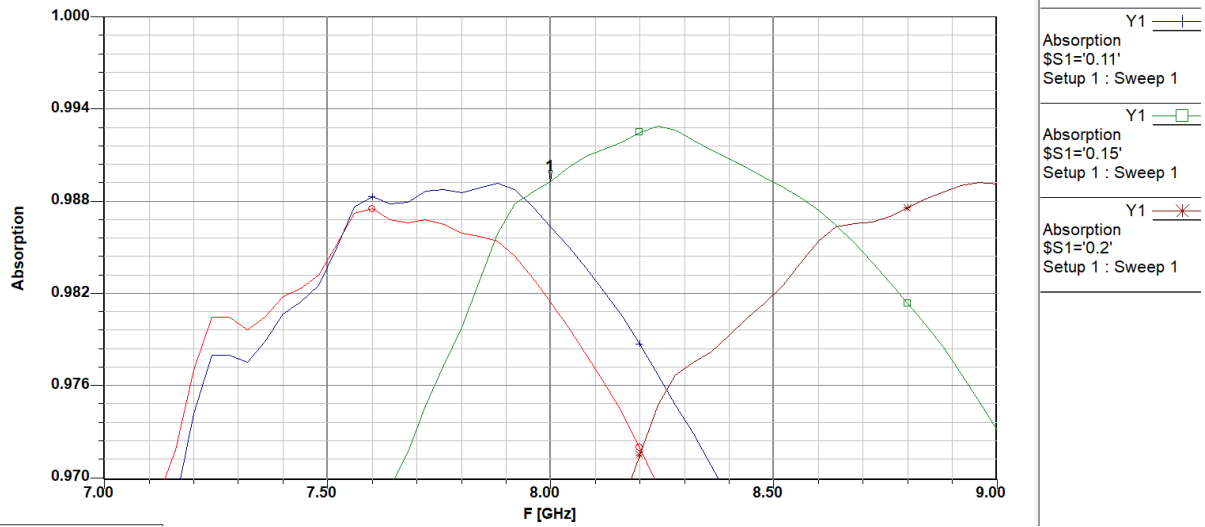


Fig. 4.34 Absorption of the unit cell for different values of S (D=2.5 mm L=2.4 mm).

- **D=2.5mm L=2.45mm.**

Fig. 4.35 shows that the impedance (real part) of the unit cell is closer to 377Ω , but is lower than the impedance of the free space, so we must not increase more the value of L, because the absorption will decrease. The absorption has the best value when the scalar factor S is equal to 0.15; it is illustrated in Fig. 4.36. The absorption is practically one (perfect absorber) at 8 GHz, our target frequency.

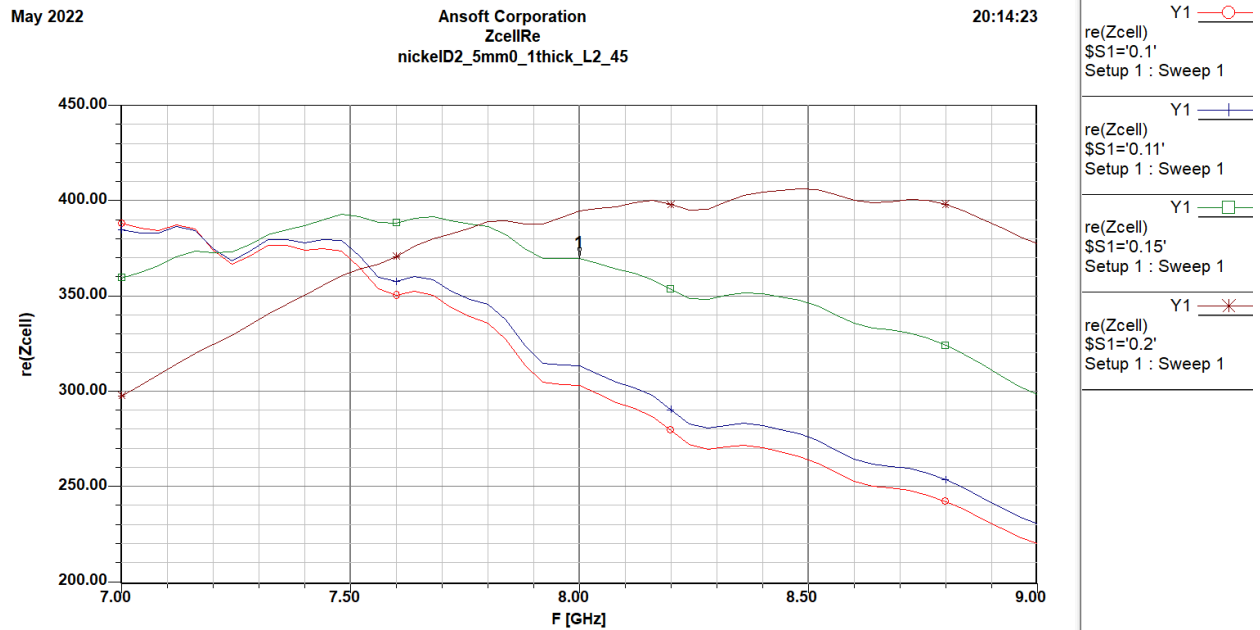


Fig. 4.35 Real part of the unit cell impedance for different values of S (D=2.5 mm L=2.45 mm).

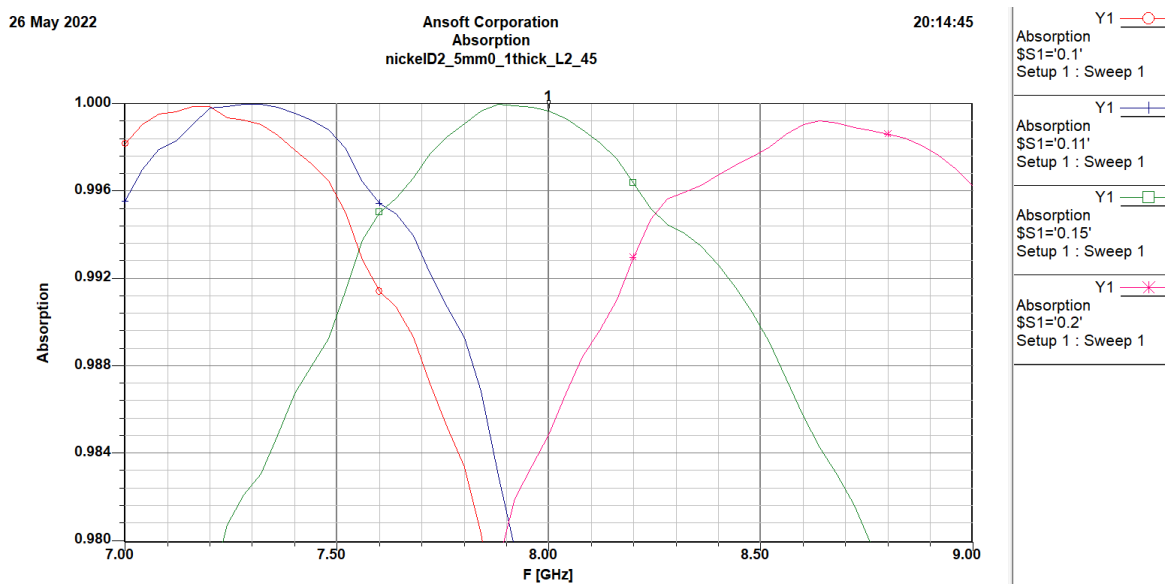


Fig. 4.36 Absorption of the unit cell for different values of S (D=2.5 mm L=2.45 mm).

Fig. 4.37 shows a comparison for different values of L with a scaling factor equal to 0.15, if the patch dimension increases the impedance of the unit cell decreases. We can see in Fig. 4.38 a comparison of the behavior of the absorption for different L-values, with S fixed to

0.15. The value of S was chosen because with this value in one of the L variation we get the best performance. The value of the absorption with $L=2.45\text{mm}$ is practically equal to 1.

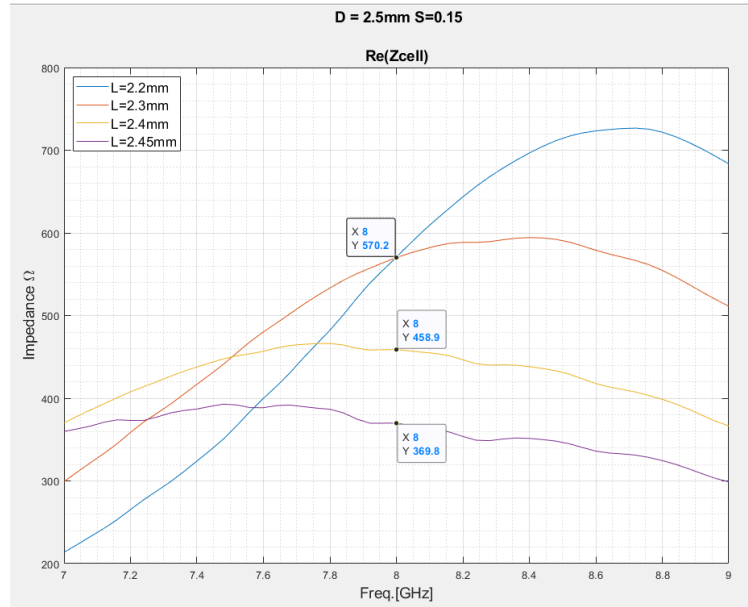


Fig. 4.37 Unit cell impedance for different values of L and $S=0.15$ ($D=2.5$ mm).

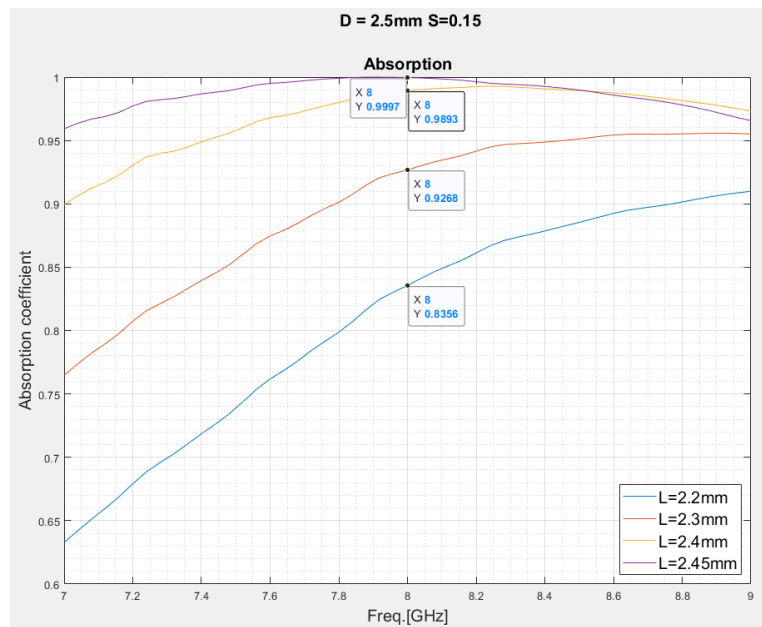


Fig. 4.38 Absorption of the unit cell for different values of L and $S=0.15$ ($D=2.5$ mm).

Table 4.2 shows the relationship between the ratio $\frac{A_p}{A_c}$ and the impedance of the unit cell for different resonant cells.

Furthermore, Fig. 4.39 shows that, for all considered cases, the traces have a similar behavior.

When the ratio $\frac{A_p}{A_c}$ increases the value of the impedance decreases. However, a smaller unit cell

has a higher impedance than larger unit cells for the same value of the ratio $\frac{A_p}{A_c}$

D	S	L	area	MetallicPatchArea/CellArea	Impedance
3.2	0.15	2.75	6.881875	0.672058105	528.2
3.2	0.15	2.8	7.1344	0.69671875	528.2
3.2	0.15	2.9	7.6531	0.747373047	495.3
3.2	0.15	3	8.19	0.799804688	416.2
2.5	0.15	2.2	4.4044	0.704704	570.2
2.5	0.15	2.3	4.8139	0.770224	570.2
2.5	0.15	2.4	5.2416	0.838656	458.9
2.5	0.15	2.45	5.462275	0.873964	369.8

Table 4.2 Unit cells behaviors versus the ratio $\frac{A_p}{A_c}$

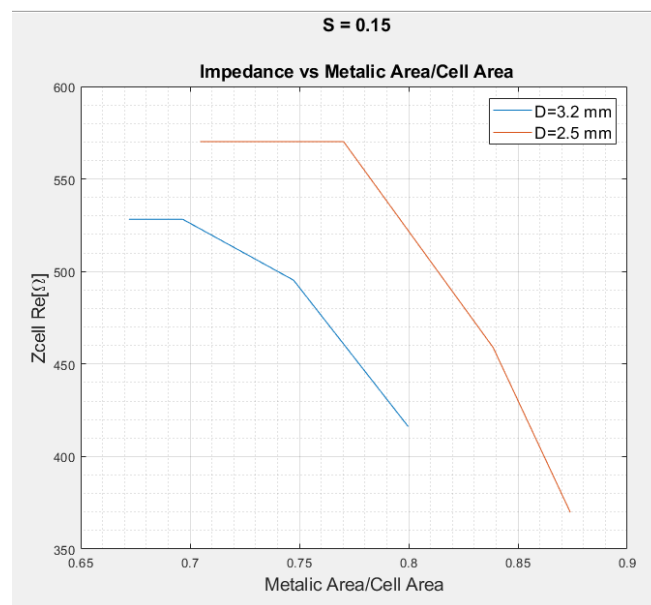


Fig. 4.39 Unit cell impedance Vs Relationship Metallic Patch Area/Unit Cell Area.

4.4 Final considerations

In the tables 4.1 and 4.2 is the summary of the relationship between the ratio $\frac{A_p}{A_c}$ and the impedance of the unit cell for different resonant cells. With this data we can concluded that if the ratio $\frac{A_p}{A_c}$ has a high value, the impedance is near to the impedance of the free space or lower, for these reason we have to take in consideration a limit to the value of the ratio $\frac{A_p}{A_c}$, if it is so high the absorption begins to decrease due the mismatch of the impedance of the unit cell and the impedance of the free space.

Another limit that we must consider is the reduction of the length size of the resonant cell, we can confirm that if the size of D decreases the length size of the metal patch (L), to obtain a perfect absorber at the target frequency, decreasing too, but it not in the same proportion. Each time L is more near to the size of D, and the behavior of the resonant cell is not stable.

In our case the smallest resonant cell, with a behavior that could be considered stable, has a length size dimension of the unit cell (D) equal to 2.5mm and the best match between to the resonant cell impedance and the free space impedance, is when the length size of the metal patch (L) is equal to 2.45mm. The absorption for this resonant cell is practically 1, a perfect absorber at 8 GHz, our target frequency.

CHAPTER V

ANGULAR STABILITY OF THE DESIGNED FRACTAL METAMATERIAL ABSORBERS

5.1 Introduction

As an additional analysis, a good angular stability is required for a perfect absorber in preventing and reducing radiated emission. To do this, the absorption and reflection coefficients are calculated against the frequency for different incidence angles, both for TE and TM polarizations.

The angle of incidence is the angle between a wave incident on a surface and the line perpendicular to the surface at the point of incidence, called the normal.

In addition, the analysis is performed both for the horizontally polarized E-field (TE mode) as well as for the vertically polarized E-field (TM mode).

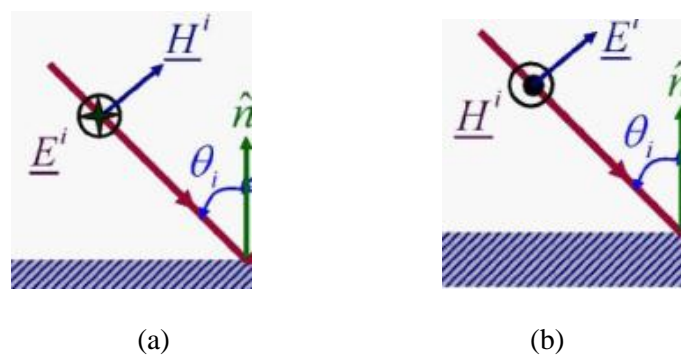


Fig. 5.1 Polarization of the incident E-field: (a) Horizontal polarization (TE-mode); (b) Vertical polarization (TM-mode)

5.2 Analysis for the horizontally polarized E-field (TE mode) and vertically polarized E-field (TM mode).

The unit cells defined in the previous chapter, which behave like a perfect absorber, have been analyzed to different incident angles. The incident angle changes from 0° to 60° in steps of 15° for the horizontally polarized E-field (TE mode) and similarly for the vertically polarized E-field (TM mode). A comparison of the reflection coefficient and absorption of the unit cells was also developed using Matlab for different incident angles.

The unit cell structures are those with the best performances in terms of absorption:

- **D=4.7mm, L=4.2mm and S=0.15.**

Fig. 5.2 illustrates the reflection coefficient computed for different values of the incident angle in the case of the TE mode. We can see that when the incident angle increases the reflection coefficient increases too. In Fig. 5.3, we can see the behavior of the absorption for different incident angles for the TE mode. If the incident angle increases, the absorption decreases. In any case, an absorption coefficient greater than 80% is obtained up to an angle of incidence of 60 degrees.

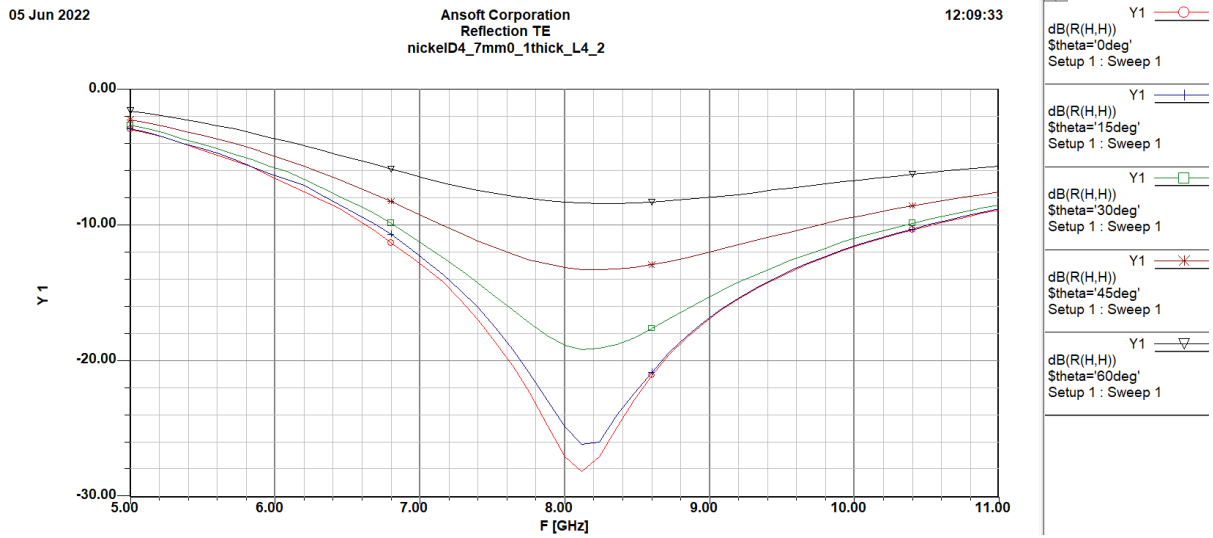


Fig. 5.2 Reflection coefficient for different values of incident angle (TE mode) (D=4.7 mm L=4.2 mm S=0.15).

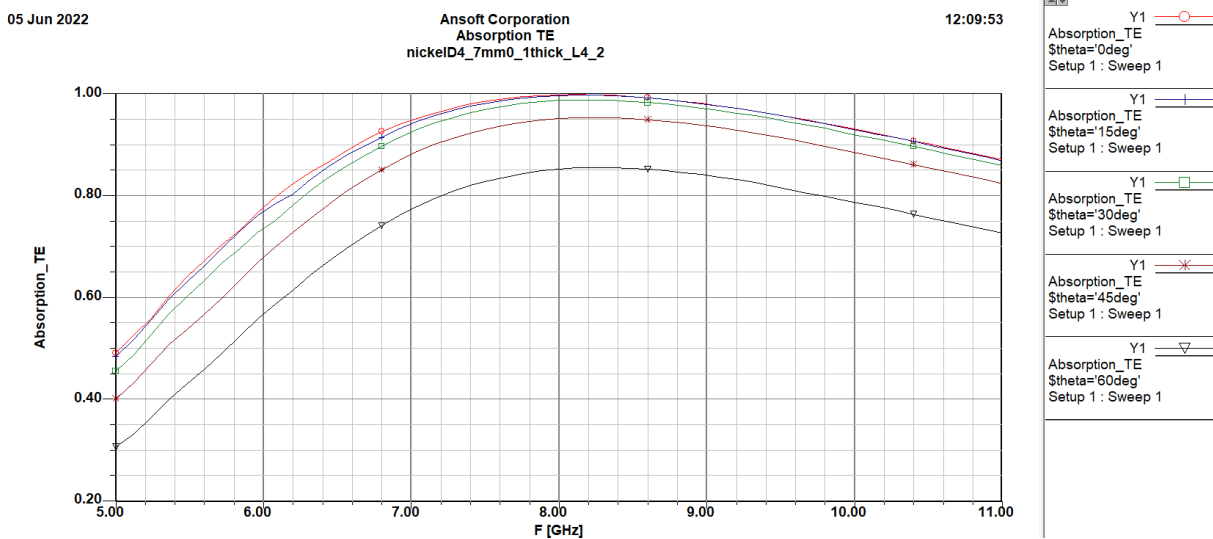


Fig. 5.3 Absorption for different values of incident angle (TE-mode) (D=4.7 mm L=4.2 mm S=0.15).

Fig. 5.4 shows the reflection coefficient for different incident angles in the case of the TM mode. If the incident angle increases, the resonance frequency increases too. In addition, the

reflection coefficient increases at our frequency target (8GHz). Furthermore, Fig. 5.5 shows the behavior of the absorption for different incident angles. When the incident angle increases, the absorption decreases at our frequency target (8GHz).

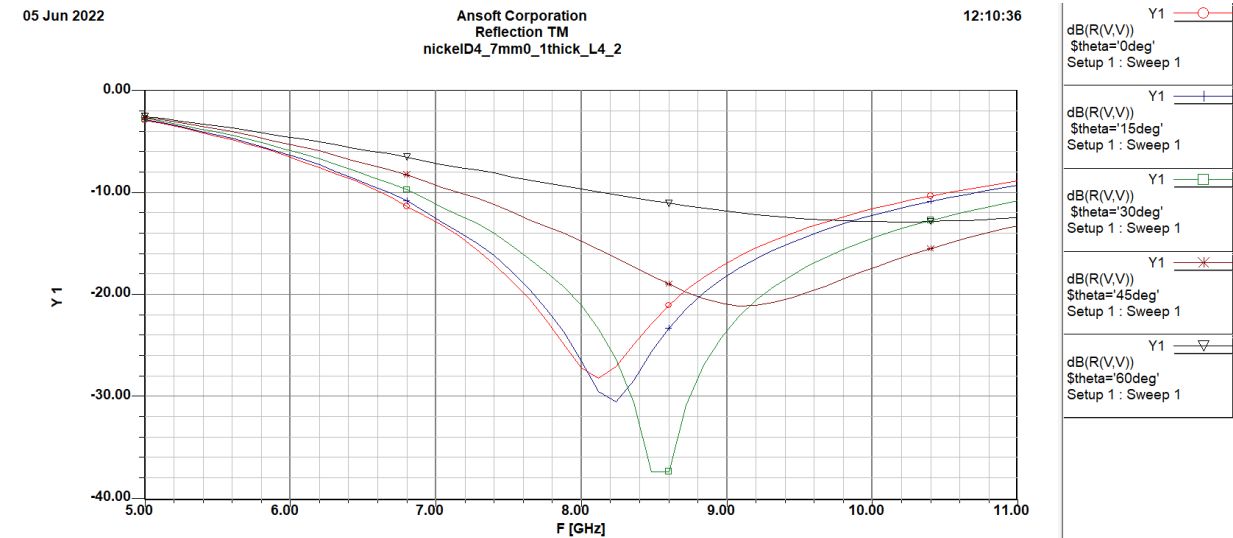


Fig. 5.4 Reflection coefficient to TM mode for different values of incident angle (D=4.7 mm L=4.2mm S=0.15).

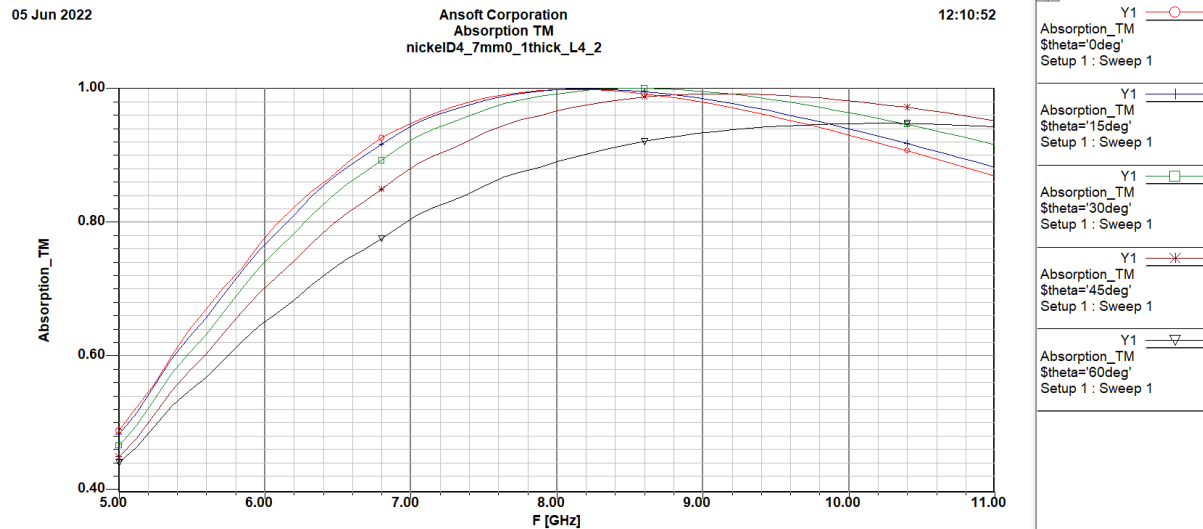


Fig. 5.5 Absorption to TM mode for different values of incident angle ($D=4.7$ mm $L=4.2$ mm $S=0.15$).

Fig. 5.6 shows a comparison between the absorption coefficient for the TE mode and the TM mode. We can observe that the maximum value of the reflection coefficient, at 8GHz, in the TE mode is -8.314 dB, for an incident angle of 60° . And the maximum value of the reflection coefficient, at 8GHz, for the TM mode is -9.614 dB, in the case of an incident angle of 60° . These values correspond to an absorption of about 85.26% (Fig. 5.7(a) - TE mode) and 89% (Fig. 5.7(b) - TM mode), respectively.

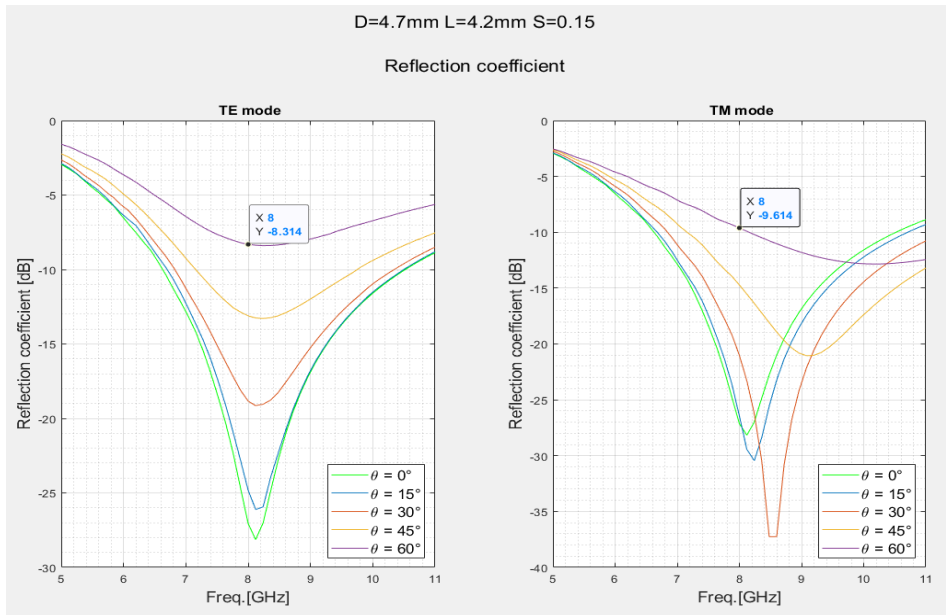


Fig. 5.6 Comparison of reflection coefficient for TE mode and TM mode (D=4.7 mm L=4.2 mm S=0.15).

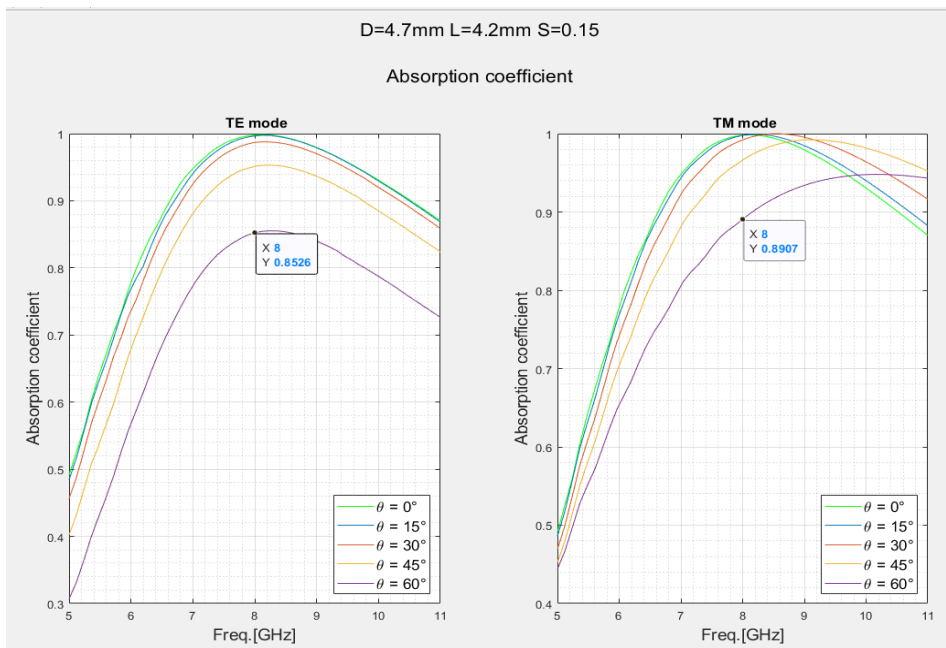


Fig. 5.7 Comparison of absorption for TE mode and TM mode (D=4.7 mm L=4.2 mm S=0.15).

- **D=4.2mm, L=3.8mm and S=0.15.**

Fig. 5.8 shows a comparison between the reflection coefficient computed for the TE mode and the TM mode.

The highest value of reflection coefficient, at 8GHz, in the TE mode is equal to -8.773dB, for an incident angle of 60°. Whilst the highest value of the reflection coefficient, at 8GHz, for the TM mode is -9.376dB, for an incident angle of 60°. A comparison of the absorption for the TE mode and the TM mode is illustrated in Fig. 5.9. We can observe an absorption of about 86.7% (Fig. 5.9(a) - TE mode) and 88.45% (Fig. 5.9(b) - TM mode), respectively.

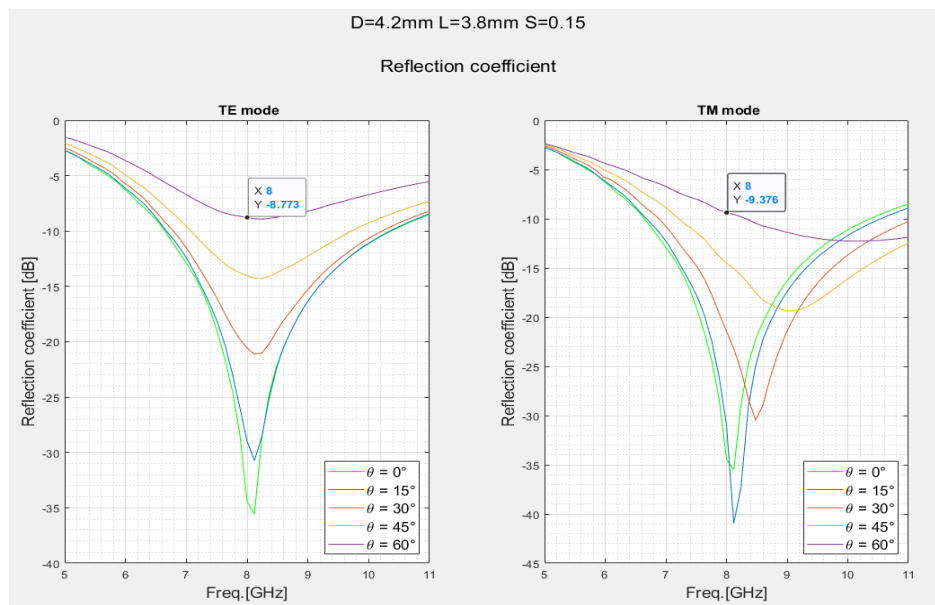


Fig. 5.8 Comparison of reflection coefficient for TE mode and TM mode (D=4.2 mm L=3.8 mm S=0.15).

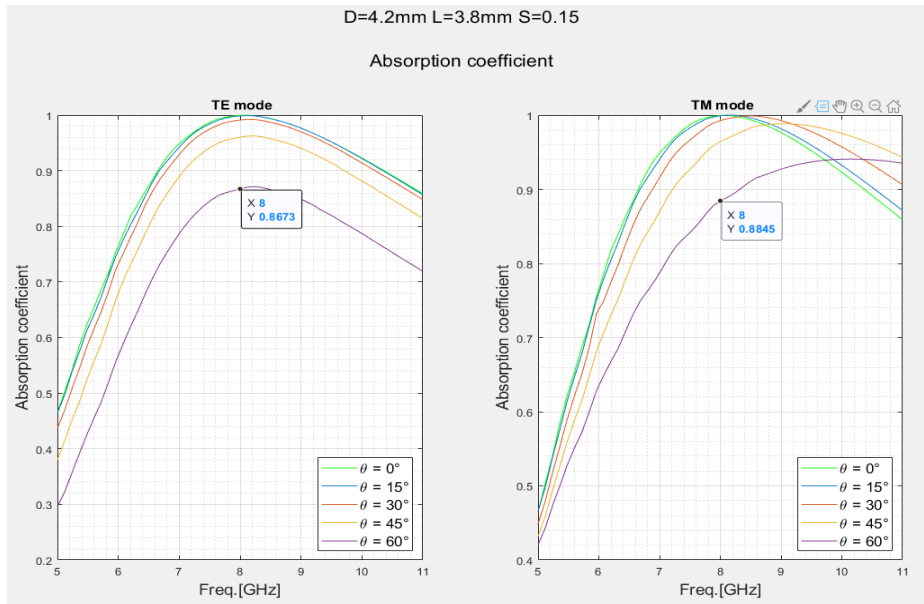


Fig. 5.9 Comparison of absorption for TE mode and TM mode (D=4.2 mm L=3.8 mm S=0.15).

- **D=3.8mm, L=3.5mm and S=0.15.**

Fig. 5.10 shows a comparison of the reflection coefficient simulated for the TE mode and the TM mode. We can see that the maximum value of the reflection coefficient, at 8GHz, for the TE mode is -8.961dB for an incident angle of 60° . Whilst the maximum value of the reflection coefficient, at 8GHz, in TM mode is -9.262dB, for an incident angle of 60° .

Fig. 5.11 shows the absorption coefficient for the TE mode and the TM mode. We can see that the minimum value of the absorption, at 8GHz, is 87.3% for an incident angle of 60° (TE mode). Whilst the minimum value of the absorption, at 8GHz, is 88.15% for an incident angle of 60° (TM mode).

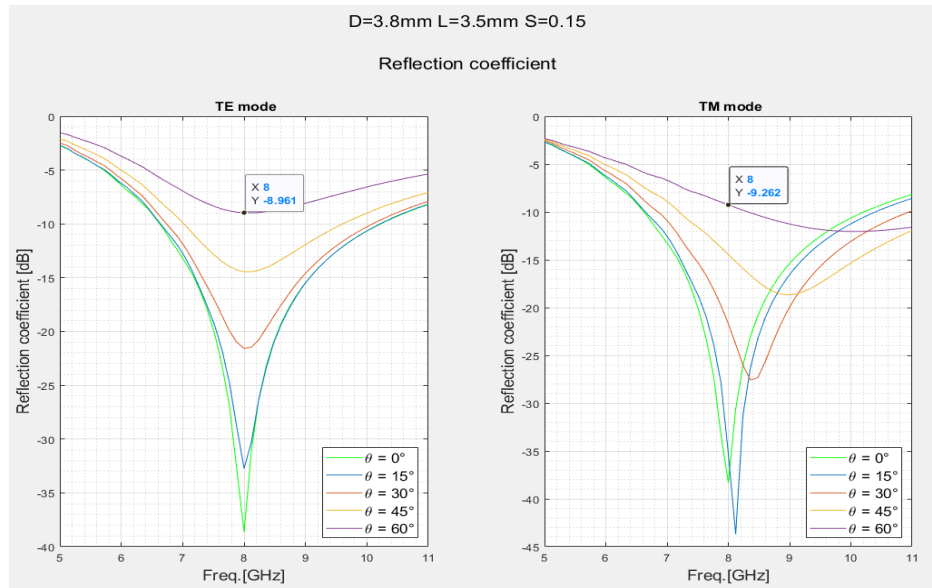


Fig. 5.10 Comparison of reflection coefficient for TE mode and TM mode ($D=3.8$ mm $L=3.5$ mm $S=0.15$).

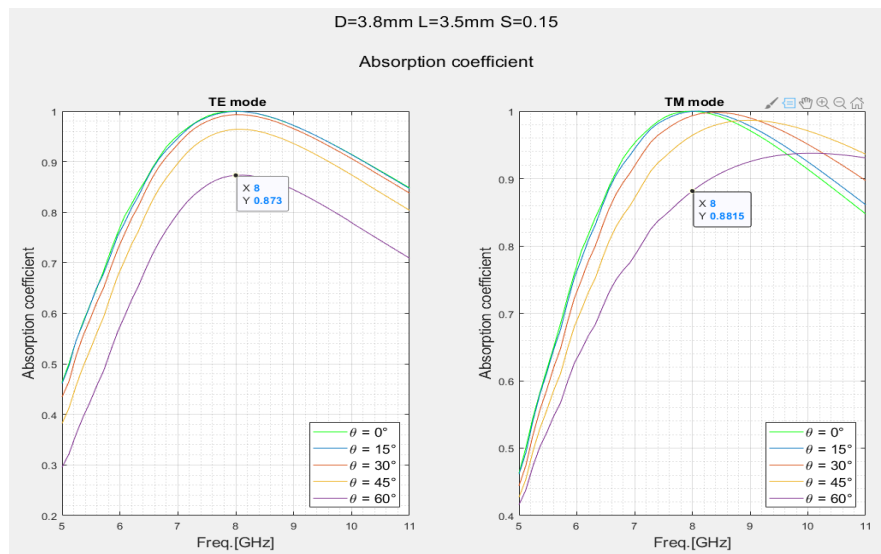


Fig. 5.11 Comparison of absorption for TE mode and TM mode ($D=3.8$ mm $L=3.5$ mm $S=0.15$).

- $D=3.2$ mm, $L=3$ mm and $S=0.15$.

Fig. 5.12 shows the reflection coefficient for the TE and the TM modes. We can observe that the maximum value of the reflection coefficient, at 8GHz, is -9.905 for an incident angle of

60° (TE mode). Whilst the maximum value of the reflection coefficient, at 8GHz, is -8.343 dB for an incident angle of 60° (TM mode). Fig. 5.13 shows the absorption computed for the TE mode and the TM mode. We can see that the minimum value of the absorption, at 8GHz, is equal to 89.78%, for an incident angle of 60° (TE mode), whilst the minimum value for the TM mode is 85.35%, for an incident angle of 60°.

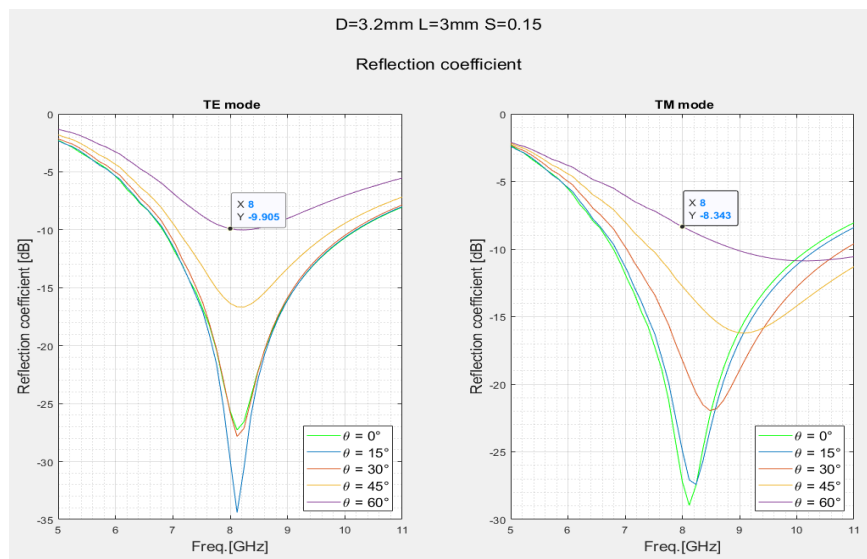


Fig. 5.12 Comparison of reflection coefficient for TE mode and TM mode (D=3.2 mm L=3 mm S=0.15).

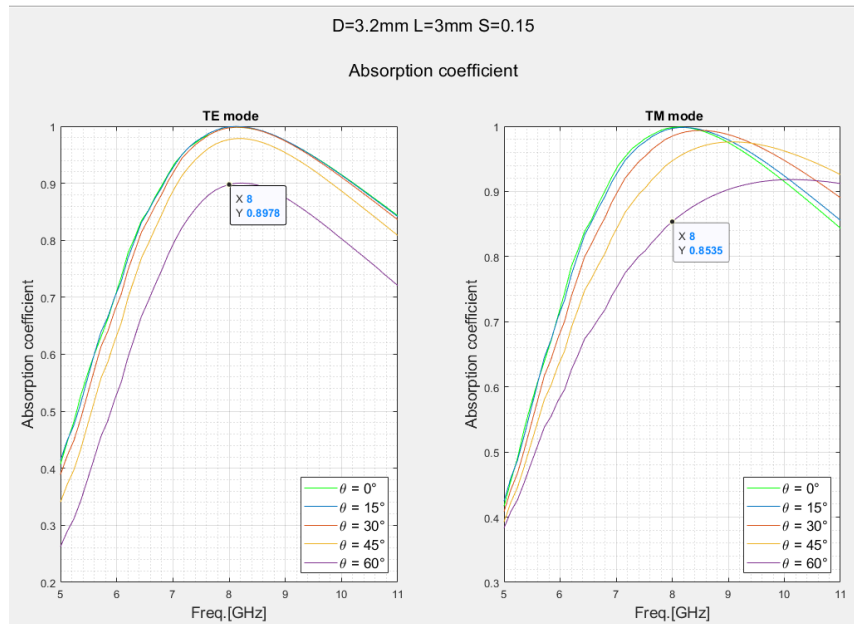


Fig. 5.13 Comparison of absorption for TE mode and TM mode (D=3.2 mm L=3 mm S=0.15).

- **D=2.5mm, L=2.45mm and S=0.15.**

Fig. 5.14 shows the reflection coefficient for the TE mode and the TM mode. We can see that the maximum value of the reflection coefficient, at 8GHz, in the TE mode is -9.2 dB for an incident angle of 60° . Whilst the maximum value of the reflection coefficient, at 8GHz, in the TM mode is -9.492dB, for an incident angle of 60° . The absorption computed for the TE and the TM modes are illustrated in Fig. 5.15. We can observe an absorption of about 87.98% (Fig. 5.15(a) - TE mode) and 88.76% (Fig. 5.15(b) - TM mode).

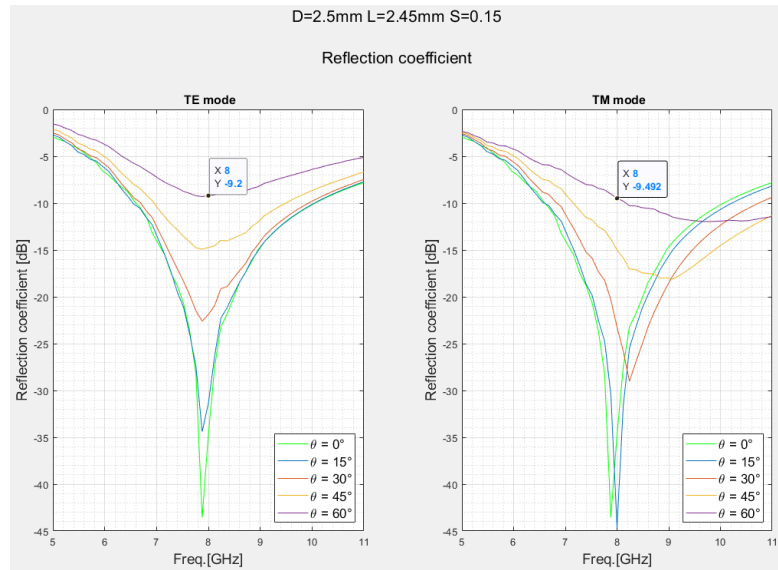


Fig. 5.14 Comparison of reflection coefficient for TE mode and TM mode (D=2.5 mm L=2.45 mm S=0.15).

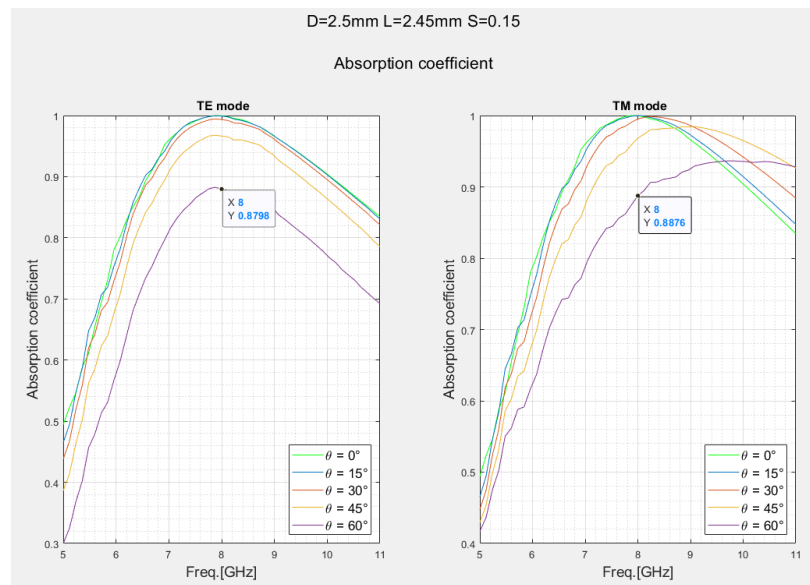


Fig. 5.15 Comparison of absorption for TE mode and TM mode (D=2.5 mm L=2.45 mm S=0.15).

5.3 Final comments

In Table 5.1 there is a summary of the absorption coefficients computed for the unit cells designed in this thesis. Different incident angles, ranging from 0° up to 60° , are considered, both for the TE and TM modes.

For all the cells, in the worst case scenario (angle of incidence equal to 60°), the absorption is higher than 85%, for this reason we can affirm that the designed absorbing structure is stable with respect to the angle of incidence, allowing the reduction of unwanted radiated emissions from random and unknown directions.

Furthermore, the smallest unit cell ($D=2.5\text{mm}$) could be the best option for the realization of a perfect absorber shield, as it allows to achieve a 53% size reduction. For this reason, more unit cells could be placed in the same area of the shield surface than the basic unit cells ($D=4.7\text{mm}$), with that we can have a better imitation of an infinite plane and ensure excellent performance of the absorber.

Incident Angle	Absorption of Unit Cell D=4.7mm L=4.2mm S=0.15		Absorption of Unit Cell D=4.2mm L=3.8mm S=0.15		Absorption of Unit Cell D=3.8mm L=3.5mm S=0.15		Absorption of Unit Cell D=3.2mm L=3mm S=0.15		Absorption of Unit Cell D=2.5mm L=2.45mm S=0.15	
	TE mode	TM mode	TE mode	TM mode	TE mode	TM mode	TE mode	TM mode	TE mode	TM mode
	0°	0.9980	0.9981	0.9996	0.9996	0.9999	0.9999	0.9973	0.9981	0.9997
15°	0.9967	0.9977	0.9987	0.9992	0.9995	0.9997	0.9990	0.9968	0.9993	0.9997
30°	0.9869	0.9921	0.9912	0.9928	0.9931	0.9932	0.9974	0.9849	0.9935	0.9953
45°	0.9512	0.9663	0.9604	0.9646	0.9641	0.9641	0.9769	0.9469	0.9664	0.9684
60°	0.8526	0.8907	0.8673	0.8845	0.8730	0.8815	0.8978	0.8535	0.8798	0.8876

Table 5.1 Summary of the absorption coefficient for different incident angles (TE and TM modes) from all unit cells.

CONCLUSIONS

This thesis dealt with the problem of unintentional radiated emissions and shielding solutions. In particular, metamaterial EM absorbers were discussed and analyzed, showing their advantages over the traditional absorbers.

In the last part of the second chapter is presented a study of the metamaterial absorber proposed in the paper [36], to mitigate the unwanted radiated electromagnetic emissions from a high-speed system with digital interfaces. PCIe Gen 3 interface operating with 8Gbps data rate shows an 8 GHz radiated emission, and it faults the proof of electromagnetic compatibility at this frequency, so in this system was implemented a frequency selective surface absorber.

The goal of this thesis was to design a smaller perfect metamaterial absorber with respect to that presented in the paper [36]. The reduction of the unit cell size is necessary to assure a good functionality of the absorber and reduce the area of the shield.

To reduce the unit cell dimensions was necessary to understand how the parameters of the unit cell, such as conductivity, loss tan, etc., affect its impedance and the others features.

A Minkowski fractal geometry was proposed in chapter 4, to reduce the dimensions of the unit cell. An analysis of the features of the unit cell was done for some unit cell's dimensions. A miniaturized metamaterial structure was finally designed (53% size reduction with respect to existing solutions) achieving very high absorption values close to 100%.

Finally, in Chapter 5 was performed the angular stability analysis of the designed fractal structures, both for the TE mode as well as the TM mode. In conclusion, the designed

absorbing structures were stable with respect to the angle of incidence, allowing the reduction of unwanted radiated emissions from random and unknown directions.

REFERENCES

- [1] Raimond Grimberg, Electromagnetic metamaterials, *Materials Science and Engineering: B*, Volume 178, Issue 19, 2013.
- [2] Castellanos, Luis M.; Lopez, Francisco e Reyes-Vera, Erick. Metamaterials: main features and applications. *Rev. acad. colomb. cienc. exact. fis. nat.* [online]. 2016, vol.40, n.156, pp.395-401. ISSN 0370-3908.
- [3] Simovski, Constantin; Tretyakov, Sergei, An Introduction to Metamaterials and Nanophotonics, University Printing House, Cambridge CB2 8BS, United Kingdom, 2020.
- [4] Rakesh Kumar, Manoj Kumar, Jasgurpreet Singh Chohan, Santosh Kumar, Overview on metamaterial: History, types and applications, *Materials Today: Proceedings*, Volume 56, Part 5, 2022, ISSN 2214-7853.
- [5] Olof Sjödin, *Electromagnetic Phase Engineering With Metamaterials*, October, 2021.
- [6] R. A. Shelby, D. R. Smith, and S. Schultz, "Experimental verification of a negative index of refraction," *Science* 292, 77–79 (2001).
- [7] Yadgar I. Abdulkarim, Ayesha Mohanty, Om Prakash Acharya, Bhargav Appasani, Mohammad S. Khan, S. K. Mohapatra, Fahmi F. Muhammadsharif and Jian Dong, A Review on Metamaterial Absorbers: Microwave to Optical, *Front. Phys.* 10:893791, 2022.

- [8] I.A. Buriak, V.O. Zhurba, G.S. Vorobjov, *Metamaterials: Theory, Classification and Application Strategies (Review)*, *J. Nano- Electron. Phys.* 8 No 4(2), 04088 (2016).
- [9] Kaushal Gangwar, Dr. Paras and Dr. R.P.S. Gangwar, *Metamaterials: Characteristics, Process and Applications*, *Advance in Electronic and Electric Engineering*. ISSN 2231-1297, Volume 4, Number 1 (2014)
- [10] *Metamaterial Market Size, Share & Trends Analysis Report By Product, Application, End-use, & Segment Forecasts 2018–2025*. Available at: <https://www.grandviewresearch.com/industry-analysis/metamaterials-market>.
- [11] *Metamaterials: An Overview*. Available at: <https://medium.com/sigma-xi-vit/metamaterials-an-overview-2eb8380b4283>.
- [12] K. Sato, T. Nomura, S. Matsuzawa, H. Iizuka, *Metamaterial techniques for automotive applications*. In: *PIERS proceedings*. Hangzhou, China, 2008, pp. 1122–1125.
- [13] *Future Opportunities for Metamaterials in Aerospace and Defense Markets*, ntech Research Article, 2016.
<http://www.ntechresearch.com/wpcontent/uploads/2017/12/metamaterials.pdf>.
- [14] P. Alitalo, S. Tretyakov, *Metamaterials for Space Applications*. , 2008, pp. 1–97. Available at. <https://www.esa.int/gsp/ACT/doc/ARI/ARI%20Study%20Report/ACT-RPT-NAN-ARI-07-7001d-Metamaterials.pdf>.
- [15] G. Palma, H. Mao, L. Burghignoli, et al., *Acoustic metamaterials in aeronautics*, *Appl. Sci.* 8 (6) (2018) 971, <https://doi.org/10.3390/app8060971>.

- [16] A. Valipour, H. Kargozarfard, M. Rakhshi, *Metamaterials and their applications: an overview*. *Proceedings of the Institution of Mechanical Engineers Part L, J. Mater. Des. Appl.* (2021), <https://doi.org/10.1177/1464420721995858>.
- [17] M. Askari, David A. Hutchins, Peter J. Thomas, *Additive manufacturing of metamaterials: A review*, *Addit. Manuf.* 36 (2020) 1–36.
- [18] Lee, Youngpak; Rhee, Joo; Yoo, Young Joon; Kim, Won; *Metamaterials for Perfect Absorption* - 2016/01/01.
- [19] Landy, N. I., Sajuyigbe, S., Mock, J. J., Smith, D. R. & Padilla, W. J. *Perfect metamaterial absorber*. *Phys. Rev. Lett.* 100, 1–4, doi:10.1103/PhysRevLett.100.207402 (2008).
- [18] Claire M. Watts, Xianliang Liu, and Willie J. Padilla, *Metamaterial Electromagnetic Wave Absorbers*, *materials views*, 2012, 24, OP98–OP120.
- [19] W. Zhu, “*Electromagnetic Metamaterial Absorbers: From Narrowband to Broadband*,” *Metamaterials and Metasurfaces*, 2019, doi: 10.5772/intechopen.78581.
- [20] G.T. Ruck, D.E. Barrick, W.D. Stuart, A.C.K. Krichbaum, *Radar Cross Section Handbook*, vol. 2 (Plenum, 1970)
- [21] Tom F. Grimes, Eric D. Church, William K. Pitts, and Lynn S. Wood, *Explanation of Unintended Radiated Emission Classification via LIME*. (2020)
- [22] Vann, J.M., Karnowski, T.P., & Anderson, A.L. (2019). *Classification of Unintended Radiated Emissions in a Multi-Device Environment*. *IEEE Transactions on Smart Grid*, 10, 5506-5513.

- [23] Clayton R. Paul, Introduction to Electromagnetic Compatibility, JOHN WILEY & SONS, INC. PUBLICATION, Second Edition, 2006.
- [24] Salvatore Celozzi, Rodolfo Araneo, Giampiero Lovat, Electromagnetic Shielding, JOHN WILEY & SONS, INC., PUBLICATION, 2008.
- [25] Linares y Miranda, Roberto, & López Bonilla, José Luis. (2012). Compatibilidad electromagnética. *Ingeniare. Revista chilena de ingeniería*, 20(1), 5-7.
<https://dx.doi.org/10.4067/S0718-33052012000100001>
- [26] https://www.electronics-notes.com/articles/analogue_circuits/emc-emi-electromagnetic-interference-compatibility/what-is-emc-basics-tutorial.php
- [27] Hernandez Flores Gerardo Abraham, Consideraciones Para Realizar Un Analisis De Compatibilidad Electromagnetica En Una Plataforma Satelital, Ciudad Universitaria, Mexico D. F. 2015.
- [28] Stenumgaard, Peter, Radiated Emission Limits to Protect Digital Wireless Communication Systems, ISSN 1650-1942, Swedish defense research agency, 2004.
- [29] <https://www.academyofemc.com/emc-standards>
- [30] <https://learnemc.com/emc-regulations-and-standards>
- [31] P.Donohoe, “EMC STANDARDS” Mississippi State University Course Notes, EMC Requirements
- [32] Module 8: EMC Regulations, www.egr.msu.edu/em/research/goali/notes/module8_regulations.pdf

- [33] Dr.Lyn'kov L.M. Dr.Nasonova N.V. Mohammed Shakir Mahmood. Boiprav O.V,Shielding Properties of Electromagnetic Radiation Absorbers with Geometrical and Structure Heterogeneities, Eng. &Tech.Journal, Vol. 32,Part (A), No.12, 2014.
- [34] Yue Zhao,Lele Hao,Xindan Zhang,Shujuan Tan, Haohang Li,Jing Zheng, Guangbin Ji, A Novel Strategy in Electromagnetic Wave Absorbing and Shielding Materials Design: Multi-Responsive Field Effect, Small Science,Volume 2, Issue 2, 2021
- [35] Manish Mathew Tirkey and Nisha Gupta, Electromagnetic Absorber Design Challenges, 2019 IEEE Electromagnetic Compatibility Magazine – Volume8 – Quarter 1.
- [36] Ali Khoshniat, d Ramesh Abhari, Design and Evaluation of Radiated Emission Metamaterial Absorbers, IEEE TRANSACTIONS ON ELECTROMAGNETIC COMPATIBILITY, VOL. 61, NO. 4, AUGUST 2019.
- [37] Venneri,,F.; Costanzo, S.; Di Massa,G.; Fractal-Shaped Metamaterial Absorbers for Multireflections Mitigation in the UHF Band, IEEE Antennas And Wireless Propagation Letters, Vol. 17, No. 2, February 2018.